

State of Oregon  
Department of Geology and Mineral Industries  
Vicki S. McConnell, State Geologist

# **EVALUATION OF EROSION HAZARD ZONES FOR THE DUNE-BACKED BEACHES OF TILLAMOOK COUNTY, OREGON**

**Technical Report to the Oregon Department of Land Conservation and Development**

By  
Laura L. Stimely<sup>1</sup> and Jonathan C. Allan<sup>1</sup>



2014

---

<sup>1</sup>Oregon Department of Geology and Mineral Industries, Coastal Field Office, 313 SW 2nd, Suite D, Newport OR 97365

## NOTICE

This product is for informational purposes and may not have been prepared for or be suitable for legal, engineering, or surveying purposes. Users of this information should review or consult the primary data and information sources to ascertain the usability of the information. This publication cannot substitute for site-specific investigations by qualified practitioners. Site-specific data may give results that differ from the results shown in the publication.

*Cover photograph: Oblique photo overlooking the community of Rockaway, Oregon.  
Photo taken by D. Best, May 30, 2008.*

Oregon Department of Geology and Mineral Industries O-14-02  
Published in conformance with ORS 516.030

---

For copies of this publication or other information about Oregon's geology and natural resources, contact:

Nature of the Northwest Information Center  
800 NE Oregon Street, Suite 965  
Portland, Oregon 97232  
(971) 673-2331  
<http://www.NatureNW.org>

For additional information:  
Administrative Offices  
800 NE Oregon Street, Suite 965  
Portland, OR 97232  
Telephone (971) 673-1555  
Fax (971) 673-1562  
<http://www.oregongeology.org>  
<http://egov.oregon.gov/DOGAMI/>



## TABLE OF CONTENTS

<b>EXECUTIVE SUMMARY .....</b>	<b>1</b>
<b>1.0 INTRODUCTION.....</b>	<b>2</b>
<b>2.0 STUDY AREA.....</b>	<b>4</b>
<b>2.1 Coastal geomorphology .....</b>	<b>6</b>
<b>2.2 Historical shoreline change and coastal erosion .....</b>	<b>10</b>
2.2.1 Neskowin cell.....	11
2.2.2 Sand Lake cell .....	15
2.2.3 Netarts cell .....	17
2.2.4 Rockaway cell .....	25
<b>2.3 Cascadia subduction zone .....</b>	<b>32</b>
<b>3.0 METHODOLOGY .....</b>	<b>33</b>
<b>3.1 Models of foredune erosion .....</b>	<b>33</b>
3.1.1 Geometric model .....	33
3.1.2 Kreibel and Dean model .....	35
<b>3.2 Wave and tide processes .....</b>	<b>36</b>
3.2.1 Pacific Northwest wave climate .....	36
3.2.2 Tides .....	38
3.2.3 El Niño .....	39
3.2.4 Storm surge .....	40
3.2.5 Sea level rise.....	40
<b>3.3 Wave runup and total water levels .....</b>	<b>43</b>
<b>3.4 Beach and shoreline morphology .....</b>	<b>44</b>
<b>3.5 Cascadia subduction zone .....</b>	<b>46</b>
<b>3.6 Scenarios of coastal change in Tillamook County .....</b>	<b>46</b>
<b>4.0 RESULTS .....</b>	<b>47</b>
<b>4.1 Projected coastal erosion hazard zones.....</b>	<b>47</b>
<b>4.2 Cascadia subduction zone hazard.....</b>	<b>52</b>
<b>4.3 Kreibel and Dean model.....</b>	<b>53</b>
4.1.1 Estimates of hazard zone uncertainty .....	53
<b>5.0 DISCUSSION AND CONCLUSION .....</b>	<b>55</b>
<b>6.0 ACKNOWLEDGMENTS .....</b>	<b>61</b>
<b>7.0 REFERENCES.....</b>	<b>61</b>
<b>APPENDIX A: EROSION SCENARIOS.....</b>	<b>64</b>
<b>APPENDIX B: MAPS OF MODELED EROSION HAZARD ZONES .....</b>	<b>65</b>
<b>Neskowin .....</b>	<b>65</b>
<b>Pacific City .....</b>	<b>75</b>
<b>Tierra Del Mar/Sand Lake .....</b>	<b>78</b>
<b>Netarts .....</b>	<b>84</b>
<b>Cape Meares/Bayocean Spit .....</b>	<b>92</b>
<b>Rockaway .....</b>	<b>99</b>
<b>Nehalem Spit.....</b>	<b>108</b>
<b>Manzanita .....</b>	<b>112</b>

## LIST OF FIGURES

<b>Figure 2-1.</b>	Location map of Tillamook County coastline .....	5
<b>Figure 2-2.</b>	Looking north along Bayocean spit, the Tillamook jetties, Rockaway just north of the jetties, Nehalem Spit, and Neahkahnie Mountain in the far distance .....	7
<b>Figure 2-3.</b>	Tillamook County dune crest elevations .....	8
<b>Figure 2-4.</b>	Tillamook County beach slopes .....	8
<b>Figure 2-5.</b>	Looking east at Neahkahnie Mountain and extensive gravel/boulder berm .....	9
<b>Figure 2-6.</b>	Costal bluffs of the Astoria Formation north of Sand Lake .....	9
<b>Figure 2-7.</b>	Extensive gravel/boulder berm that backs a dissipative sand beach in the Cape Meares community .....	10
<b>Figure 2-8.</b>	Historical and contemporary shoreline positions identified at Neskowin .....	12
<b>Figure 2-9.</b>	Erosion at Neskowin and rebuilding of the sandy beach at Neskowin in 1949 .....	13
<b>Figure 2-10.</b>	Positional changes in the beach/dune toe (elevation of 6 m) along the Neskowin Cell between 1997 and 2013 .....	14
<b>Figure 2-11.</b>	Historical and contemporary shoreline positions identified adjacent to the Nestucca Bay mouth .....	14
<b>Figure 2-12.</b>	Shoreline variability adjacent to the Sand Lake estuary mouth .....	16
<b>Figure 2-13.</b>	Historical and contemporary shoreline positions identified along the southern end of Netarts Spit, adjacent to Cape Lookout State Park. ....	18
<b>Figure 2-14.</b>	De-measured shoreline changes derived from a comparison of 1997 and 1998 lidar along the Netarts littoral cell .....	19
<b>Figure 2-15.</b>	Wooden bulkhead constructed at Cape Lookout State Park and the same area in February 1998 .....	19
<b>Figure 2-16.</b>	Dynamic revetment “cobble beach” constructed at Cape Lookout State Park .....	20
<b>Figure 2-17.</b>	Historical and contemporary shoreline positions identified along the northern end of Netarts Spit, adjacent to Cape Lookout State Park. ....	21
<b>Figure 2-18.</b>	Historical shoreline positions identified at the mouth of Netarts Bay .....	22
<b>Figure 2-19.</b>	Historical shoreline positions identified along the toe of The Capes development near the mouth of Netarts Bay .....	23
<b>Figure 2-22.</b>	Shoreline positions north of Tillamook Bay jetty, 1914-1972 .....	25
<b>Figure 2-23.</b>	Historical shoreline positions identified adjacent to the mouth of Tillamook Bay in the Rockaway littoral cell .....	26
<b>Figure 2-24.</b>	Historical shoreline positions identified at the southern end of the Rockaway littoral cell near the Cape Meares community .....	27
<b>Figure 2-25.</b>	The breach of Bayocean Spit on November 13, 1952 .....	28
<b>Figure 2-26.</b>	Historical shoreline positions identified near Twin Rocks .....	28
<b>Figure 2-27.</b>	Historical shoreline positions at Manzanita .....	29
<b>Figure 2-28.</b>	Alongshore beach volume changes derived from an analysis of available lidar data for the period 1997–2002 .....	30
<b>Figure 2-29.</b>	The Rockaway cell beach monitoring network maintained by DOGAMI showing the measured changes in the position of the dune toe from 1997 to 2014. ....	31
<b>Figure 3-1.</b>	Foredune erosion model and the geometric model used to assess the maximum potential beach erosion in response to an extreme storm. ....	33
<b>Figure 3-2.</b>	Maximum potential erosion ( $R_{\infty}$ ) due to a change in water levels. ....	35
<b>Figure 3-3.</b>	Location map of NDBC (black) and CDIP wave buoys, tide gauges, and GROW wave hindcast stations .....	37
<b>Figure 3-4.</b>	Daily tidal elevations measured at Southbeach, Newport on the central Oregon coast .....	38
<b>Figure 3-5.</b>	Seasonal cycles in monthly-mean water levels based on data from the combined Southbeach/Garibaldi measured tides .....	39
<b>Figure 3-6.</b>	Projections of future sea level rise for the central Oregon coast .....	41
<b>Figure 3-7.</b>	Example cross-section established adjacent to Camp Winema in the Neskowin cell showing recent RTK-DGPS surveys and measurements from 1997, 1998, and 2009 lidar data. ....	44
<b>Figure 3-8.</b>	Storm-wave-damaged riprap structure in Neskowin, January 2008, and rip embayment at Shorewood RV park, Twin Rocks .....	46
<b>Figure 4-1.</b>	Modeled erosion hazard zones for Neskowin showing 83 scenarios of change .....	48
<b>Figure 4-2.</b>	Plot showing the difference between calculating total water levels using the Allan and Priest (2001) deterministic approach versus total water levels calculated using a combined wave/tide time series approach for a range of beach slopes .....	50
<b>Figure 5-1.</b>	New dune-backed hazard zones for Neskowin .....	58
<b>Figure 5-2.</b>	New dune-backed hazard zones for Tierra Del Mar .....	59
<b>Figure 5-3.</b>	New dune-backed hazard zones for Rockaway Beach .....	60

## LIST OF TABLES

<b>Table 2-1.</b> Average uncertainties for Pacific Northwest shorelines .....	11
<b>Table 3-1.</b> Relative sea level rise (SLR) values for the north-central Oregon coast for low, medium, and high hazard zone scenarios ...	42
<b>Table 3-2.</b> Summary of the estimated erosion associated with sea level rise .....	42
<b>Table 4-1.</b> Calculated erosion distances determined for Tillamook County using the geometric model. ....	47
<b>Table 4-2.</b> Summary statistics of the width of the calculated hazard zones based on all Tillamook profiles .....	49
<b>Table 4-3.</b> Hazard characteristics calculated for each subcell .....	51
<b>Table 4-4.</b> Worst-case erosion distances calculated using the geometric model assuming a sudden land level drop after a Cascadia subduction zone (CSZ) earthquake causing relative sea level (aka $T_{wl}$ ) to rise along with a worst-case storm-induced erosion (geometric foredune erosion) and SLR rise .....	52
<b>Table 4-5.</b> Maximum K&D erosion distance calculated for each subcell from Allan and others (2013) as described in Section 3.2.2 ...	53
<b>Table 4-6.</b> Estimates of uncertainty due to variations in the beach slope and its effect on the calculated widths of the erosion hazard zones. ....	54
<b>Table 5-1.</b> Summary of erosion distance characteristics for Tillamook County .....	56
<b>Table 5-2.</b> Summary of erosion distance characteristics for each recommended hazard zone by subcell .....	56

## GEODATABASE AND SPREADSHEET INCLUDED WITH DIGITAL PUBLICATION

**TillamookCountyErosionHazardZonesDatabase.gdb** is an Esri® ArcGIS® version 10.1 geodatabase:

Feature class, polygons: TillamookCountyHazardZones\_Active\_Allan\_Priest\_2001  
 Feature class, polygons: TillamookCountyHazardZones\_BluffBacked\_Allan\_Priest\_2001  
 Feature class, polygons: TillamookCountyHazardZones\_DuneBacked  
 Feature class, polylines: TillamookCountyHazardZones\_DuneBacked\_AllScenarios  
 Feature class, polylines: TillamookCountyHazardZones\_Kreibel\_and\_Dean  
 Feature class, polylines: TillamookCountyHazardZones\_LandwardEj

*See metadata embedded in geodatabase for more information.*

**TillamookErosionHazardZonesData2014.xlsx** is a Microsoft® Excel® spreadsheet listing morphology parameters and erosion distances at each dune-backed transect along the Tillamook County shoreline.





## EXECUTIVE SUMMARY

This report describes and documents a range of coastal erosion hazards zones determined for the Tillamook County coastline, which may be used for general hazard planning purposes. The hazard zones were determined using two approaches:

- A storm-induced erosion distance was first determined using a geometric model (Komar and others, 1999), whereby property erosion occurs when the total water level ( $T_{WL}$ ) produced by the combined effect of extreme wave runup ( $R$ ) plus the tidal elevation ( $T$ ), exceeds the elevation of the beach-dune juncture ( $E_j$ ); the latter parameter effectively distinguishes the seaward toe of the dune or a coastal engineering structure. On average, the storm-induced erosion contributes ~10 m (10% event) to 79 m (1% event, 33 to 258 ft) to the overall erosion distances identified in Tillamook County.
- Erosion due to the projected future increase in sea level was calculated using a Bruun (1962) model. The latter was accomplished for a suite of sea level rise (SLR) projections (high, middle, and low) at the year 2030, 2050, and 2100 time frames. Results from the Bruun modeling indicated that the projected erosion ranged from negligible at 2030 to as much as 94 m (308.4 ft) by 2100.

The final derived hazard zones reflect the combined effect of both sets of processes.

Processes driving coastal change are exceedingly complex, making future predictions of erosion challenging. With that in mind, 83 scenarios of future coastal change were developed: 81 scenarios were developed using three beach-dune juncture elevations ( $E_j$ ), three  $T_{WL}$ s, and SLR projections for 2030, 2050, and 2100; two other scenarios incorporate the effects of regional subsidence due to the occurrence of a Cascadia subduction zone (CSZ) earthquake and the effects of a single storm. From modeled beach and dune erosion data we identified six scenarios (out of the suite of 81) for the purposes of defining future erosion hazard zones for the dune-backed beaches of Tillamook County. The recommended zones include:

- A **High** hazard zone (Hhz), which includes a **2%  $T_{WL}$**  and a **medium SLR** projected for 2030. In this scenario the final designated hazard zone was found to range from a mean of 43 to 60 m (140 to 196 ft), varying between the Tillamook County sublittoral cells due to differences in beach morphologies and calculated  $T_{WL}$ s;
- A **Medium** hazard zone (Mhz), which includes a **2%  $T_{WL}$**  and a **medium SLR** projected for 2050. In this scenario the designated hazard zone was found to range from 52 to 72 m (170 to 236 ft).
- A **Low 1** hazard zone (Lhz1), which includes a **1%  $T_{WL}$**  and **medium SLR** projected for 2100. In this scenario the designated hazard zone was found to range from 79 to 108 m (259 to 354 ft).
- A **Low 2** hazard zone (Lhz2), which includes a **1%  $T_{WL}$**  and **high SLR** projected for 2100. In this scenario the designated hazard zone was found to range from 125 to 171 m (410 to 561 ft).
- A **Low 3** hazard zone (Lhz3), which provides a worst-case future scenario, which may be of value to coastal communities when planning well into the future. It includes a **1%  $T_{WL}$** , **high SLR** projected for 2100, and erosion due to subduction from a CSZ earthquake. In this scenario the designated hazard zone was found to range from 175 to 228 m (574 to 748 ft).

A sixth hazard zone was defined using a technique developed by Kriebel and Dean (1993) to account for the fact that storms are rarely capable of fully eroding a dune (as predicted by the geometric model) due to their limited storm duration. Overall, the Kriebel and Dean approach yielded generally narrower hazard zones (~up to 22 m [72 ft] wide) for Tillamook County. Because the Oregon coast rarely experiences a single event over an entire winter season, *the actual degree of erosion associated with a major storm(s) is likely to span the spectrum between the duration-limited storm-induced erosion calculated using Kriebel and Dean and the maximum potential erosion ( $DE_{MAX}$ ) defined using the geometric model.* From our modeling, we argue that the Kriebel and Dean model is suitable for defining the minimum width of a coastal erosion setback zone for Tillamook County, while the other five hazard zones provide more conservative calculations of future erosion potential.

## 1.0 INTRODUCTION

The Oregon Department of Geology and Mineral Industries (DOGAMI) was commissioned to develop an updated suite of coastal erosion hazard zones for Tillamook County, Oregon, using improved methodologies for modeling dune-backed beach erosion and incorporating up-to-date information on ocean water levels and waves, topographic change data, and recent projections of future regional sea level changes. The ultimate purpose of these maps is to assist the County and the cities within Tillamook County in dealing with existing and future property and infrastructure needs along a coastline that is subject to risks from coastal erosion hazards.

Coastal communities located along the coast of Oregon are increasingly under threat from a variety of natural hazards, including coastal erosion hazards due to the occurrence of major storms, long-term sea level rise, landslides, earthquakes, and potentially catastrophic tsunamis generated by the Cascadia subduction zone (CSZ). Over time, community risk from hazards is increasing, in part due to the degree of development that has occurred along the coast in recent decades and in part by planning and land-use development practices that have not fully considered geologic hazards (Allan and others, 2009). In particular, the local geology and geomorphology of the coastline restricts development to low-lying areas, chiefly along dunes and barrier spits, or along the coastal bluffs and steep sides of coastal hills, which are directly impacted by the intensification of the erosion processes that drive coastal change and, ultimately, beach and bluff erosion.

Beaches and dunes are particularly susceptible to the occurrence of large storms coupled with high ocean water levels. Along the Tillamook County coast, coastal erosion hazards have been especially acute over the past decade due to the occurrence of multiple storm events, coupled with the occurrence of the 1997-1998 El Niño. Collectively, such events have resulted in extensive erosion in several communities (e.g., Neskowin, Tierra Del Mar, and Rockaway), resulting in the proliferation of coastal engineering structures in order to protect back-shore properties from the erosion hazard. Due to the prevalence of sandy beaches and dunes along the Tillamook County coast and projected regional increases in sea level, coastal erosion in the county will almost certainly increase in the future (NRC, 2012). Coastal

erosion in response to an abrupt lowering of the coast during a great earthquake on the CSZ will be especially significant, effectively raising local sea level instantaneously and initiating massive coast-wide changes as the coast adjusts to the new level.

Following the establishment of a new coastal field office in Newport, Oregon, in 2000, DOGAMI was commissioned by Tillamook County to develop coastal erosion hazard zones spanning various time frames for the entire county (Allan and Priest, 2001). The past decade has seen considerable improvements in the methods used to derive erosion hazard zones on dune-backed beaches (Baron, 2011), as well as the collection of more up-to-date information on ocean water levels and waves (Ruggiero and others, 2010; Allan and others, 2011), topographic change data (Allan and Hart, 2008; Allan and Harris, 2012), and recent projections of future regional and global sea level changes (NRC, 2012). These new data and findings are the reason for developing new maps that contain up-to-date coastal information and erosion hazard zones in Tillamook County.

The development of coastal erosion maps is complicated due to a dependence on many factors (oceanographic, atmospheric, and geologic) that combine to influence the coast at some point in the future. These factors include the beach sediment budget (the availability of sediment supply and losses), the incident wave energy particularly during storms, variations in ocean water levels, nearshore bathymetry, shoreline orientation, the presence of coastal engineering structures, and the geology of the region, combinations of which ultimately determine the shape of a beach and, importantly, whether the beach will erode or accrete. Because of the challenges with modeling coastal change and the volume of data necessary to calibrate more sophisticated models that try to account for sediment transport physics (as summarized by Komar and others, 1991a), the approach adopted here is based on a simple fore-dune erosion model originally proposed by Komar and others (1999) and Ruggiero and others (2001). This is essentially the same approach used in the original study by Allan and Priest (2001), but updated to reflect the following enhancements:

- The new modeling involves a fully probabilistic approach based around 27 scenarios of potential forcing conditions (including the effects of projected future sea level increases and a worst-case



Cascadia earthquake scenario). This contrasts with the deterministic approach used by Allan and Priest (2001), which involved three scenarios of future storm-induced erosion.

- The addition of two new (2009 and 2011) high-resolution lidar flights of the Oregon coast, used to measure and document the state of the beach and adjacent backshore.
- Integration of beach morphology results derived from repeat Real-Time Kinematic Differential Global Positioning System (RTK-DGPS) surveys of selected areas of the Tillamook County coast.
- New coastal nearshore hydraulic modeling of the Tillamook County coastline for the purposes of defining new Federal Emergency and Management (FEMA) coastal flood insurance rate maps (Allan and others, coastal flood insurance study, Tillamook County, Oregon unpub. data, 2014).

To facilitate mapping up-to-date erosion hazard zones in Tillamook County, we proposed to undertake the following tasks:

1. Evaluate previous mapping approaches (e.g., the geometric model versus other techniques) used to identify and map coastal erosion hazards along both dune- and bluff-backed coastal sections;
2. Evaluate existing map products (e.g., active hazard zone, high-hazard, etc.) in order to better define the number of coastal erosion hazard zones that will best assist coastal planners with their day-to-day activities. For example, new erosion hazard maps may be better aligned with future projections of sea level rise such that they target specific time periods (e.g., 2030, 2050, and 2100). However, implementing this approach may be challenging when dealing with mapping similar zones along coastal bluffs. Other important questions that need to be addressed include whether coastal managers would prefer a single line for each period of interest, multiple lines that encompass uncertainty bands, or both. For this task, DOGAMI worked with DLCD and the Tillamook County Planning Department to identify an approach to display analysis results in a way most suitable for local land use planning applications;
3. Acquire the necessary data to be used to implement the development of new coastal erosion hazard zones for Tillamook County. For the updated maps, we performed the following tasks:

- a. Evaluate all existing lidar data sets (1997, 1998, 2002, 2009, 2010, and 2011) flown previously in order to define the necessary morphological parameters (i.e., the beach slope and beach-dune juncture elevation) that are used to model future erosion hazard zones;
  - b. Evaluate the variability in the morphology of the beach in order to document the effect (uncertainty) on hazard zones;
  - c. Use the Stockdon and others (2006) empirical runup model to define the total water levels ( $T_{wLs}$ ) that are ultimately used to model future erosion hazard zones. This latter model is a refined version of the model developed by Ruggiero and others (2001) and has been thoroughly tested on a wide range of beach conditions;
  - d. Incorporate climate change effects associated with future sea level rise (SLR) in modeling future erosion hazard zones. Here we proposed to model the erosion response due to SLR by calculating the degree of erosion using the Bruun (1962) model based on the mean and maximum SLR values identified in the NRC (2012) study. Specifically, we proposed to model SLR erosion based on the following projections:
    - Mean: +0.07 m (+0.23 ft) by 2030, +0.17 m (+0.56 ft) by 2050, and +0.63 m (+2.1 ft) by 2100.
    - Maximum: +0.23 m (0.75 ft) by 2030, +0.48 m (1.57 ft) by 2050, and +1.42 m (4.66 ft) by 2100.
  - e. Undertake probabilistic analyses of the total water levels ( $T_{wLs}$ ) for a wide range of conditions in order to assess the erosion response.
4. Develop a report detailing the methods used and results.

This report documents the approaches taken to model coastal erosion hazards in Tillamook County, Oregon. The investigation is not intended for use as a site-specific analysis tool but may be used by local governments within Tillamook County to address and plan for coastal hazards. This study did not re-evaluate bluff erosion hazards for Tillamook County. As a result, the map layers developed originally by Allan and Priest (2001) remain unchanged, while new erosion hazard zones are developed for the dune-backed beaches.

The report first examines, in Section 2, the coastal geology and geomorphology of the Tillamook County shoreline, including a discussion of the erosion history of the coast. The results presented in this section provide context for understanding future erosion hazard zones presented in this study.

Section 3 presents the data and methods used to derive erosion hazard zones for the dune-backed beaches of Tillamook County. Two models of foredune erosion used to define the future erosion hazard zones are presented and discussed. Section 3 includes an examination of the ocean and beach parameters used in the modeling process. Finally, Section 3 describes the scenarios taken to draft new erosion hazard zones for the dune-backed sections of the Tillamook County shoreline.

Section 4 presents projected coastal erosion hazard zones and discusses the variations and uncertainty in the calculated erosion hazard zones.

Finally, Section 5 discusses and summarizes the recommended hazard zones along with possible applications for their use within the Tillamook County Hazard Mitigation Plan.

## 2.0 STUDY AREA

Tillamook County is located on the northwest Oregon coast, between latitudes 45°45'49.49"N (Cape Falcon) and 45°3'54.88"N (Cascade Head), and longitudes 124°1'15.57"W and 123°17'59.88"W. The terrain varies from low-elevation sandy beaches and dunes on the coast to elevations up to 1,130 m [3,706 ft] farther inland. The coastal strip is approximately 104 km long and varies in its geomorphology: broad, gently sloping sandy beaches backed by dunes, beaches backed by engineered structures, cobble and boulder beaches adjacent to the headlands, and bluff shorelines. Prominent headlands formed of resistant basalt (e.g., Cascade Head, Cape Meares, Cape Lookout, and Neahkahnie Mountain) provide natural barriers to alongshore sediment transport (Komar, 1997), effectively dividing the

county coastline into four littoral cells (Figure 2-1). (A littoral cell is a headland bounded stretch of coast that traps sediment to within its confines. As a result, sand transport is contained within the cell, with limited or no sand exchange between adjacent littoral cells.) The four cells are:

- Neskowin littoral cell, which extends from the north side of Cascade Head to Cape Kiwanda. This particular shore section includes the communities of Neskowin, North Neskowin, and Pacific City.
- Sand Lake littoral cell, which extends from Cape Kiwanda north to Cape Lookout. This section includes the community of Tierra Del Mar.
- Netarts littoral cell, which extends from Cape Lookout to Cape Meares. This section includes Cape Lookout State Park and the communities of Happy Camp (Netarts), Oceanside, and Short Sand Beach.
- Rockaway littoral cell, which extends from the north side of Cape Meares to Neahkahnie Mountain in the north. This section includes the communities of Cape Meares, Twin Rocks, Rockaway, Nedonna Beach, Nehalem State Park, and Manzanita.

Each of these cells is further broken up into a series of subcells due to the presence of five estuaries (in order from south to north, Nestucca, Sand Lake, Netarts, Tillamook, and Nehalem), two of which (Tillamook and Nehalem) are bounded by prominent jetties. The county also is characterized with several major rivers (Nestucca, Nehalem, Miami, Tillamook, Trask, Kilchis, and Wilson Rivers) that terminate in the estuaries. Due to their generally low flows and the terrain, these rivers carry little beach sediment out to the open coast today; instead, they deposit most of their sediment in the estuaries. Hence, the coastal beaches of Tillamook County receive very little sediment today other than from erosion of the backshore (Allan and others, unpub. data, 2014).

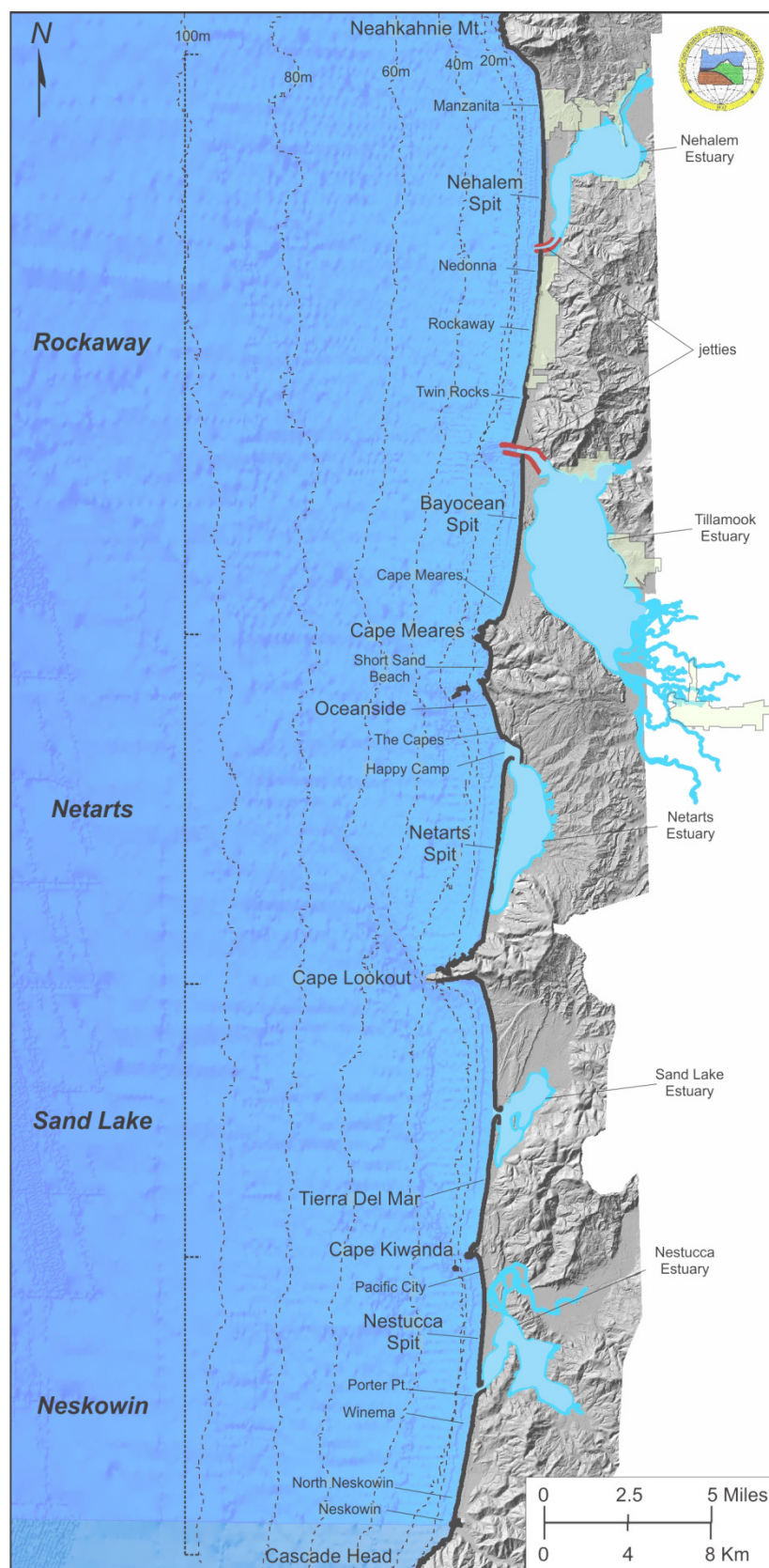


**Figure 2-1.** Location map of Tillamook County coastline (Allan and others, unpub. data, 2014). Littoral cells are labeled on the left-hand side of the figure..



## 2.1 Coastal geomorphology

On the basis of geology and geomorphology the Tillamook County shoreline can be broadly divided into five morphological beach types (Allan and others, unpub. data, 2014). These are:

**Dune-backed beaches:** Dune-backed beaches make up the bulk (50.9%) of the Tillamook County shoreline, much of which is associated with barrier spits (e.g., Nestucca, Sand Lake, Netarts, Bayocean, and Nehalem spits). The geomorphology of the beaches can be generalized as wide, dissipative surf zones with low-sloping foreshores that are backed by high dunes containing significant sand volume (Figure 2-2). Dune crest elevations reach their highest peak along Bayocean Spit (39 m [128 ft]) and Netarts Spit (25 m [82 ft]) (Figure 2-3). However, these dunes reflect ancient parabolic dunes that are now being truncated by wave erosion. Dune crest elevations are generally lowest in the Rockaway subcell (Twin Rocks, Rockaway, and Nedonna Beach) (Figure 2-1). Along the length of the county, mean dune crest heights are 10.5 m (35.5 ft), with most dune crest heights in the range of 5 to 16 m (16 to 54 ft). The average beach slope ( $\tan \beta$ ) for dune-backed beaches is summarized in Figure 2-4, where it is apparent that slopes vary significantly along the coast, with the lowest mean slopes occurring near Oceanside (mean  $\tan \beta = 0.032$ ), and are generally steepest in the Neskowin littoral cell (mean  $\tan \beta = 0.06$ ).

**Cliffed shore:** Cliffed shores make up the second largest (30.5%) geomorphic type in the county (Figure 2-5). Examples of this type of shore exist around each of the major headlands. This particular shore type consists of near-vertical cliffs that plunge into the ocean. In some cases, the cliffs may be fronted by rock platforms and/or talus.

**Bluff-backed beaches:** Bluff-backed beaches fronted by a wide, dissipative sand beach are the third most prominent geomorphic type in Tillamook County, comprising approximately 14.3% of the shore (Figure 2-6). This particular geomorphic type dominates the shoreline near Oceanside and Short Sand Beach, south

of Cape Lookout, the south end of Cape Lookout State Park, north of Cape Kiwanda and south of Tierra Del Mar, and adjacent to the mouth of Nestucca Bay. The bluffs that back the beaches vary in height from ~7 m (23 ft) to greater than 50 m (164 ft). Beach slopes ( $\tan \beta$ ) seaward of the bluffs are similar to those observed throughout Tillamook County, averaging about 0.037 ( $\sigma = 0.009$ ). Geomorphically, these beaches may be characterized as “composite” using the terminology of Beaulieu (1973) and Jennings and Shulmeister (2002). Such beaches consist of a wide dissipative sandy beach, backed by a steeper upper foreshore composed of gravels. In addition, several of the bluff-backed sections (e.g., Manzanita and Oceanside) are characterized by well-vegetated faces, indicating that they have not been subject to significant wave erosion processes along the toes of the bluffs.

**Bluff-backed beaches fronted by gravel and sand:** This particular geomorphic type makes up approximately 3.3% of the Tillamook County shoreline and is prevalent on the south side of Neahkahnie Mountain (north of Manzanita), immediately north of Cape Meares, Short Sand Beach, and immediately north of Cape Lookout. The overall morphology is essentially the same as described for bluff-backed beaches except for the presence of a gravel berm along the toes of the bluffs.

**Gravel/boulder berm fronted by sand:** In the community of Cape Meares (south end of Bayocean Spit; Figure 2-1), a substantial gravel/boulder beach abuts the Cape Meares headland, where it forms a prominent, steep natural barrier to wave erosion (Figure 2-7). The berm is approximately 0.8 km long. Crest elevations of the gravel/boulder berm reach a maximum of 8.7 m, while the mean crest elevation is 6.7 m. The slope of the gravel/boulder berm is steep (mean  $\tan \beta = 0.187$  ( $\sigma = 0.060$ )), while the sand beach has a mean slope of 0.047, which is typical of much of the Tillamook County coast. Flotsam extends a significant distance landward of the crest of the berm, indicating that this stretch of shore is subject to frequent wave overtopping and inundation.



**Figure 2-2.** Looking north along Bayocean spit, with the Tillamook jetties (Tillamook Bay to the right), Rockaway just north of the jetties, Nehalem Spit, and Neahkahnie Mountain in the far distance [photo: E. Harris, DOGAMI, 2011].

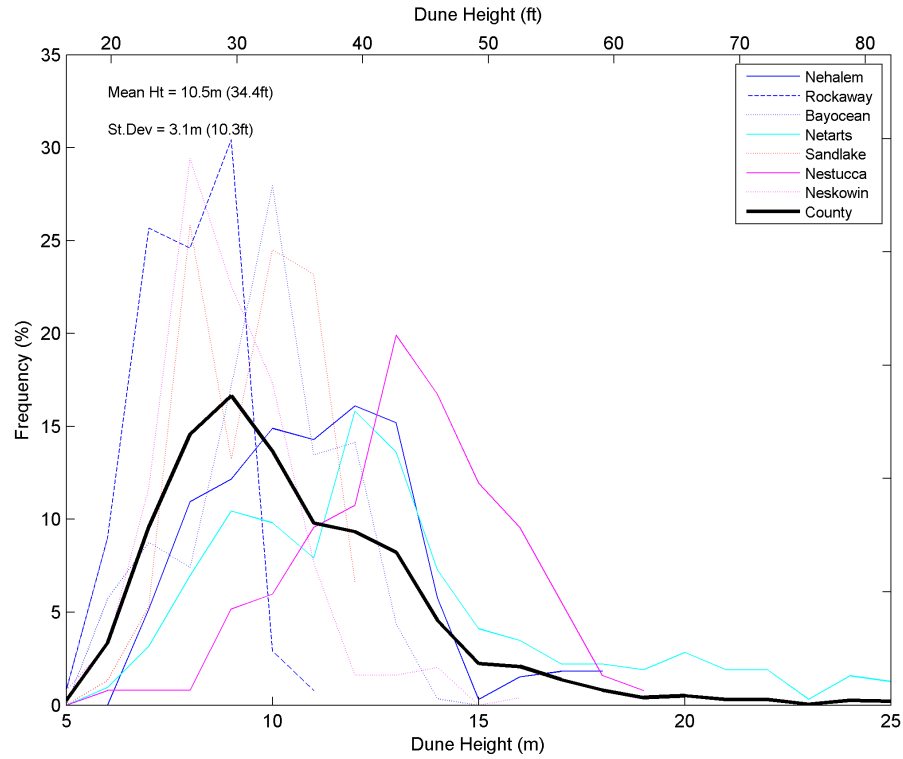


**Figure 2-3.** Tillamook County dune crest elevations (data from Allan and Harris, 2012).

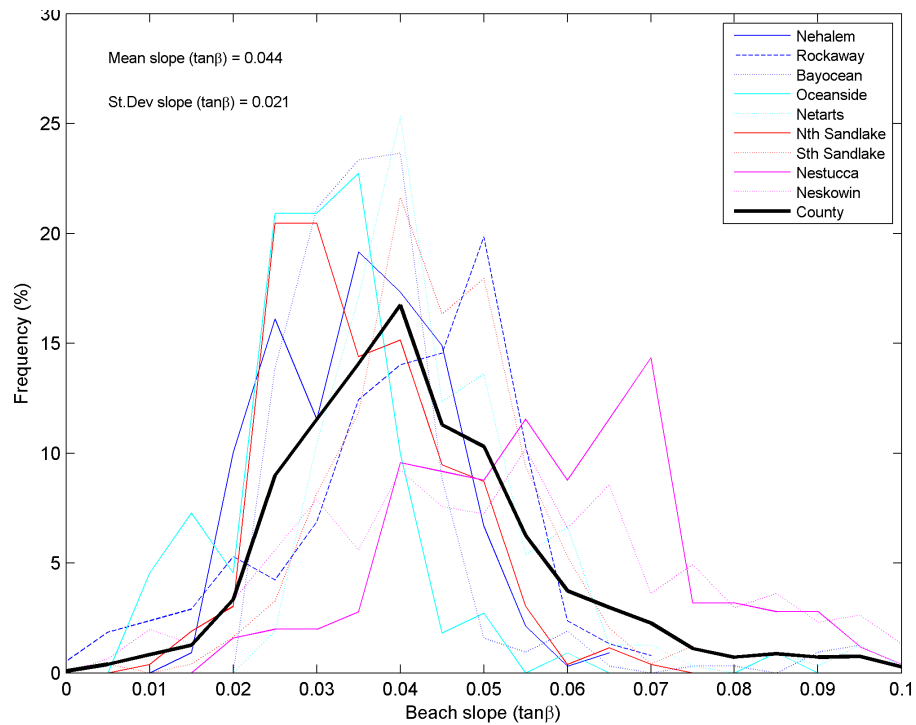


**Figure 2-4.** Tillamook County beach slopes (data from Allan and Harris, 2012).





**Figure 2-5.** View is looking east toward Neahkahnie Mountain. U.S. Highway 101 can be seen around mid photo tracking along the mountain. To the right and along the toe of the cliff is an extensive gravel/boulder berm that has formed as a result of rockfalls and landslides off the headland. (Photo: L. Stimely, DOGAMI, 2011)



**Figure 2-6.** Coastal bluffs of the Astoria Formation characterize much of the shore north of Sand Lake. Note the presence of cobbles to the left of the photo, which serve to protect the bluff toe. View is looking south toward Cape Kiwanda in the distance. (Photo: J. Allan, DOGAMI, 2011)



**Figure 2-7.** An extensive gravel/boulder berm that backs a dissipative sand beach in the Cape Meares community. View is looking south toward the Cape Meares headland. An exposed tree stump located in situ is exposed due to lowering of the sand beach following late winter storms. (Photo: J. Allan, DOGAMI, 2008)

## 2.2 Historical shoreline change and coastal erosion

This section presents a qualitative discussion of large-scale morphological changes derived from analyses of historical and contemporary shorelines along the Tillamook County coastline. This summary stems from work undertaken by researchers at DOGAMI and Oregon State University (OSU) over the past two decades (Preist and others, 1993; Allan and Priest, 2001; Allan and others, 2003; Allan and Hart, 2007, 2008; Allan and Harris, 2012; Allan and Stimely, 2013; Ruggiero and others, 2013).

Historical shoreline positions have been derived from a variety of sources including National Ocean Service (NOS) Topographic (T)-sheets (Allan and Priest, 2001), 1967 digital orthophotos (Ruggiero and others, 2013), 1980s era U.S. Geological Survey topographic maps, 1994 digital orthophotos, and from 1997, 1998, 2002, 2009, and 2012 lidar data (Allan and Priest, 2001; Allan and others, unpub. data, 2014). Pre-lidar historical

shorelines use the High Water Line (HWL) as a shoreline proxy. The HWL has been used by researchers for more than 150 years because it could be visually identified in the field or from aerial photographs. In contrast, shorelines derived from lidar data are datum based and can be extracted objectively using a tidal datum, such as Mean High Water (MHW) or Mean Higher High Water (MHHW). Studies by Moore (2000) and Ruggiero and others (2003) noted that HWL-type shoreline proxy are virtually never coincident with datum-based MHW-type shorelines. In fact, they are almost universally estimated to be higher (landward) on the beach profile when compared to MHW shorelines (Ruggiero and others, 2013). According to Ruggiero and others, the average absolute horizontal offset between the HWL and MHW ranges from ~6 m (~19 ft) to as much as 50 m (164 ft), while the average is typically less than 20 m (65 ft). Offsets are typically greatest on flat, dissipative beaches where the wave runup may be large and smallest where beaches are steep (e.g., gravel beaches).



Estimates of the uncertainty of HWL shoreline measurements have been assessed in a number of studies (e.g., Moore, 2000; Ruggiero and others, 2013). These uncertainties reflect the following errors: 1) mapping methods and materials for historical shorelines (including the offset between the HWL and MHW shoreline), 2) the registration of shoreline positions relative to Cartesian coordinates, and 3) shoreline digitizing. Uncertainties are summarized in Table 2-1.

**Table 2-1.** Average uncertainties for Pacific Northwest shorelines (Ruggiero and others, 2013).

	<b>Total Shoreline Position Uncertainty</b>	
NOS T-sheets (1800s to 1950s)	18.3 m	60 ft
DRGs (1940s to 1990s)	21.4 m	70 ft
Aerial photography (1960s to 1990s)	15.1 m	50 ft
Lidar	4.1 m	14 ft

Shorelines measured by DOGAMI staff using Real-Time Kinematic Differential Global Positioning System (RTK-DGPS) surveys of the beach are also available for two of the littoral cells: Neskowin and Rockaway (Allan and Hart, 2007, 2008). These data sets provide the most up-to-date assessments of the changes taking place within these two littoral cells on the Tillamook County coast. These data have been collected since 2004 in order to document the seasonal to interannual variability in shoreline positions along the coast. In all cases, the GPS shorelines reflect measurements of the Mean Higher High Water (MHHW) line located at an elevation of 2.3 m (7.5 ft). We have relied on the MHHW rather than the Mean High Water (MHW) line, as previous studies (e.g., Ruggiero and others, 2003) indicated that MHHW most closely approximates the MHW line surveyed by early NOS surveyors. GPS shoreline positioning errors, a function of the orientation of the GPS receiver relative to the slope of the beach, are estimated to be  $\sim\pm 0.1$  to  $\pm 0.2$  m ( $\pm 0.3$  to  $\pm 0.6$  ft).

The approach adopted here is to describe the broad morphological changes identified along the coast, beginning in the south at Neskowin, and progressing northward toward Cape Falcon.

### 2.2.1 Neskowin cell

At Neskowin, historical shoreline positions reveal little systematic pattern—all of the identified shorelines fall within a few hundred feet of one another (Figure 2-8). Many of the shorelines reveal the presence of large embayments along the coast indicative of the formation of rip currents that can result in highly localized hotspot erosion (e.g., the April 2013 shoreline in Figure 2-8). Along much of the southern half of the cell, the 1920s era shoreline tends to track landward of the other shorelines. This suggests that beach conditions in the 1920s reflected an eroded state following a period of large storm events. Erosion appears to have dominated much of the early existence of the Neskowin community. Probably the most significant storm on record occurred in January 1939. This storm affected much of the Oregon coast and caused major coastal flood hazards and significant erosion problems. Figure 2-9 provides an example of the damage sustained in Neskowin. One home had its foundation eroded from under it, which resulted in the house collapsing onto the beach. Within a decade, however, this process had effectively reversed itself, with much of the shore now having been rebuilt as sand migrated back on to the beach. This cycle of erosion followed by accretion is typical of shoreline changes on the Oregon coast. The 1967, 1980s era, and 1994 shorelines represent the most seaward extent of the shoreline, implying that significant accretion had occurred adjacent to Neskowin during those years, while the early 1960s, the 1982-1983 El Niño winter, and the storms of the late 1990s represent eroded states.

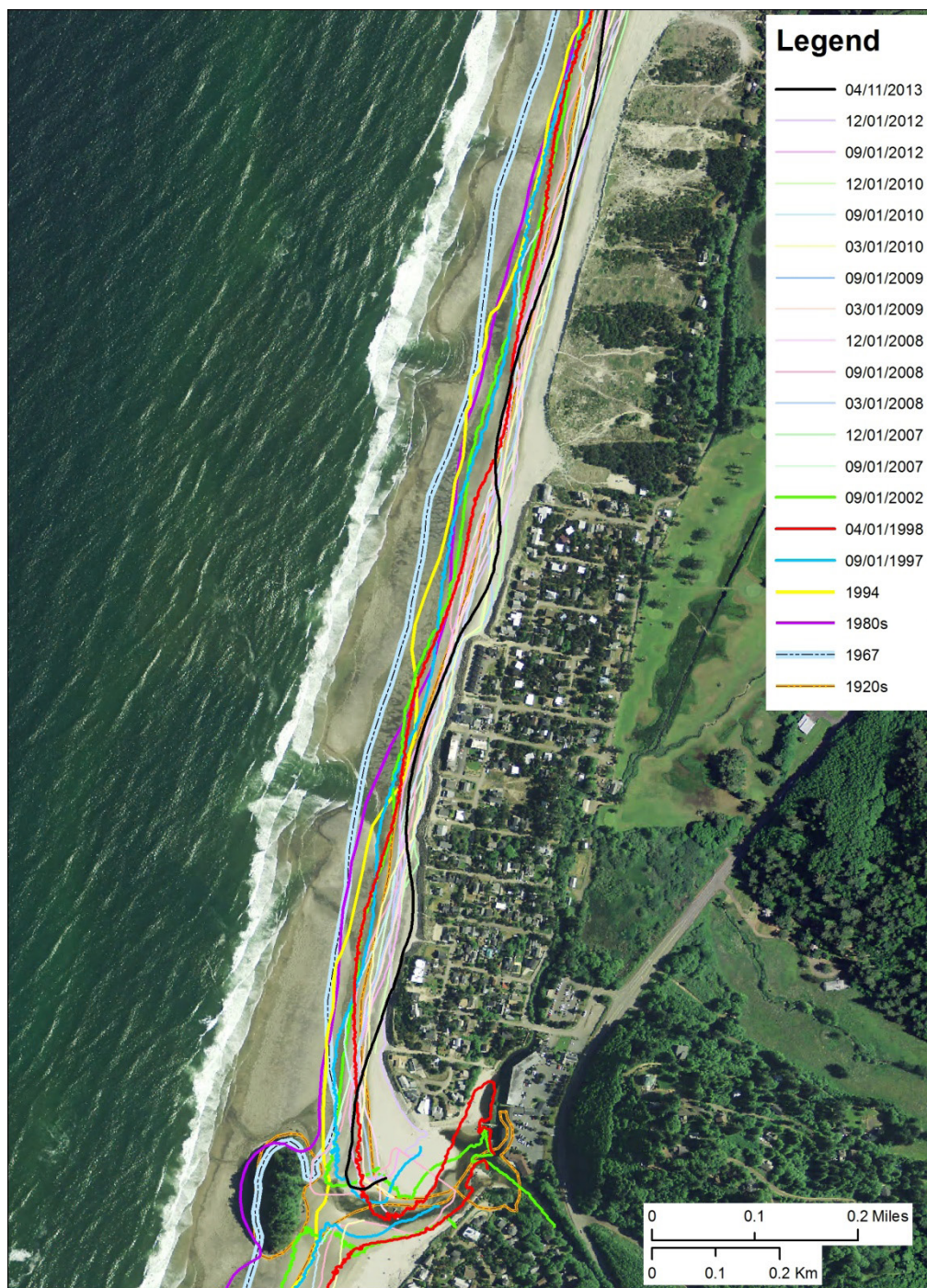


**Figure 2-8.** Historical and contemporary shoreline positions identified at Neskowin. The 1920s (1927/1928) shoreline is derived from NOST T-sheets, 1967 and 1994 shorelines are from orthorectified aerial photographs, 1980s (1985/1986) shorelines are from U.S. Geological Survey topographic maps, 1997–2002 shorelines are derived from lidar, and post 2007 shorelines were measured using GPS.



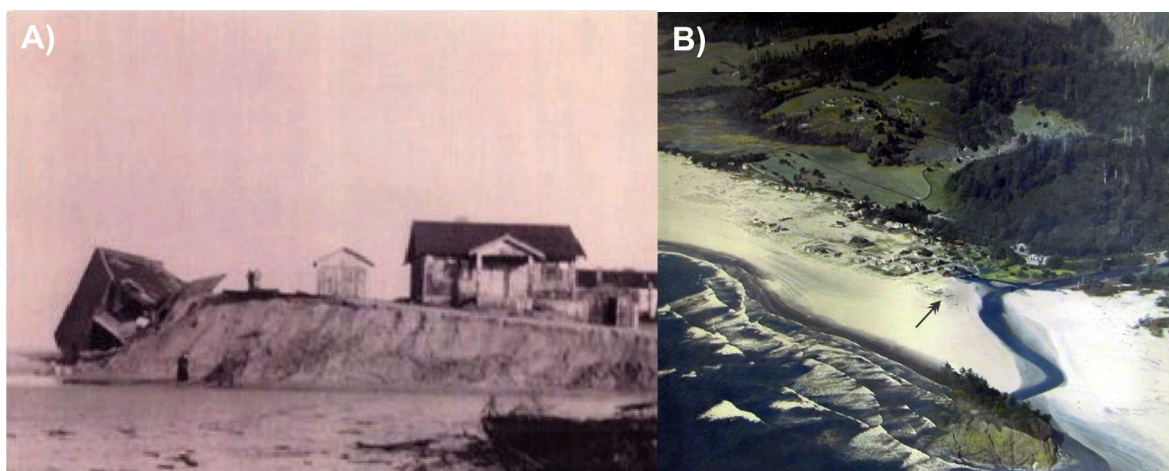


**Figure 2-9.** A) Erosion at Neskowin (adjacent to the juncture between Neskowin and Hawk creeks) following the January 1939 storm; B) Rebuilding of the sandy beach at Neskowin in 1949. The arrow indicates the approximate position of the erosion shown in A). (Photos courtesy of Neskowin community archives.)

Following the major storms of the late 1990s, erosion hazards in the community of Neskowin reached acute levels (Allan and others, 2003; Allan and Hart, 2007), with the beach and dune having eroded landward some 50 m (~150 ft) (Figure 2-10). Property owners responded to the hazard by installing riprap along much of the shore north of Proposal Rock. As of 2014, virtually the entire length of the community of Neskowin is hardened with riprap. Monitoring of the beaches in Neskowin by DOGAMI indicates that the beaches have not fully recovered from the storms of the late 1990s (several areas have continued to erode), such that the beaches today are narrower and have much less sand volume compared with the same beaches in the mid-1990s (Allan and Hart, 2008). Long-term erosion rates derived by Ruggiero and others (2013) indicate that the beaches of Neskowin have some of the highest rates of retreat in the state. Due to their narrow beaches and lack of sand volume, the community of Neskowin today remains at high risk of being affected by large winter storms and from ocean flooding.

With progress north along the Neskowin coast, the 1994 shoreline tends to track well seaward of the other shorelines. This suggests a period of accretion and was most noticeable adjacent to Porter Point near the

mouth of Nestucca Bay (~transect 8 in Figure 2-10). The pattern of accretion appears to be consistent with a general decline in wave energy and storm incidence observed during the early part of the 1990s (Allan and Komar, 2000). However, recent GPS surveys of this section of the coast by DOGAMI staff indicate a reversal from accretion back to erosion, with the shoreline having now retreated almost back to the toe of the marine cliffs that back the beach.

Along Nestucca spit (Figure 2-11) the spit tip and bay mouth have remained predominantly in the south, with some evidence of a northward migration in 1998. From the suite of shorelines available to us, the Nestucca spit tip has ranged over a distance of about 340 m (~1,120 ft) between 1927 and 2008 and was at its most southerly position in 2008. Following the 1997-1998 El Niño, the spit tip migrated northward, probably in response to a change in wave direction that is typical of El Niño events (e.g., Komar, 1986). Of interest also is the presence of a large bulge identified by the 1980s shoreline on the eastern side of the spit (Figure 2-11). This feature is remnant from when the spit was breached during a major storm in February 1978 (see Figure 6.15 of Komar, 1997).



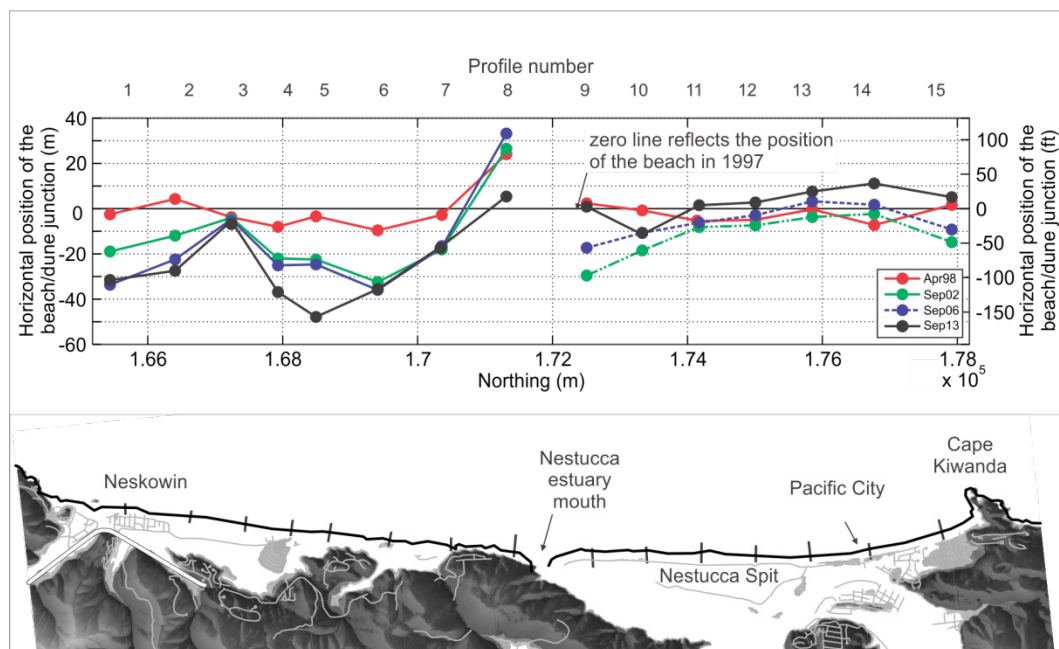


**Figure 2-10.** Positional changes in the beach/dune toe (elevation of 6 m) along the Neskowin cell between 1997 and 2013 derived from lidar data and RTK-DGPS measured surveys of the beach. Circles and numbers correspond to the locations of the Neskowin beach monitoring network established by DOGAMI in 2006 (after Allan and others, 2009).

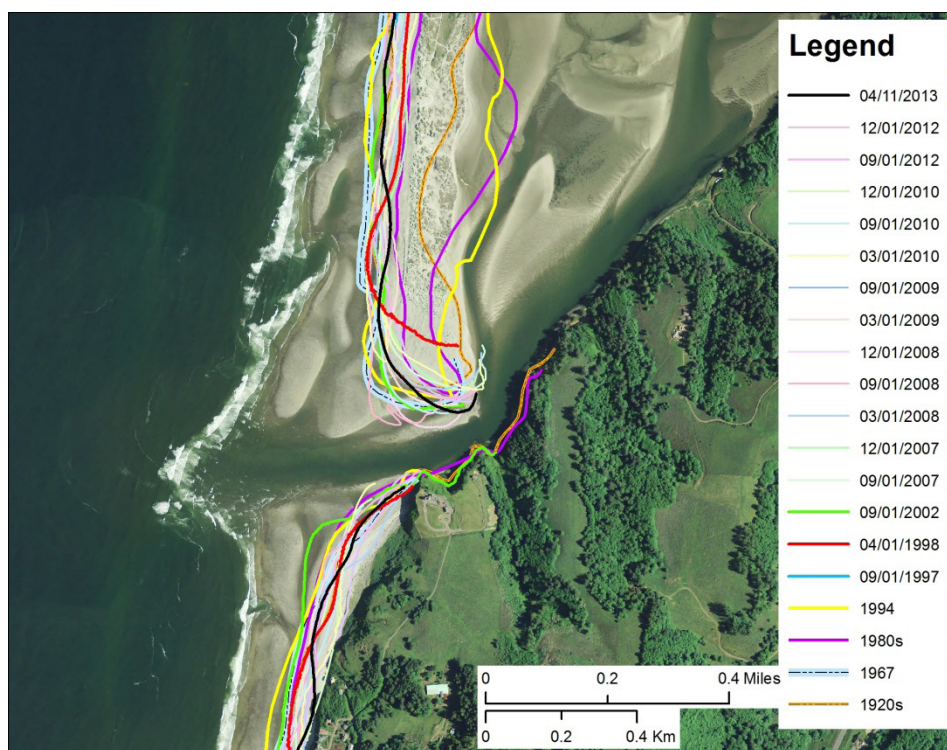


**Figure 2-11.** Historical and contemporary shoreline positions identified adjacent to the Nestucca Bay mouth. The 1920s (1927/1928) shoreline is derived from NOS T-sheets, 1967 and 1994 from orthorectified aerial photographs, 1980s (1985/1986) from U.S. Geological Survey topographic maps, 1997-2002 are derived from lidar, and post 2007 were measured using GPS.

North of Nestucca spit, the 1980s era shoreline tracks landward of the other shoreline positions and extends all the way to Pacific City at the north end of the cell. This finding is likely to be a function of erosion that occurred as a result of the 1982-1983 El Niño event (P. Komar, personal communication, 2001). In contrast, the 1994 and 2002 shoreline positions represent the most seaward extent of the shoreline (located some 45 to 76 m (150 to 250 ft) seaward of the 1980s shoreline). This indicates that large volumes of sediment had accumulated along much of the northern half of the cell, the product of a persistent net drift of beach sediments to the north. It is highly likely that this pattern is a function of the persistent El Niño conditions that have characterized the Pacific Northwest (PNW) during the 1980s and 1990s. Similar observations of net accretion around Pacific City since about 1981 were also noted in a report by Shoreland Solutions (1998). For example, considerable quantities of sand rapidly accumulated along much of the Pacific City shoreline in the early 1980s, burying a large riprap revetment that was installed in 1978. Furthermore, the continued accumulation of sand at the north end of the Neskowin cell has presented major problems for homeowners since at least 1984. Of particular concern has been the inundation of homes and property by sand (Komar, 1997; Shoreland Solutions, 1998). As can be seen from Figure 2-10, much of the Nestucca spit has now recovered from the major storms of the late 1990s.

### 2.2.2 Sand Lake cell

Along the Sand Lake cell, the 1920s and 1980s era shoreline positions represent the most landward position of the MHWL (i.e., eroded state), while the 1967 and 1994 shorelines characterize the accreted state. For the most part, this pattern is broadly similar to that identified previously in the Neskowin cell. However, unlike the Neskowin cell, the 1980s era shoreline at Sand Lake indicates cell-wide coastal erosion.

Approximately 2.8 km (1.74 mi) north of Cape Kiwanda is the community of Tierra Del Mar. As with Neskowin, much of its shoreline has now been protected with coastal engineering (riprap). These structures appear to have been built in the early 1970s and were expanded further in 1984, probably in response to the effects of the 1982-1983 El Niño. North of the Tierra Del Mar, the entire spit is undergoing considerable erosion and associated dune retreat. For example, analyses of lidar data from 1997 to 2009 indicate that the spit shoreline has eroded on average by 27.8 m (91 ft).

Some of the most interesting shoreline changes identified in the Sand Lake cell are found adjacent to the mouth of the estuary. As shown in Figure 2-12, the location of the estuary mouth has varied considerably over the past century. The 1920s era shoreline characterizes the most southerly extent of the estuary mouth (implying a period of net southerly sand transport), while the 2009 shoreline identifies its most northerly position. As a result, the estuary mouth has migrated some 580 m (~1,900 ft) during this period. These results clearly highlight the dynamic and unstable nature of spit ends. An examination of aerial photographs flown in 1939 (not shown) also reveals a southerly bay-mouth position, while the spit ends were much wider. These latter characteristics are broadly similar to the 1920s shoreline identified in Figure 2-12. In contrast, the 1980s shoreline indicates an extremely wide bay mouth (~550 m [1,800 ft] wide), so that much of the inner bay was probably fully exposed to the sea. Since the 1990s, the estuary mouth has migrated north up against the northern spit tip, causing the tip to be truncated, while also eroding a section of the shoreline within the estuary adjacent to Sand Lake Recreation Area park.



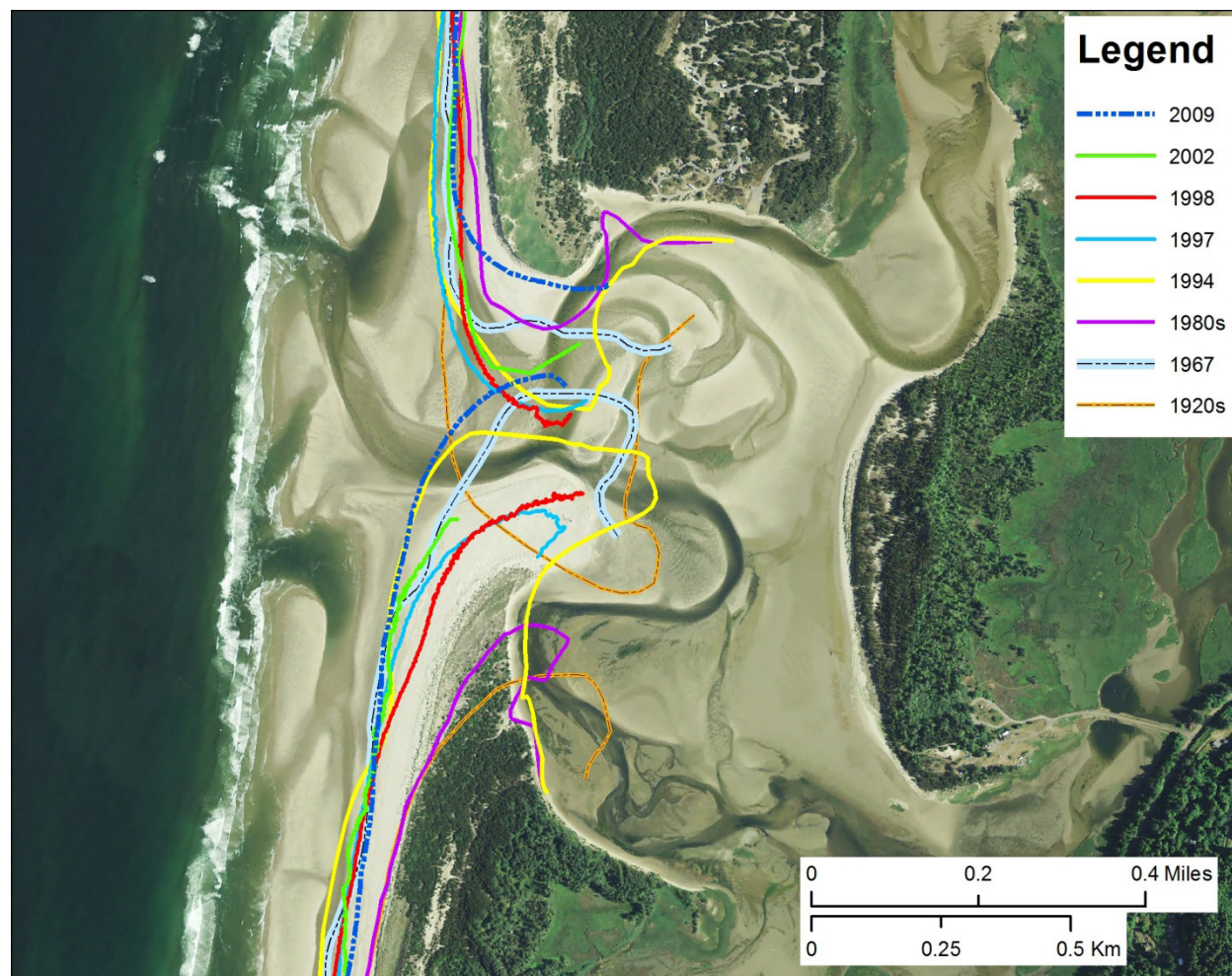


**Figure 2-12.** Shoreline variability adjacent to the Sand Lake estuary mouth. The 1920s (1927/1928) shoreline is derived from NOS T-sheets, 1967 and 1994 from orthorectified aerial photographs, 1980s (1985/1986) from U.S. Geological Survey topographic maps, and 1997–2009 are derived from lidar.

### 2.2.3 Netarts cell

The Netarts littoral cell is one of the smallest cells on the Oregon coast. As a result, it is particularly susceptible to variations in wave approach, especially changes in the predominant wave direction caused by the El Niño/La Niña Southern Oscillation. The shoreline analyses presented here demonstrate a number of morphological changes that are less apparent in the other littoral cells. At Cape Lookout State Park (CLSP), located at the southern end of the cell (Figure 2-13), the shorelines track closely to each other. The exceptions to this are the 1994 and 2009 shorelines. The former shoreline identifies the accreted state (consistent with the other littoral cells in Tillamook County), while the 2009 shoreline reveals the most eroded state. The latter is the product of erosion along the spit that accelerated in the late 1990s, due to a series of large storms that impacted the area during the 1997-1998 El Niño winter. In fact, subsequent storms over the 1998-1999 La Niña winter caused even more extensive erosion of the park. In particular, a storm on March 2-3, 1999, eventually resulted in the foredune protecting the park being breached, and waves inundating the campground, causing significant damage to campground facilities.

According to Komar and others (1989), El Niño events have produced large spatial changes in the configuration of the Netarts coastline and the morphology of the beaches, especially during the 1980s and 1990s. Allan and others (2003) analyzed terrestrial lidar measured in 1997 (pre 1997-1998 El Niño) and 1998 (post El Niño) in order to quantify the alongshore varying nature of the El Niño shoreline responses (Figure 2-14). As can be seen in the figure, the largest extent of shoreline retreat occurred along the southern 3 km (1.86 mi) of the cell, immediately north of Cape Lookout. Erosion in that area during both the 1982-1983 and 1997-1998 El Niños significantly damaged Cape Lookout State Park, eroding away a high ridge of dunes that protected the park (Komar and others, 1989; Komar, 1998). The lidar results in Figure 2-14 also capture the northward displacement of sand during the El Niño winter. In the hot spot zone in the south, the maximum shoreline retreat reached 18 m (59 ft). Shoreline accretion otherwise prevailed along the remainder of the cell, on average 5

to 10 m (~16 to 33 ft), a result of sand acquired by its northward displacement from the eroded hot spot zone at the south end of the cell. There was also an occurrence of hot spot erosion along the north shore of the inlet to Netarts Bay, which threatened the loss of condominiums perched above the estuary mouth on the north side of the bay (Komar, 1998).

Prior to the 1982-1983 El Niño, erosion on Netarts Spit had generally been minimal (Komar and others, 1989). As a result, significant erosion of CLSP did not begin to occur until the 1982-1983 El Niño and was very significantly advanced by the 1987-1988 El Niño erosion event. Interestingly, the 1980s era and 1994 shorelines presented in Figure 2-13 indicate a relatively broad beach in front of the park. This suggests that the beach had reformed somewhat following the 1982-1983 El Niño. This is consistent with observations reported by Komar and others (1989). However, they noted further that although some sand had returned, the volume of sand contained on the beach was still depleted when compared with the period prior to the 1982-1983 El Niño. Evidence for this was the extensive areas of gravel exposed on the beach and the presence of rock outcrops in the shallow offshore. Because the beach was in such a depleted state, the capacity of the beach to act as a buffer against storm waves during subsequent winter seasons was severely reduced. This was especially the case during the 1987-1988 El Niño event, which eventually caused the destruction of a bulkhead emplaced along the beach foredune during the late 1960s (Figure 2-15). By April 1998 the width of the beach in front of CLSP had narrowed significantly, from about 50 to 91 m (170 to 300 ft) wide in 1994, to around 12 to 24 m (40 to 80 ft) wide in 1998 (Figure 2-10). Furthermore, the area affected by the erosion extended about 1.4 km (0.9 mi) north and 1.1 km (0.7 mi) south of the campground. In an effort to mitigate the erosion problems, the Oregon Parks and Recreation Department responded by installing a dynamic revetment structure in the area most affected (Figure 2-16). Such structures are a "soft" form of engineering (when compared with basaltic riprap revetments) because they are less intrusive on the coastal system and are designed to respond dynamically to wave attack.



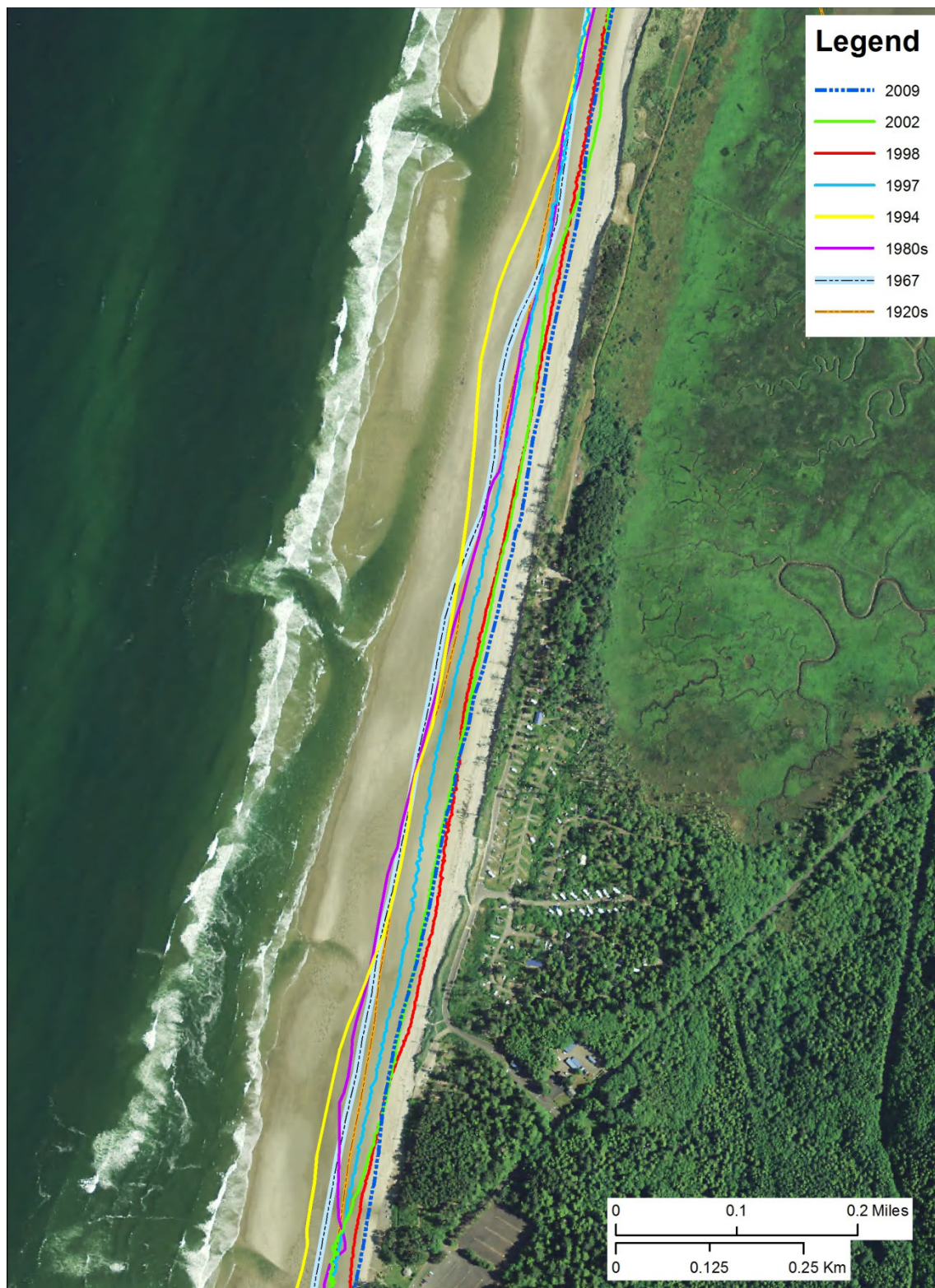


**Figure 2-13.** Historical and contemporary shoreline positions identified along the southern end of Netarts Spit, adjacent to Cape Lookout State Park. The 1920s (1927/1928) shoreline is derived from NOST T-sheets, 1967 and 1994 from orthorectified aerial photographs, 1980s (1985/1986) from U.S. Geological Survey topographic maps, and 1997–2009 are derived from lidar.

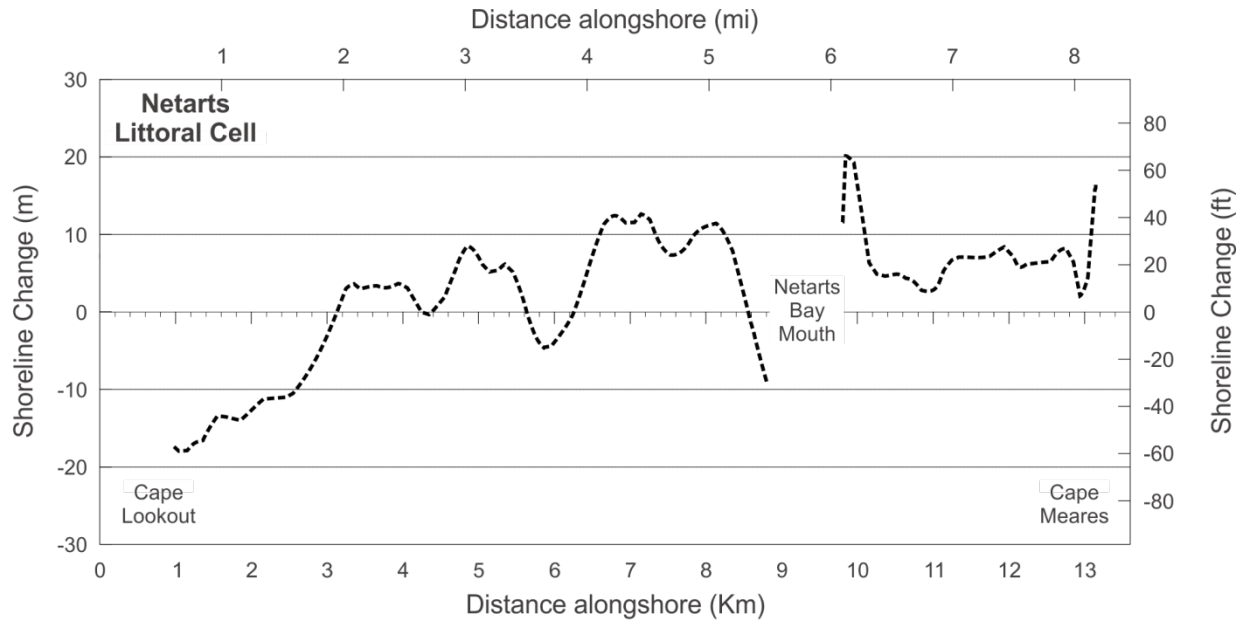


**Figure 2-14.** De-meaned shoreline changes derived from a comparison of 1997 and 1998 lidar along the Netarts littoral cell (after Allan and others, 2003).

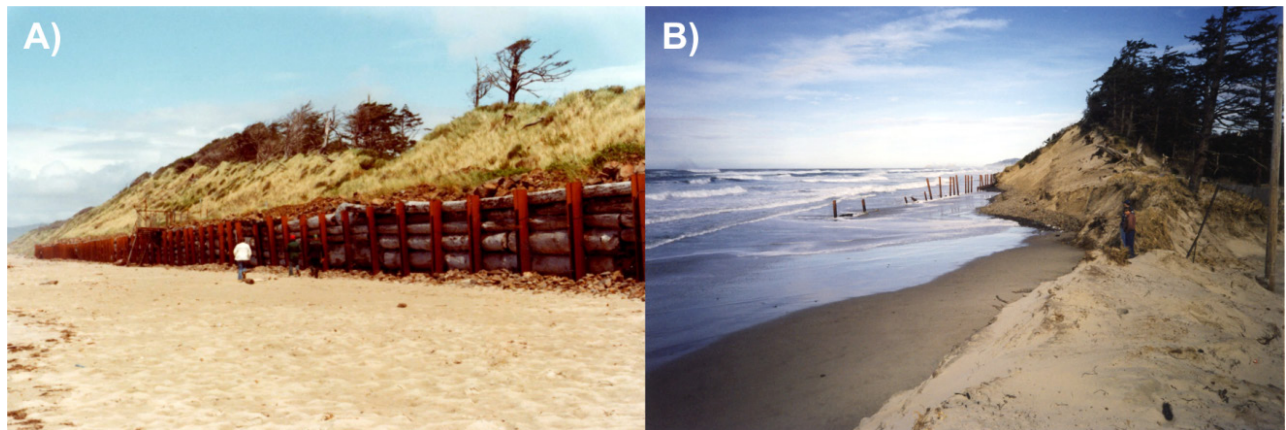


**Figure 2-15.** A) Wooden bulkhead constructed at Cape Lookout State Park (photo: Oregon Parks and Recreation Department, June 1978); B) The same area in February 1998. (Photo: P. Komar)





**Figure 2-16.** A dynamic revetment “cobble beach” constructed at Cape Lookout State Park. The cobble beach is backed by an artificial dune, which is overtopped periodically during major storms. (Photo: J. Allan, DOGAMI, 2008)

Farther north along Netarts Spit (about 2.9 km [1.8 mi] north of CLSP), the erosion of the high foredune remains acute. For the most part, the 1980s shoreline shifts landward with progress along the spit, tracking close to the vegetation line and indicating significant erosion along much of the northern end of Netarts Spit (Figure 2-17). This is characterized not only by the position of the 1980s shoreline but by the presence of a prominent erosion scarp. In contrast, the 1994, 1997, and 1998 shorelines shift seaward and track about 60 to 75 m (196 to 246 ft) seaward of the 1980s shoreline (Figure 2-17). Such a change is analogous to a pivot point in which one set of processes (erosion) gives way to another (accretion). In other words, the coastal response along Netarts Spit reflects a reorientation of the entire coastline toward the direction of wave attack, with erosion occurring along the southern end of the cell and accretion in the north (Komar and others, 1989; Revell and others, 2002). Recent measurements by DOGAMI staff using RTK-DGPS to document beach and shoreline changes along Netarts Spit have revealed that the foredune periodically undergoes 10 to 15 m (33 to 49 ft) of dune retreat during single storm events,

highlighting the intensity of the erosion processes that dominate much of this coastline. Figure 2-18 distinguishes historical shoreline positions adjacent to the end of Netarts Spit; here we have included one additional shoreline (1950s) which was derived from a NOS T-sheet not available south of Netarts Spit. Apart from the 1950s shoreline, which shows the spit end having re-curved into the bay and a much narrower mouth, the morphology of Netarts Spit has remained broadly the same. In keeping with the Nestucca and Sand Lake estuary mouths, the spit tip migrated northward some 122 m (400 ft) between the 1980s and 1994 shoreline. Part of this response is probably related to the prevalence of El Niños throughout the 1980s, which would have helped shift the mouth of Netarts Bay to the north in response to the increase in waves from the southwest typical of El Niño conditions. However, by 1998 the spit tip had returned to the south. These changes again highlight the dynamic nature of spit ends.

On the north side of Netarts Bay is The Capes development, which consists of homes built along the head scarp of a large landslide (Figures 2-18 and 2-19). During the 1997-1998 El Niño, homeowners observed

movement on the slide immediately seaward of homes built adjacent to the head scarp (Figure 2-19). The movement accelerated over the winter, resulting in several cracks opening up landward of a few of the homes. The cause of the movement was attributed to extensive

wave erosion along the toe of the landslide, the product of the northward movement of the mouth of the estuary. The erosion essentially removed the toe-supporting structure, which effectively enhanced the lateral movement of the landslide material.

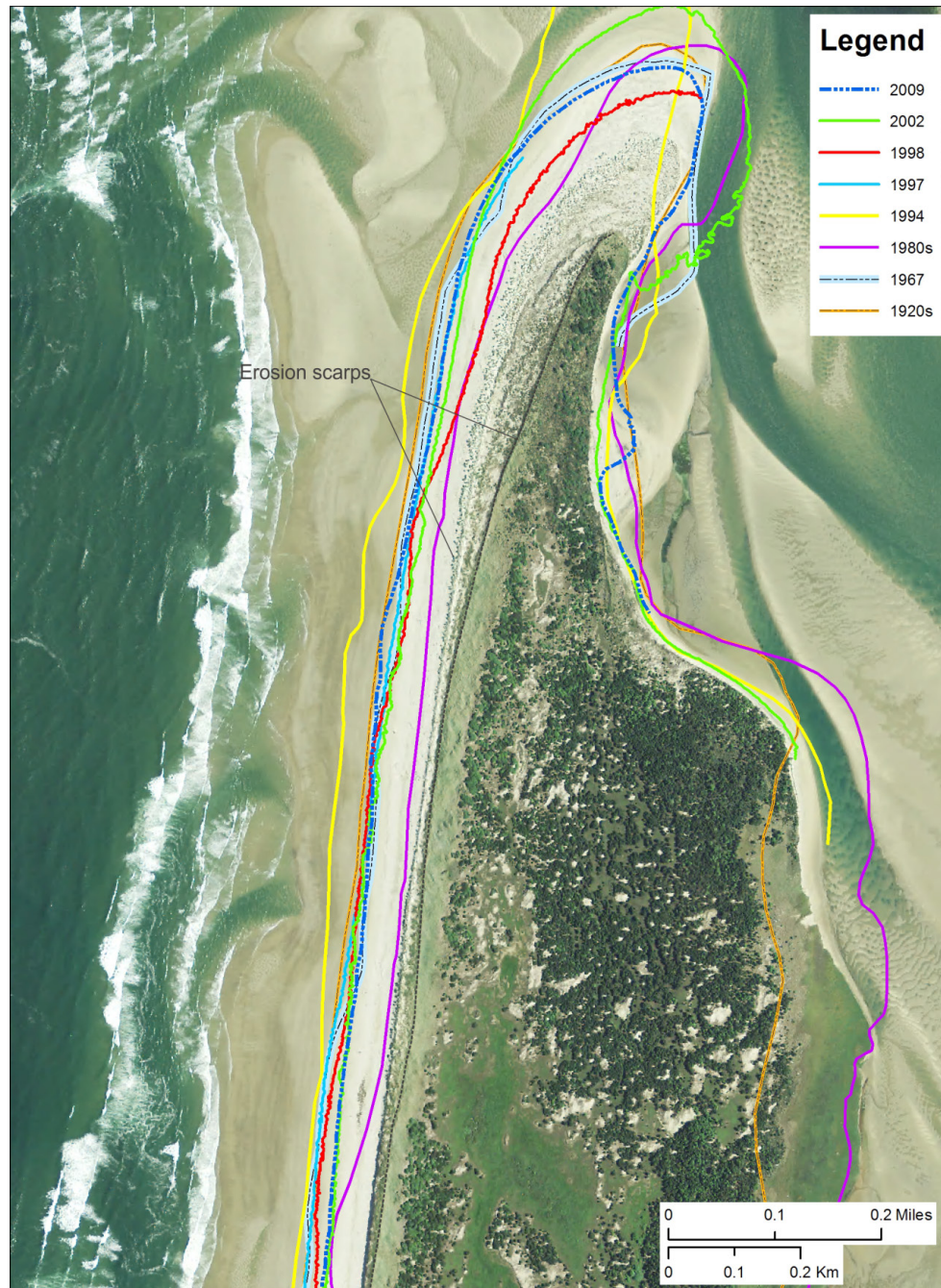


**Figure 2-17.** Historical and contemporary shoreline positions identified along the northern end of Netarts Spit, adjacent to Cape Lookout State Park. The 1920s (1927/1928) shoreline is derived from NOS T-sheets, 1967 and 1994 from orthorectified aerial photographs, 1980s (1985/1986) from U.S. Geological Survey topographic maps, and 1997–2009 are derived from lidar. Black dashed line on the dune denotes an erosion scarp.



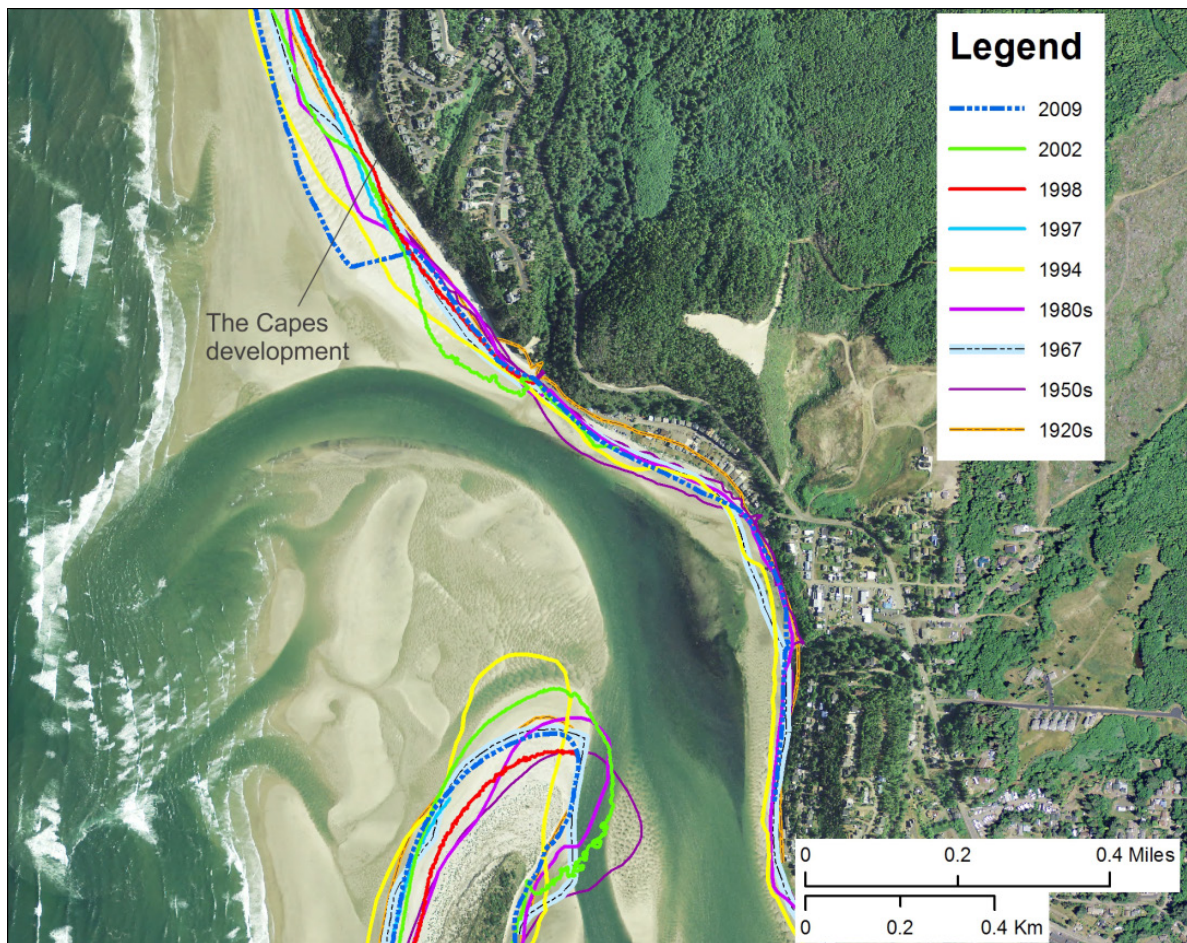


**Figure 2-18.** Historical shoreline positions identified at the mouth of Netarts Bay. The 1920s and 1950s (1927/1928, 1953/1955) shoreline is derived from NOS T-sheets, 1967 and 1994 from orthorectified aerial photographs, 1980s (1985/1986) from U.S. Geological Survey topographic maps, and 1997–2009 are derived from lidar. Black dashed line on the dune denotes an erosion scarp.

Our analyses of the shoreline data reveal that the width of the beach in front of The Capes has varied considerably in the past (Figures 2-18 and 2-19). For example, the width of the beach at the toe of the slide in 1994 was some 106 m (350 ft) wide, while small dunes had developed along a 1.1 km (0.6 mi) section of the beach. This suggests the accumulation of a significant volume of sand in the area. However, as a result of the 1997-1998 El Niño, the beach eroded back about 98 m (320 ft), into the toe of the slide (Figure 2-19). This process has been repeated over the years (e.g., 1950s shoreline) and most recently in the mild 2009-2010 El Niño. During this last event, the sand beach in front of the Capes narrowed significantly, almost approaching

the position of the shoreline in 1998. Figure 2-19 shows the magnitude of change characterized by the shift in the shoreline from 2009 and 2011, as the mouth of the bay once again shifted north.

Finally, Figure 2-20 shows the spread of shorelines adjacent to Oceanside. The 1920s and 1950s shorelines reveal the presence of an extremely narrow beach at Oceanside. This suggests a period of extensive erosion during those years. However, as can be seen from Figure 2-21, although the beach may have been narrow the bluff face is covered in vegetation with little sign of erosion. In fact, comparisons between historical and modern photos reinforce the perception that this section of shore is essentially stable.



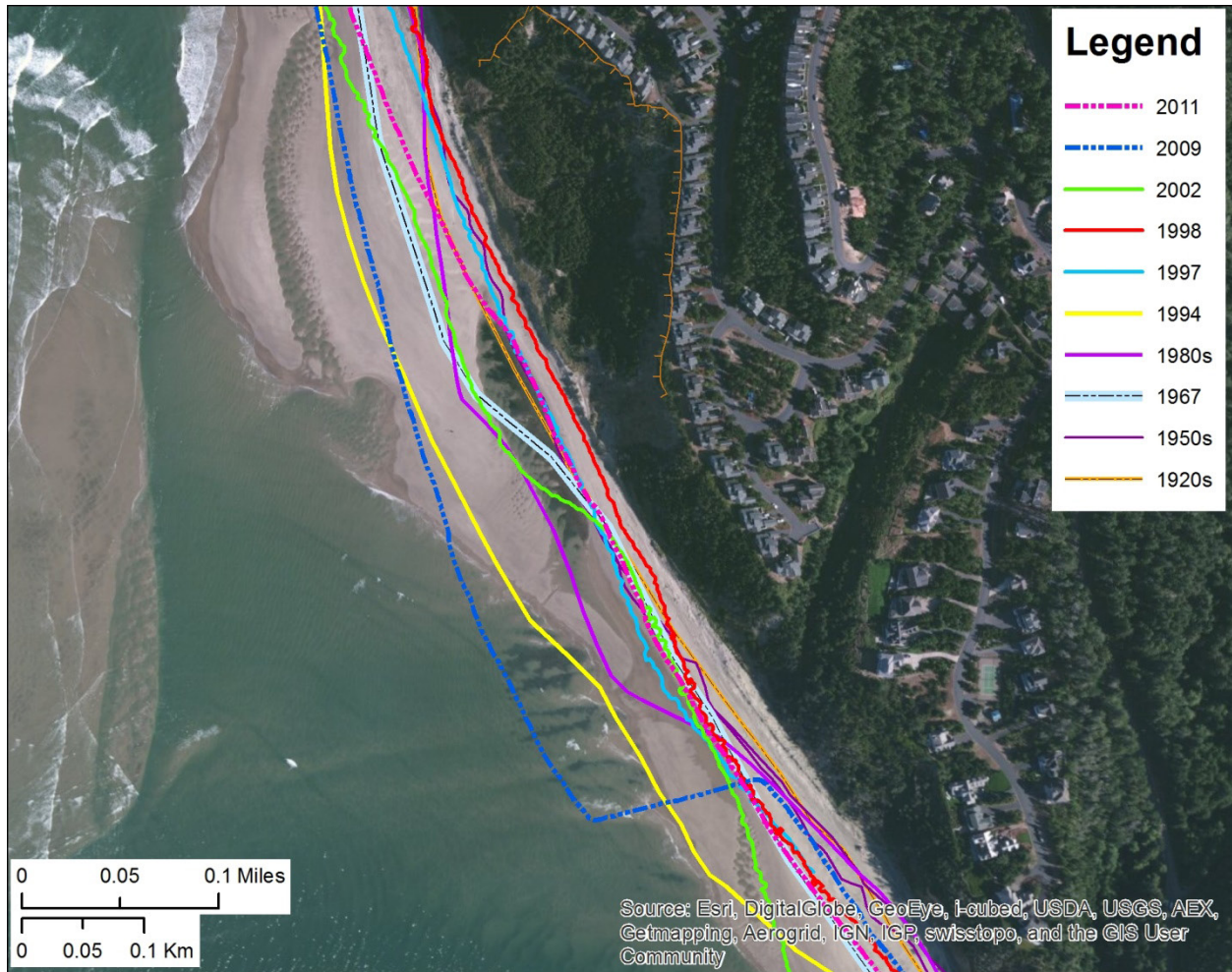


**Figure 2-19.** Historical shoreline positions identified along the toe of The Capes development near the mouth of Netarts Bay. The 1920s and 1950s (1927/1928, 1953/1955) shoreline is derived from NOST-sheets, 1967 and 1994 from orthorectified aerial photographs, 1980s (1985/1986) from U.S. Geological Survey topographic maps, and 1997–2009 are derived from lidar. One additional shoreline (2011) surveyed using GPS is included. Brown hashed line depicts the landslide head scarp.

Also of interest is the 1980s shoreline, which highlights significant differences between Oceanside and Short Sand beach to the north. At Oceanside the 1980s shoreline is located in approximately the same location as the 1994, 1997, and 1998 shorelines and indicates a relatively broad beach (Figure 2-20). In the two pocket beaches to the north, the 1980s shoreline tracks close to the base of the bluff, indicating a very narrow beach. The latter is not surprising given that this particular beach consists of gravels and, as noted previously, the shorelines tend to track much closer to each other on steep beaches. Overall, variations in the shoreline

positions along this section of coast may reflect a lag in the transport of sediment around the bluff headlands that bound the smaller pocket beaches. Furthermore, erosion events similar to what occurred at The Capes (Figure 2-18) likely contribute large slugs of sediment that progressively move northward along the coast, producing the apparent shoreline fluctuations seen at Oceanside and in the smaller pocket beaches to the north. Overall, these findings clearly highlight a very dynamic and complex coastal environment, in which many processes are operating over a broad range of spatial and temporal scales.



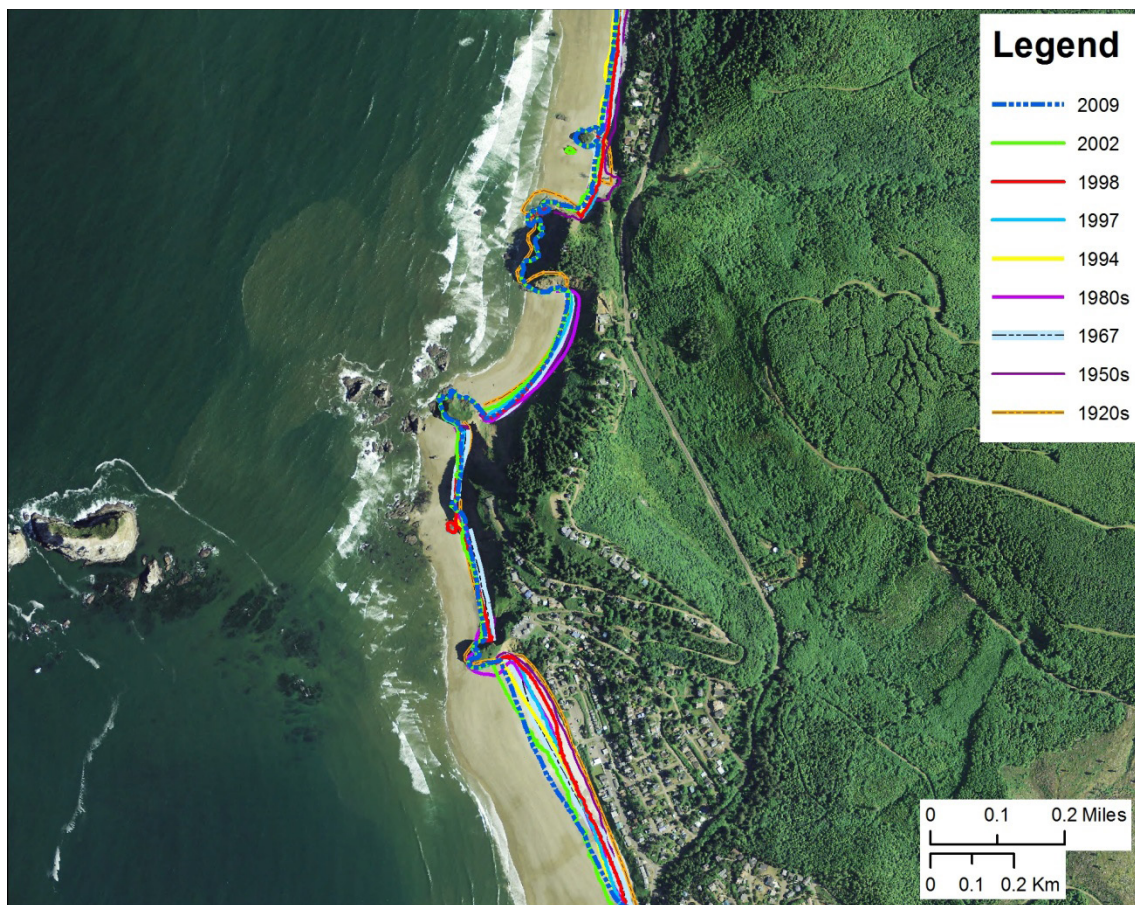


**Figure 2-20.** Historical shoreline positions identified at Oceanside and along Short Sand beach. The 1920s and 1950s (1927/1928, 1953/1955) shoreline is derived from NOS T-sheets, 1967 and 1994 from orthorectified aerial photographs, 1980s (1985/1986) from U.S. Geological Survey topographic maps, and 1997–2009 are derived from lidar. Black dashed line on the dune denotes an erosion scarp.



**Figure 2-21.** A) A 1920s era photo of the community of Neskowin looking south toward the entrance to Netarts Bay. Note well-vegetated bluffs and the presence of the gravel berm along the toe of the bluffs (photos courtesy of Neskowin community archives); B) Oceanside in March 1998 following the 1997-1998 El Niño winter. Note again the well-vegetated bluff and gravel berm at the back of the beach (Photo: P. Komar).

### 2.2.4 Rockaway cell

Some of the most dramatic shoreline changes identified on the Oregon coast have occurred in the Rockaway littoral cell, particularly in response to the construction of the north jetty at the mouth of Tillamook Bay (Figures 2-22 and 2-23). Previous descriptions of the response of Tillamook Bay mouth to jetty construction were provided by Terich and Komar, 1973,1974), while (Komar, 1997) provided a historical summary of the destruction of Bayocean spit.

Construction of Tillamook's north jetty was completed in October 1917. During the construction phase, changes in the inlet channel and the adjacent shorelines soon became evident (Figure 2-22). North of the jetty, sand began to accumulate rapidly, and the shoreline advanced seaward at a rate almost equal to the speed at which the jetty was being constructed (Komar, 1997). Between 1914 and 1927 the coastline just north of the jetty advanced seaward about 1 km (0.62 mi). However, by 1920 the rate of sand accumulation on the north side of the jetty had slowed dramatically, so that the position of the shoreline was much the same as it is today (Figure 2-23). According to Komar and others (1976), the volume of sand that accumulated north of the jetty caused some to speculate that the predominant net sand transport was to the south. However, Komar and others argued that this was not the case. They observed that if a net southward drift of sediment was occurring, why was there no evidence of an accumulation of sand

adjacent to Cape Meares, located at the southern end of the Rockaway littoral cell? Instead, the Cape Meares beach is narrow and is composed mainly of cobbles and gravels.

Although the coastline from Rockaway to Manzanita experienced some erosion (discussed below) due to jetty construction, the most dramatic changes were observed farther south along Bayocean Spit. In particular, significant coastal retreat occurred at the south end of the Rockaway cell near the community of Cape Meares (Figure 2-24). As shown in the figure, the 1927 shoreline previously extended well seaward (up to 260 m [850 ft]) of the present-day shoreline; in the community of Cape Meares, 3rd Street is now the most seaward street with 1st and 2nd located out on the beach. Over time the shoreline has progressively retreated landward to its present position. Between the 1920s and 1950s, the shoreline retreated by about 67 to 85 m (220 to 280 ft) at an average erosion rate of ~2 to 3 m/yr (6 to 10 ft/yr). In particular, significant coastal erosion occurred at Cape Meares as a result of a major storm on January 3–6, 1939 (Komar, 1997). Additional large storm wave events during the winter of 1940 continued to erode the spit. This process was repeated throughout the 1940s, and culminated with the removal of a 1.2 km (0.75 mi) section of Bayocean spit on November 13, 1952, breaching the spit (Figure 2-25).

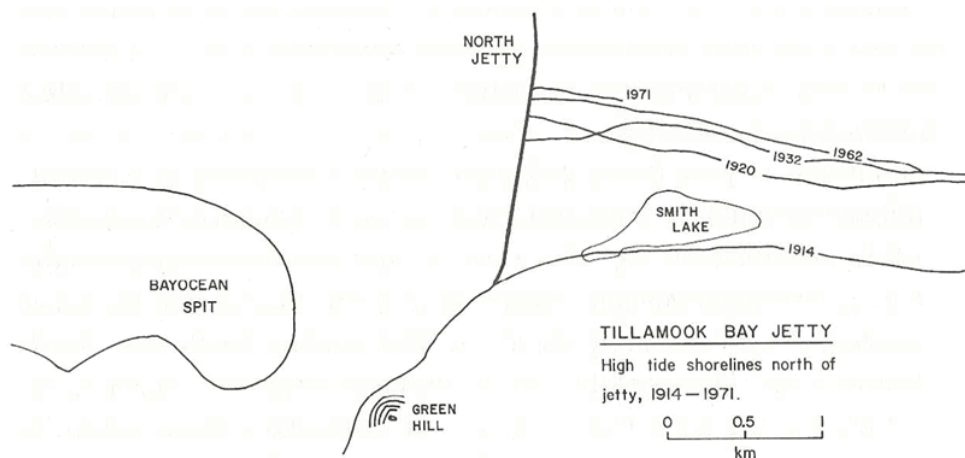


**Figure 2-22.** Shoreline positions north of Tillamook Bay jetty, 1914–1972 (from Terich, 1973; cited by Komar, 1997).



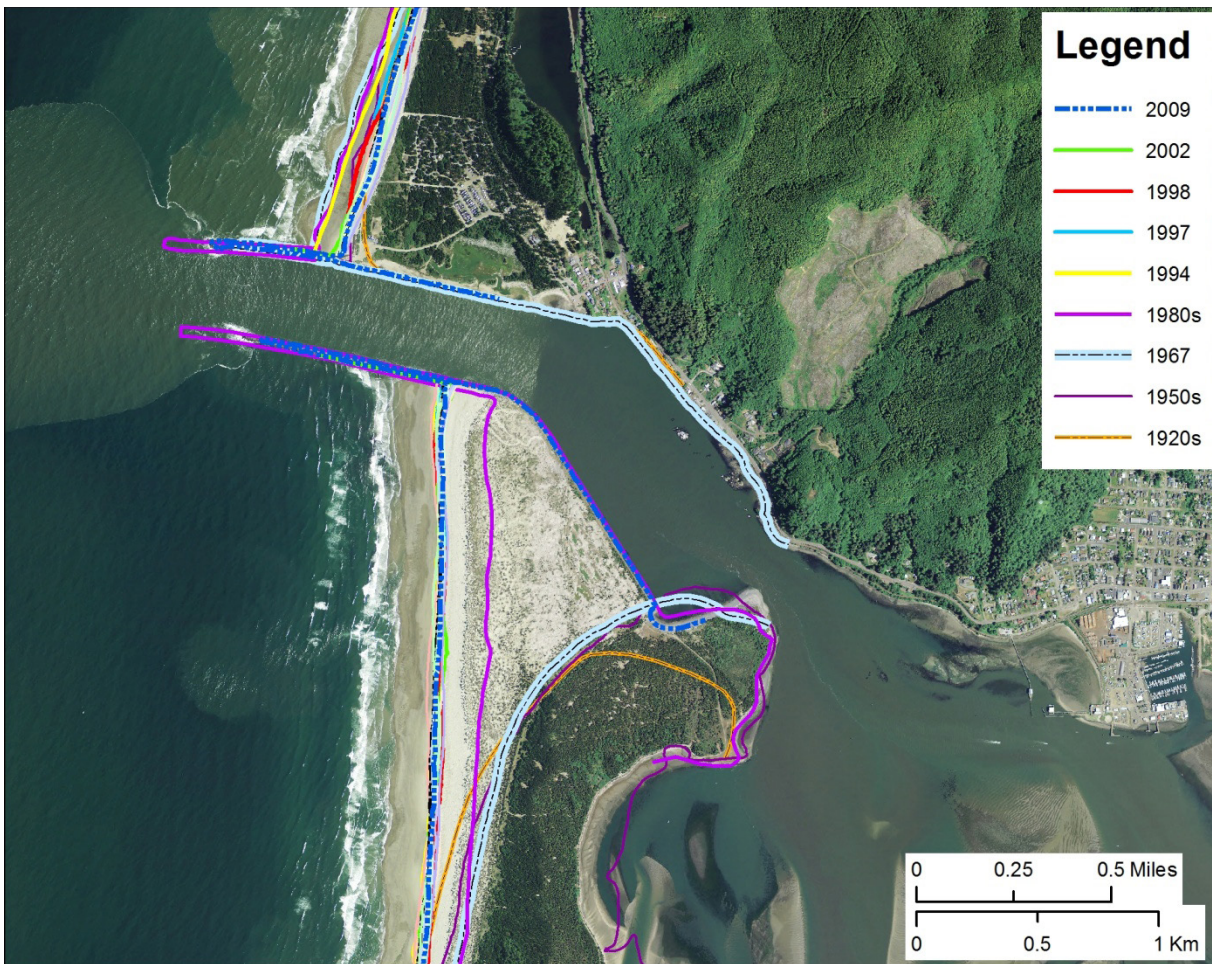


**Figure 2-23.** Historical shoreline positions identified adjacent to the mouth of Tillamook Bay in the Rockaway littoral cell. The 1920s and 1950s (1927/1928, 1953/1955) shoreline is derived from NOS T-sheets, 1967 and 1994 from orthorectified aerial photographs, 1980s (1985/1986) from U.S. Geological Survey topographic maps, and 1997–2009 are derived from lidar.

The estimated erosion rate ( $\sim 2$  to  $3$  m/yr [ $6$  to  $10$  ft/yr]) for the area around Cape Meares appears to have been sustained from the 1950s to the 1980s, as the shoreline continued to retreat landward by an additional  $90$  m ( $295$  ft). However, since then the lidar and GPS shorelines indicate that the coastline may have stabilized, as it appears to be oscillating around its present location. The absence of a south jetty at Tillamook Bay prior to 1974 probably enhanced the erosion of Bayocean spit, because a lot of sediment accumulated as shoals at the spit end or was washed into the bay (Komar, 1997). However, with the completion of the

south jetty in November 1974, sand quickly began to accumulate at the north end of the spit, causing the shoreline to prograde seaward by some  $300$  to  $760$  m ( $1,000$  to  $2,500$  ft) (Figure 2-23). Since then, the shoreline along Bayocean Spit has stabilized, so that it now responds in a manner similar to other littoral cells on the Oregon coast (Komar, 1997). Repeat GPS surveys of Bayocean Spit undertaken by DOGAMI staff since 2004 indicate that the northern one-third of the spit has been accreting at an average rate of  $\sim 0.7$  to  $1$  m/yr ( $2.3$  to  $3.3$  ft/yr).



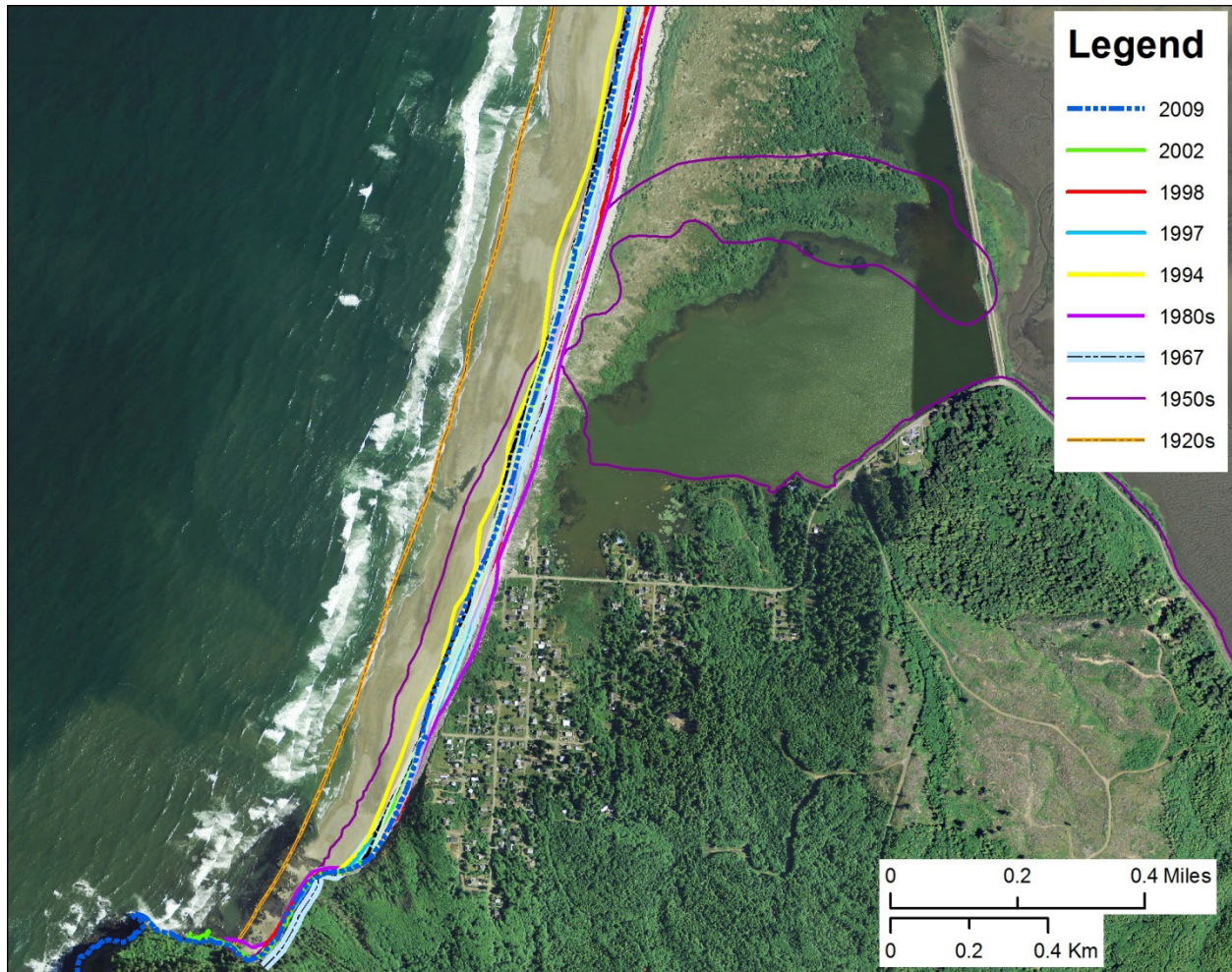


**Figure 2-24.** Historical shoreline positions identified at the southern end of the Rockaway littoral cell near the Cape Meares community. The 1920s and 1950s (1927/1928, 1953/1955) shoreline is derived from NOST-sheets, 1967 and 1994 from orthorectified aerial photographs, 1980s (1985/1986) from U.S. Geological Survey topographic maps, and 1997–2009 are derived from lidar.



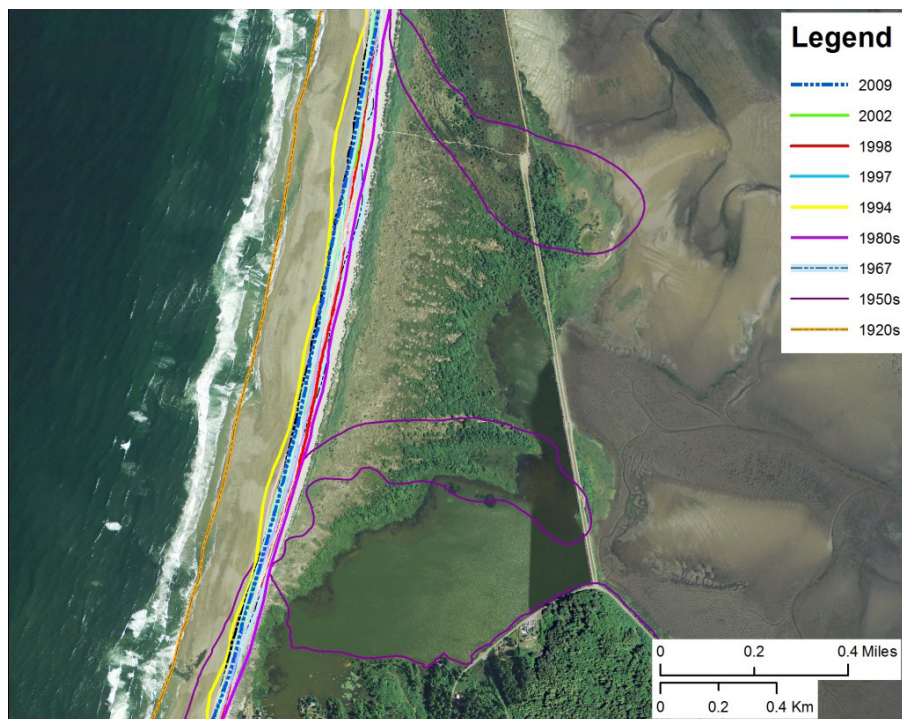


**Figure 2-25.** The breach of Bayocean Spit on November 13, 1952. The 1920s and 1950s (1927/1928, 1953/1955) shoreline is derived from NOS T-sheets, 1967 and 1994 from orthorectified aerial photographs, 1980s (1985/1986) from U.S. Geological Survey topographic maps, and 1997–2009 are derived from lidar.

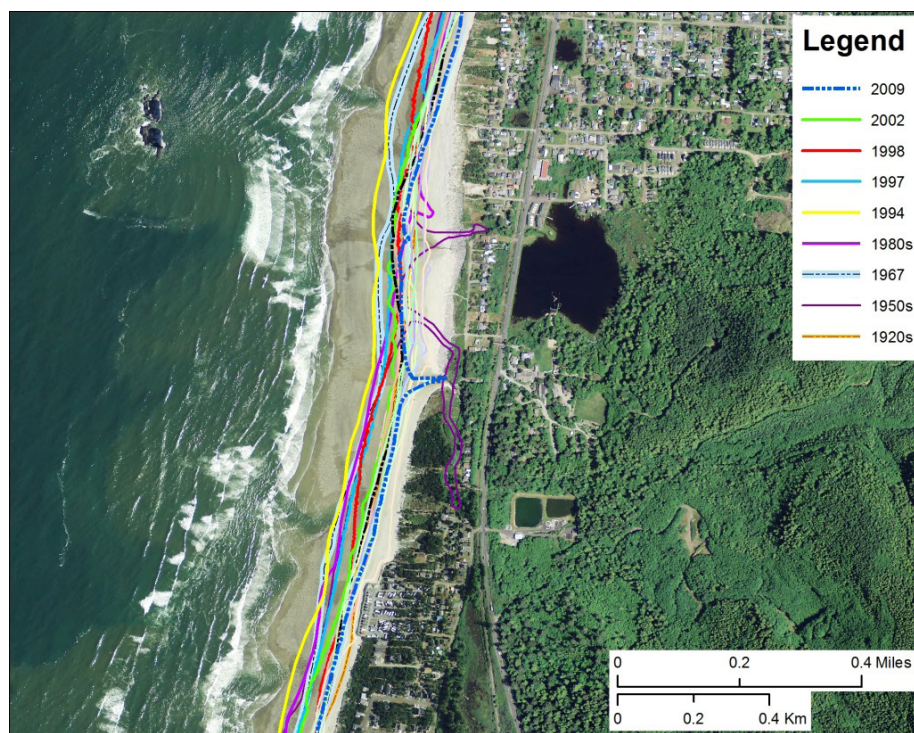


**Figure 2-26.** Historical shoreline positions identified near Twin Rocks. The 1920s and 1950s (1927/1928, 1953/1955) shoreline is derived from NOS T-sheets, 1967 and 1994 from orthorectified aerial photographs, 1980s (1985/1986) from U.S. Geological Survey topographic maps, and 1997–2009 are derived from lidar.



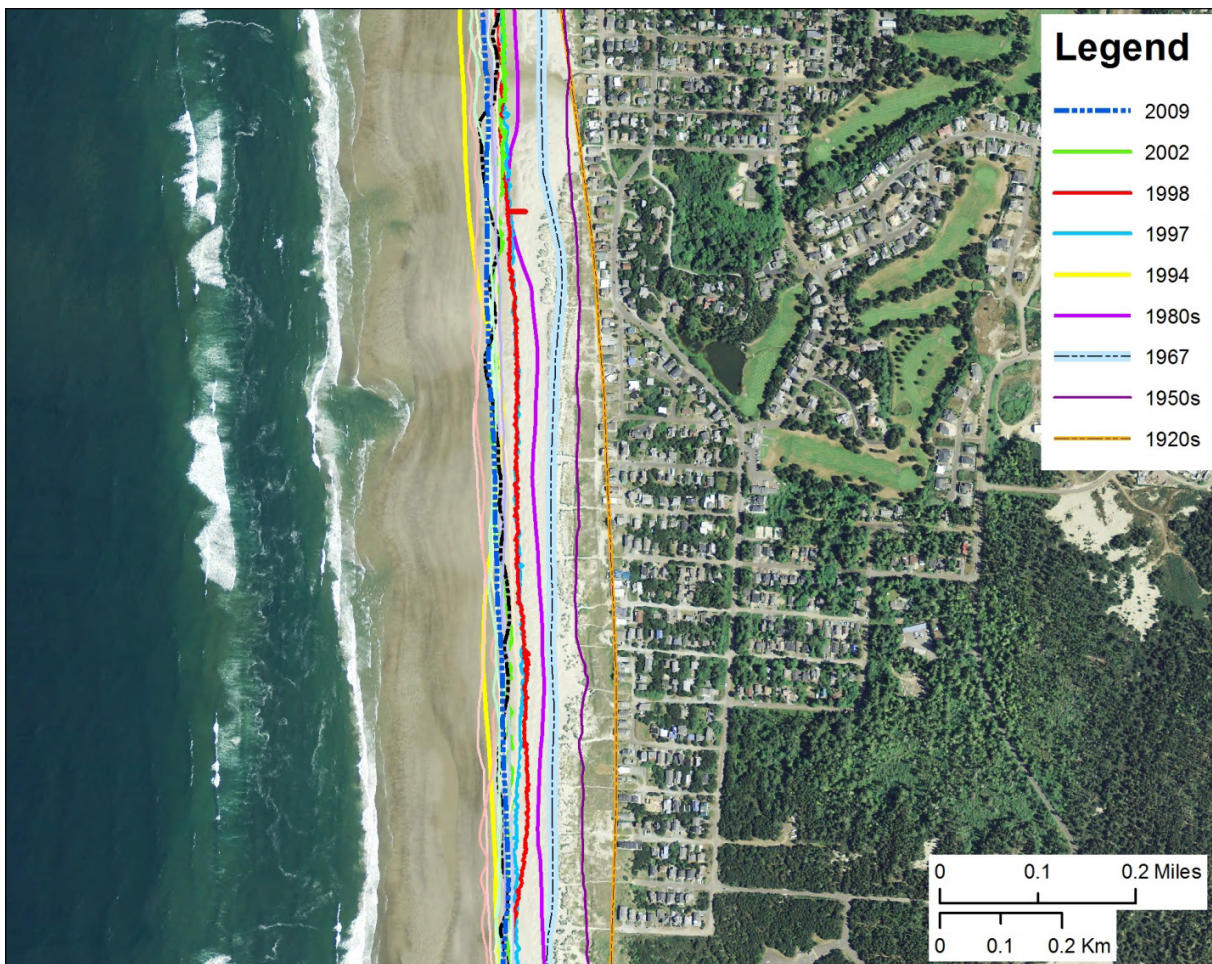


**Figure 2-27.** Historical shoreline positions at Manzanita. The 1920s and 1950s (1927/1928, 1953/1955) shoreline is derived from NOS T-sheets, 1967 and 1994 from orthorectified aerial photographs, 1980s (1985/1986) from U.S. Geological Survey topographic maps, and 1997–2009 are derived from lidar.

Farther north along the Rockaway-Manzanita coastline, the 1920s and 1950s shorelines track well landward of the contemporary shorelines (Figures 2-26 and 2-27). This type of pattern is a direct response to construction of the north Tillamook jetty. However, the erosion that occurred along the Rockaway-Manzanita beaches was generally much less than on Bayocean Spit (Komar, 1997). This is because the length of shoreline along the Rockaway-Manzanita coastline is much greater than along Bayocean spit. As a result, only a small amount of sand had to be eroded from those beaches, per unit length of shoreline, to supply sand to the accreting area around the north jetty. Erosion along the Rockaway-Manzanita coastline probably stabilized some time after the 1950s, enabling the coastline to enter an accretionary phase (Figures 2-26

and 2-27). As shown in Figures 2-26 and 2-27, the 1994 shoreline reflects the seaward extent of this rebuilding phase. This view is also supported from observations of dune growth around Manzanita, culminating with the initiation of a dune management program to control the growth of the foredunes (J. Marra, personal communication 2001). More recently, the Rockaway subcell (north of Tillamook Bay and south of the Nehalem Bay mouth) has experienced extensive erosion as a result of the 1997-1998 El Niño. The erosion was further enhanced during the even more severe 1998-1999 La Niña winter, so that the coast experienced a “one-two punch,” with little time to recover (Figure 2-28). Figure 2-28 was derived by analyzing topographic changes collected using airborne lidar flown in 1997 and 2002. The volume change estimated using this approach is

confined to just the subaerial beach and hence excludes the vegetated foredune. The results indicate that the Rockaway subcell lost  $\sim 1.4 \times 10^6 \text{ m}^3$  ( $1.8 \times 10^6 \text{ yd}^3$ ) of sand between 1997 and 2002 (Figure 2-28). Sand volume losses can also be seen for Nehalem Spit, which lost an estimated  $1.5 \times 10^5 \text{ m}^3$  ( $1.96 \times 10^5 \text{ yd}^3$ ) of sand, while Bayocean Spit gained  $\sim 1.3 \times 10^5 \text{ m}^3$  ( $1.7 \times 10^5 \text{ yd}^3$ ) of sand. It is not clear where the sand has gone. One hypothesis is that most of the eroded sand was removed offshore into deeper water; the other potential sink is the estuaries. However, we speculate that the volume of sand removed into the estuaries is likely to be quite small. As can be seen from Figure 2-29, which is derived from

our repeated monitoring of the Rockaway cell beaches up to February 2014, the overall pattern of erosion within the Rockaway subcell has continued. In contrast, the northern half of Bayocean Spit (along with portions of Nehalem Spit) has essentially recovered from the storms of the late 1990s and has gained a considerable volume of sand (Figure 2-29). A large proportion of this sand may be sediment eroded from the Rockaway beach in the late 1990s. However, the volume of sand gained along Bayocean and Nehalem Spit remains relatively small when compared with overall losses in the Rockaway subcell.

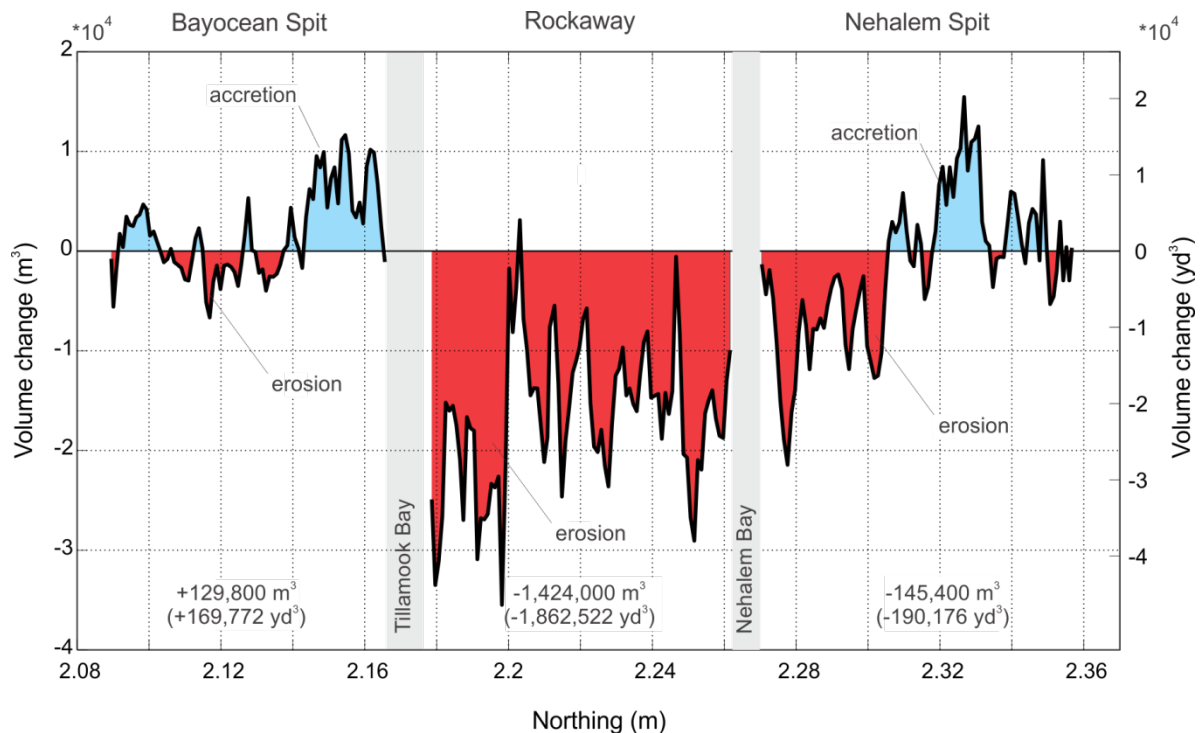


**Figure 2-28.** Alongshore beach volume changes derived from an analysis of available lidar data for the period 1997–2002. Red (darker) shading denotes erosion, while blue (lighter) shading indicates accretion (after Allan and others, 2009).

In summary, this section has presented information on historical shoreline changes that have occurred along the Tillamook County coastline over the past century. The analyses indicate that for the most part the dune-backed shorelines respond episodically to such processes as the El Niño/La Niña Southern Oscillation and as a result of rip current embayments that cause highly localized “hotspot erosion” of the coast. Accordingly, the coastline undergoes periods of both localized and widespread erosion, with intervening periods in which the beaches and dunes slowly rebuild. Perhaps the most significant coastal changes identified in Tillamook

County have occurred in response to humans, particularly as a result of jetty construction during the early part of last century. In particular, jetty construction has had a dramatic influence on the morphology of Bayocean Spit and, to a lesser extent, between the north Tillamook jetty and the Rockaway-Manzanita beaches to the north. Finally, the present analyses have shown that the mouths of the estuaries and the spit ends are extremely dynamic features, migrating over large distances in response to changes in both the sediment supply and the predominant wave conditions, making these areas hazardous for any form of development.

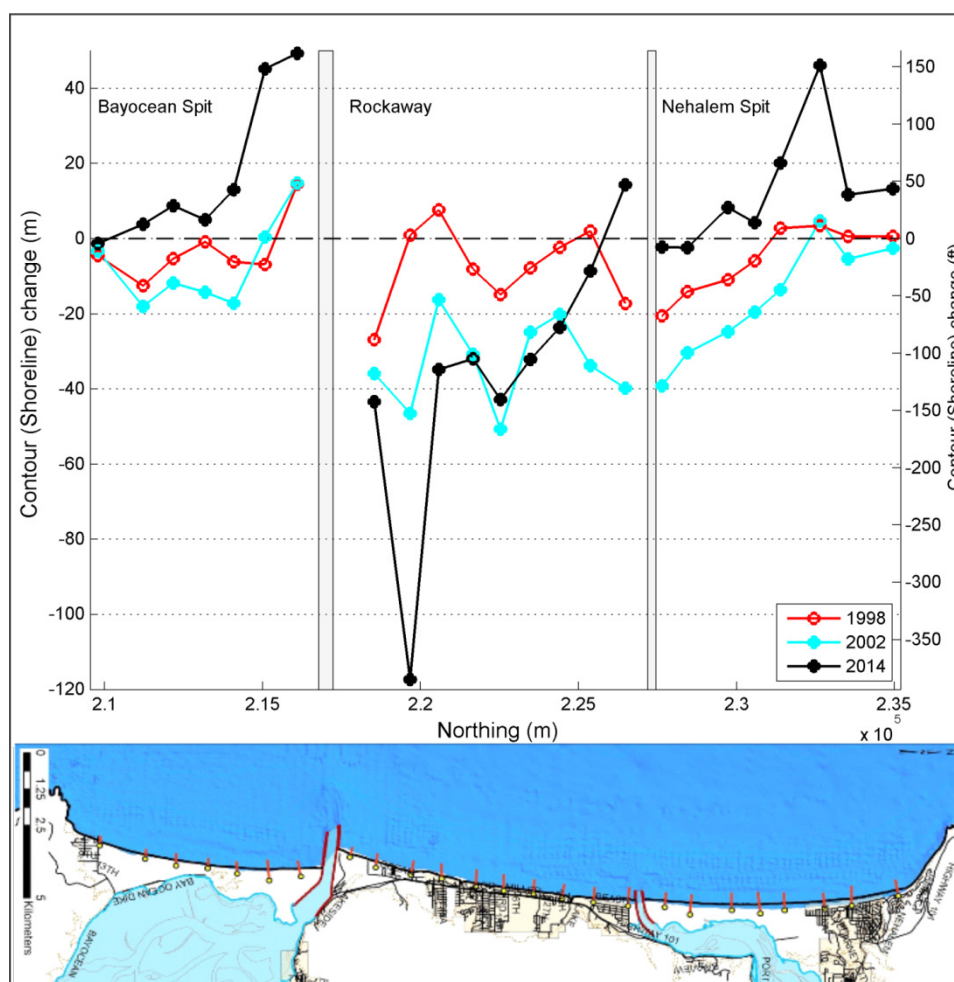


**Figure 2-29.** The Rockaway cell beach monitoring network maintained by DOGAMI showing the measured changes in the position of the dune toe (6 m [19 ft] elevation) from 1997 to 2014.



### 2.3 Cascadia subduction zone

Considerable geologic evidence from estuaries and coastal lakes along the Cascadia subduction zone supports the episodic occurrences of abrupt coastal subsidence immediately followed by significant ocean flooding associated with major tsunamis that swept across the ocean beaches and traveled well inland through bays and estuaries. Coastal paleoseismic records document the impacts of as many as 13 major subduction zone earthquakes and associated tsunamis over the past ~7,000 years (Witter and others, 2003; Kelsey and others, 2005; Witter and others, 2010), while recent studies of turbidite records within sediment cores collected in deep water at the heads of Cascadia submarine canyons provide evidence for at least 41 distinct tsunami events over the past ~10,000 years (Goldfinger and others, 2003; Goldfinger, 2009; Goldfinger and others, 2009). The length of time between these events varies from as short as a century to as long as 1,200 years, with the average recurrence interval for major Cascadia earthquakes (magnitude > [MW] 9) estimated to be ~530 years (Goldfinger and others, 2009; Witter and others, 2010).

The most recent Cascadia subduction zone earthquake occurred on January 26, 1700 (Satake and others, 1996; Atwater and others, 2005) and is estimated to have been a magnitude (MW) 9 or greater from the size of the tsunami documented along the coast of Japan. This event probably ruptured the full length (~1,200 km [~750 mi]) of the subduction zone, on the basis of correlations between tsunami deposits identified at multiple sites along the length of the PNW coast.

Associated with great Cascadia earthquakes is a nearly instantaneous lowering (subsidence) of the coast by ~0.4 m (~1.3 ft) to as much as 3 m (~10 ft) (Witter and others, 2003). This process equates to raising sea

level by the same amount, which would effectively cause considerable erosion as the beaches and shorelines adjust to the change in water levels. Over time it can be expected that the rate of change would decrease asymptotically as the coast approaches a new equilibrium (Komar and others, 1991b). Komar and others have argued that the extensive number of sea stacks offshore from Bandon are evidence for that massive erosion following the 1700 earthquake. Subsequent uplift (estimated to be ~0.6 to 1.1 m [2 to 3.6 ft]) due to the locked subduction zone has resulted in the progressive decline and eventual cessation of measurable erosion. Strain is now building toward the next major earthquake. When it is released during the next CSZ earthquake, there will be land subsidence and cliff erosion along the Bandon shore would be expected to begin again.

In 2009, DOGAMI initiated a multi-year study to accelerate remapping of the Oregon coast for tsunami inundation using state-of-the-art computer modeling and laser-based terrain mapping (lidar) (Witter and others, 2011). The outcome of this effort is the creation of new and more accurate tsunami evacuation maps for the entire length of the coast. DOGAMI, in collaboration with researchers at the Oregon Health and Science University (Joseph Zhang and Antonio Baptista), Oregon State University (Chris Goldfinger), and the Geological Survey of Canada (Kelin Wang), have developed a new approach to produce a suite of next-generation tsunami hazard maps for Oregon (Priest and others, 2009; Witter and others, 2010). New evacuation maps and many other tsunami hazard resources can be found at DOGAMI's online tsunami clearinghouse ([www.OregonTsunami.org](http://www.OregonTsunami.org)). With the next Cascadia event an inevitable reality (whether in the next year or in 500 years), we have included a hazard zone depicting the erosion distance associated with a worst-case earthquake scenario.

### 3.0 METHODOLOGY

This section describes the models and data used to generate projected future erosion hazard zones for Tillamook County.

#### 3.1 Models of foredune erosion

Two coastal erosion models were used to project future erosion hazard zones along the Tillamook County coastline:

- the geometric model developed by Komar and others (1999), and
- the Kriebel and Dean (1993) dune erosion model.

##### 3.1.1 Geometric model

The erosion potential of sandy beaches and foredunes along the PNW coast of Oregon is a function of the total water level produced by the combined effect of

the wave runup produced during a storm, coupled with the tidal elevation, exceeding some critical elevation of the fronting beach, typically the elevation of the beach-dune junction ( $E_J$ ). This basic concept is depicted conceptually in Figure 3-1A from the model developed by Ruggiero and others (1996) and, in the case of erosion of a foredune backing the beach, the application of a geometric model (Equation 3-1, Figure 3-1B) formulated by Komar and others (1999):

$$DE_{MAX} = \frac{(T_{WL} - E_J)}{\tan \beta} \quad (3-1)$$

where  $DE_{MAX}$  is the maximum potential dune erosion,  $T_{WL}$  is the calculated wave runup plus the measured tide, and  $\tan \beta$  is the beach slope. Thus, the more extreme the total water level elevation, the greater the resulting erosion that occurs along both dunes and bluffs.

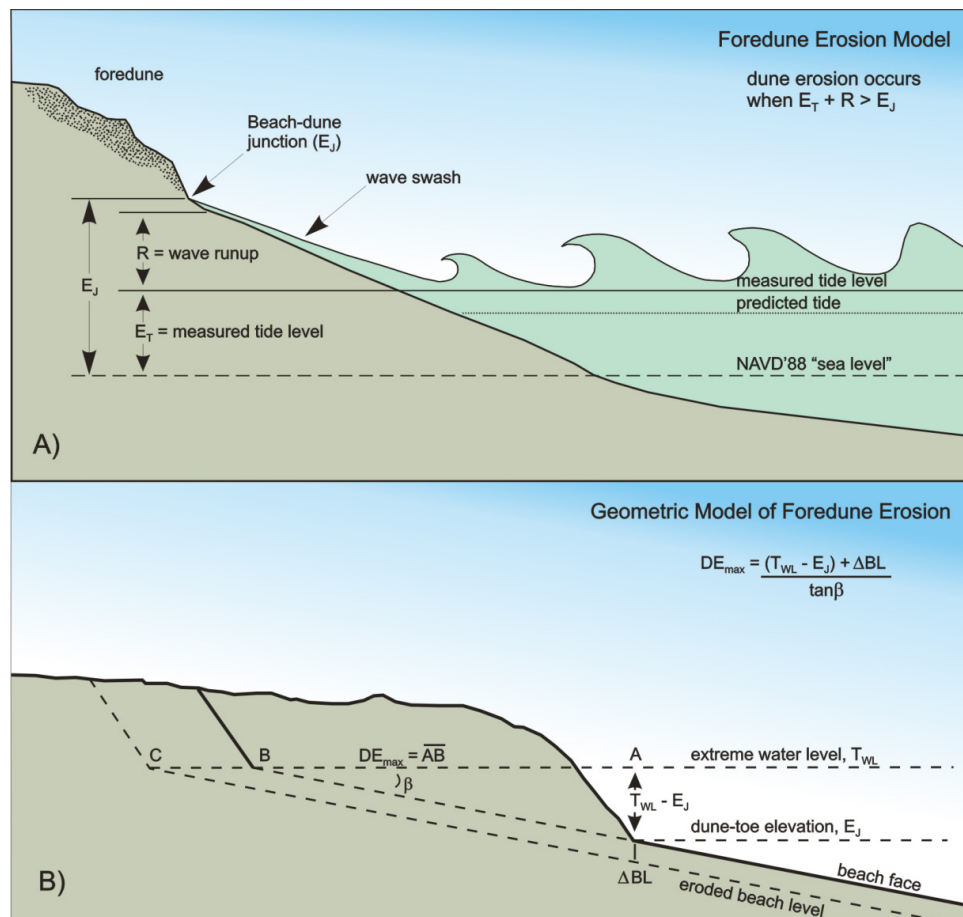


**Figure 3-1.** A) The foredune erosion model (Ruggiero and others, 1996; 2001). B) The geometric model used to assess the maximum potential beach erosion in response to an extreme storm (Komar and others, 1999).

As can be seen from Figure 3-1B, estimating the maximum potential dune erosion ( $DE_{MAX}$ ) is dependent on first determining the total water level elevation,  $T_{WL}$ , diagrammed in Figure 3-1A, which includes the combined effects of extreme high tides plus storm surge plus wave runup, relative to the elevation of the beach-dune junction ( $E_j$ ). Therefore, when  $T_{WL} > E_j$ , the foredune retreats landward by some distance, until a new beach-dune junction is established, the elevation of which approximately equals the extreme water level. Because beaches along the high-energy Oregon coast are typically wide and have a nearly uniform slope ( $\tan \beta$ ), the model assumes that this slope is maintained and the dunes are eroded landward until the dune face reaches point B in Figure 3-1B. As a result, the model is geometric in that it assumes an upward and landward shift of a triangle, one side of which corresponds to the elevated water levels, and then an upward and landward translation of that triangle and beach profile to account for the total possible retreat of the dune (Komar and others, 1999).

The geometric model gives the maximum potential equilibrium cross-shore change in the shoreline position landward of the most likely winter profile resulting from a major storm. However, in reality it is unlikely that this extreme degree of response is ever fully realized, because of the assumptions made in deriving the geometric model with the intent of evaluating the maximum potential dune erosion. As noted by Komar and others (1999), in the first instance the geometric model projects a mean linear beach slope. As a result, if the beach is more concave, it is probable that the amount

of erosion would be less, though not by much. Perhaps of greater significance is that the geometric model assumes an instantaneous erosional response, with the dunes retreating landward as a result of direct wave attack. However, the reality of coastal change is that it is far more complex, there in fact being a lag in the erosional response behind the forcing processes. As noted by Komar and others (1999), the extreme high runup elevations typically occur for only a relatively short period of time (e.g., the period of time in which the high wave runup elevations coincide with high tides). Because the elevation of the tide varies with time (e.g., hourly), the amount of erosion can be expected to be much less when water levels are lower. Thus, it is probable that several storms during a winter may be required to fully realize the degree of erosion estimated by the geometric model; this did, for example, occur during the winter of 1998-1999, with the last five storms the most extreme and erosive (Allan and Komar, 2002). In addition, as beaches erode, sediment is removed offshore (or farther along the shore) into the surf zone where it accumulates in near shore sand bars. This process helps mitigate the incoming wave energy by causing the waves to break farther offshore, dissipating much of the wave energy, and forming the wide surf zones that are characteristic of the Oregon coast. In turn, this process helps to reduce the rate of beach erosion that occurs. In summary, the actual amount of beach erosion and dune recession is dependent on many factors, the most important of which include incident wave conditions,  $T_{WL}$ , and the duration of storm event(s).



### 3.1.2 Kriebel and Dean model

Kriebel and Dean (1993), hereafter known as K&D, developed a dune erosion model that is broadly similar to the geometric model but assumes the beach to be in statistical equilibrium (Bruun, 1962) with respect to the prevailing wave climate and mean water levels. As water levels increase, the beach profile is shifted upward by an amount equal to the change in water level ( $S$ ) and landward by an amount  $R_\infty$  until the volume of sand eroded from the subaerial beach matches the volume deposited offshore in deeper water (Figure 3-2); *note that  $DE_{MAX}$  and  $R_\infty$  are synonymous with each other.* Thus, the maximum erosion potential,  $R_\infty$ , was determined by K&D to be a function of the increase in mean water level ( $S$ ) caused by a storm, the breaking wave water depth ( $h_b$ ), surf zone width ( $W_b$ ), berm or dune height ( $B$  or  $D$ ), and the slope ( $\beta_f$ ) of the upper foreshore beach face.

As a result of the above concepts, K&D developed two approaches for determining the maximum erosion potential::

- A beach backed by a low sand berm

$$R_\infty = \frac{S(W_b - h_b/\beta_f)}{B + h_b - S/2} \quad (3-2)$$

- A beach backed by high sand dune

$$R_\infty = \frac{S(W_b - h_b/\beta_f)}{D + h_b - S/2} \quad (3-3)$$

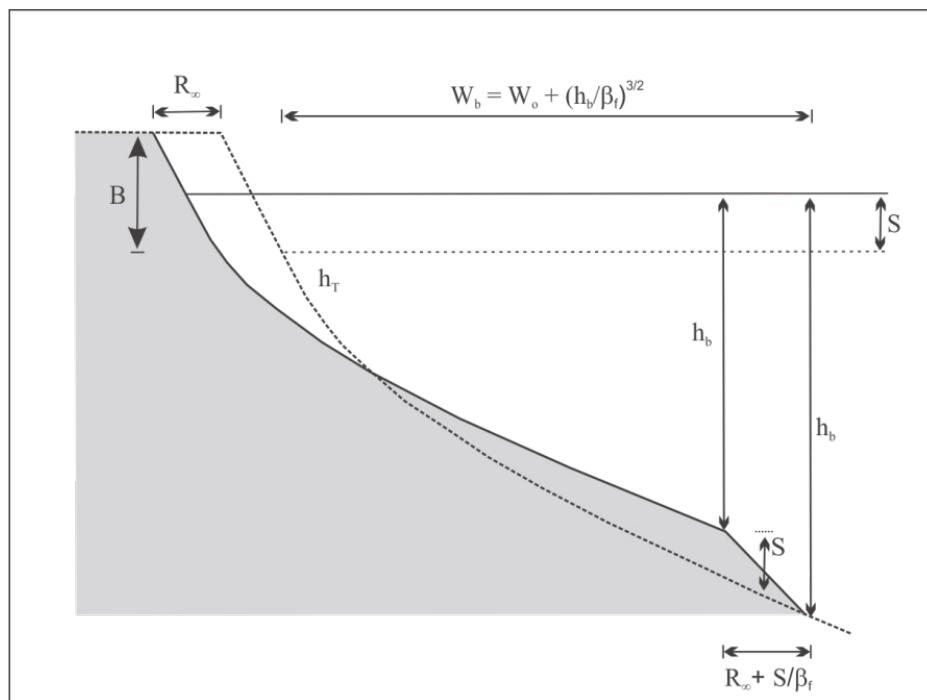


**Figure 3-2.** Maximum potential erosion ( $R_\infty$ ) due to a change in water levels (after Kriebel and Dean, 1993).

Application of the Komar and others (1999) and Kriebel and Dean (1993) dune erosion models provides estimates of the maximum potential erosion ( $DE_{MAX}$  or  $R_{\infty}$ ) associated with a major storm, and assume that a particular storm will last sufficiently long enough to fully erode the dune. As noted previously, in reality  $DE_{MAX}$  is almost never fully realized, because storms rarely last long enough to fully erode the dune. Because the duration of a storm is a major factor controlling beach and dune erosion, K&D developed an approach to account for duration effects of storms with respect to the response time scale required to fully erode a beach profile. The time scale for the erosion of a dune can be estimated using Equation 3-4:

$$T_s = C_1 \frac{H_b^{3/2}}{g^{1/2} A^3} \left( 1 + \frac{h_b}{B} + \frac{\beta_f W_b}{h_b} \right)^{-1} \quad (3-4)$$

where  $T_s$  is the time scale of response,  $C_1$  is an empirical constant (320),  $H_b$  is the breaker height,  $h_b$  is the breaker depth,  $g$  is acceleration due to gravity,  $B$  is the berm elevation, is the slope of the foreshore,  $W_b$  is the surf zone width, and  $A$  is the beach profile parameter that defines an equilibrium profile. Using Equation 3-4 yields typical response times for complete profile erosion that are on the order of 10 to 100 hours (Allan and others, unpub. data, 2014). In general, as the surf zone width increases due to larger wave heights, smaller grain-sizes or gentler slopes, the response time increases. The response time will also increase as the height of the berm increases.

The actual beach profile response is dependent on the storm hydrograph and, specifically, the duration of the storm. Thus, if the storm duration,  $T_D$ , is long relative to the time scale of profile response,  $T_s$ , then a significant portion of the estimated erosion determined by the K&D or geometric model will occur. As the ratio of these two values decreases, the amount of erosion also decreases. Solving the degree of beach erosion due to the duration of a storm is complicated and is fully described by Allan and others (unpub. data, 2014). However, the end product is a reduction factor ( $\alpha$ ) that is used to reduce the amount of erosion:

$$DE_m = \alpha DE_{MAX} \quad (3.5)$$

For the purposes of this study, we used the maximum duration-limited recession value ( $DE_m$ , per sublittoral cell) derived from the detailed FEMA coastal flood study for Tillamook County (Allan and others, unpub. data, 2014) and applied it uniformly to our dune-back lidar transects to generate a hazard scenario reflecting the erosion that may occur during a single storm. This scenario is independent of coastal erosion calculations undertaken using the geometric model. The specific values associated with the results of the K&D modeling generated from the work of Allan and others (unpub. data, 2014) is described in Section 4.1.3.

### 3.2 Wave and tide processes

Beach and dune erosion is dependent on total water levels ( $T_{WLS}$ ), which combine high wave runup, extreme high astronomical tides, and storm surges. Allan and others (unpub. data, 2014) performed a detailed analysis of the wave environment and measured tides and storm surges for the purposes of developing new FEMA coastal flood maps for Tillamook County. The product of their study included a probabilistic analysis of the calculated 10%, 2%, 1%, and 0.2%  $T_{WLS}$  (10-, 50-, 100- and 500-year storm events, respectively) at 178 study reaches along the length of the county coastline. For the purposes of this study we have leveraged many of the results from their study. For more detail, please refer to the study by Allan and others (unpub. data, 2014.)

#### 3.2.1 Pacific Northwest wave climate

The wave climate offshore from the Oregon coast is one of the most extreme in the world, with winter storm waves regularly reaching heights in excess of 8 m (26 ft); extreme waves in excess of 10 m (33 ft) are not uncommon. This is because the storm systems emanating from the North Pacific travel over fetches that are typically a few thousand miles (965–1,930 km [600–1,200 mi]) long and are characterized by strong winds, the two main factors that account for the development of large wave heights and long wave periods (Tillotson and Komar, 1997). These storm systems originate near Japan or off the Kamchatka Peninsula in Russia and typically travel in a southeasterly direction across the North Pacific toward the Gulf of Alaska, eventually crossing the coasts of Oregon and Washington or along the shores of British Columbia in Canada (Allan and Komar, 2002).

Wave statistics (heights and periods and more recently wave direction) have been measured in the Eastern North Pacific using wave buoys and sensor arrays since the mid 1970s. These data have been collected by the National Data Buoy Center (NDBC) of NOAA and by the Coastal Data Information Program (CDIP) of Scripps Institution of Oceanography (Figure 3-3). The buoys cover the region between the Gulf of Alaska and Southern California and are located in both deep and intermediate to shallow water over the continental shelf. The NDBC operates some 30 stations along the West Coast of North America, while CDIP has at various times carried out wave measurements at 80 stations. Presently, two CDIP buoys (#46243 and #46248) and three NDBC buoys (Washington [#46005], Tillamook [#46089], and Columbia River Bar [#46029]) operate offshore from the mouth of the Columbia River. Wave measurements by NDBC are obtained hourly (CDIP provides measurements every 30 minutes) and are transmitted via satellite to the laboratory for analysis of wave energy spectra, significant wave heights, and peak spectral wave periods. These data can be obtained directly from NDBC through their website (<http://www.ndbc.noaa.gov/maps/Northwest.shtml>).

Measured data obtained from wave buoys may have significant data gaps due to the instruments having come off their mooring or from instrument failure. An alternative source of wave data is hindcast, or modeled, wave data. GROW (Global Reanalysis of Ocean Waves) is a high-resolution regional (Pacific Northwest) wave model incorporating basin-specific wind adjustments based on NASA QuikSCAT (Quick Scatterometer) scatterometry, enhancements due to Southern Ocean swells, and inclusion of shallow water physics (Oceanweather, Inc., 2010). The study by Allan and others (unpub. data, 2014) explored both measured and modeled data sets in order to define the most appropriate time series of wave data to be used for coastal wave runup and flood mapping along the Tillamook County coastline.

The measured wave data were input into SWAN (Simulating WAVes Nearshore), version 40.81, a third-generation wave model developed at the Technical University of Delft, Netherlands (Booij and others, 1999; Ris and others, 1999), to transform the deepwater waves to the nearshore (typically the 20 m [65.6 ft] contour). This step is important in order to account for the effects of wave shoaling across the continental shelf,

essentially accounting for the effects of wave refraction and diffraction. After the wave were transformed, wave heights were then linearly shoaled back into deepwater to derive a refracted deepwater equivalent wave parameterization (wave height and peak period) that can be used ultimately to calculate the wave runup. These, combined with the measured tides, are used to calculate final  $T_{WLS}$  along the Tillamook County shoreline.

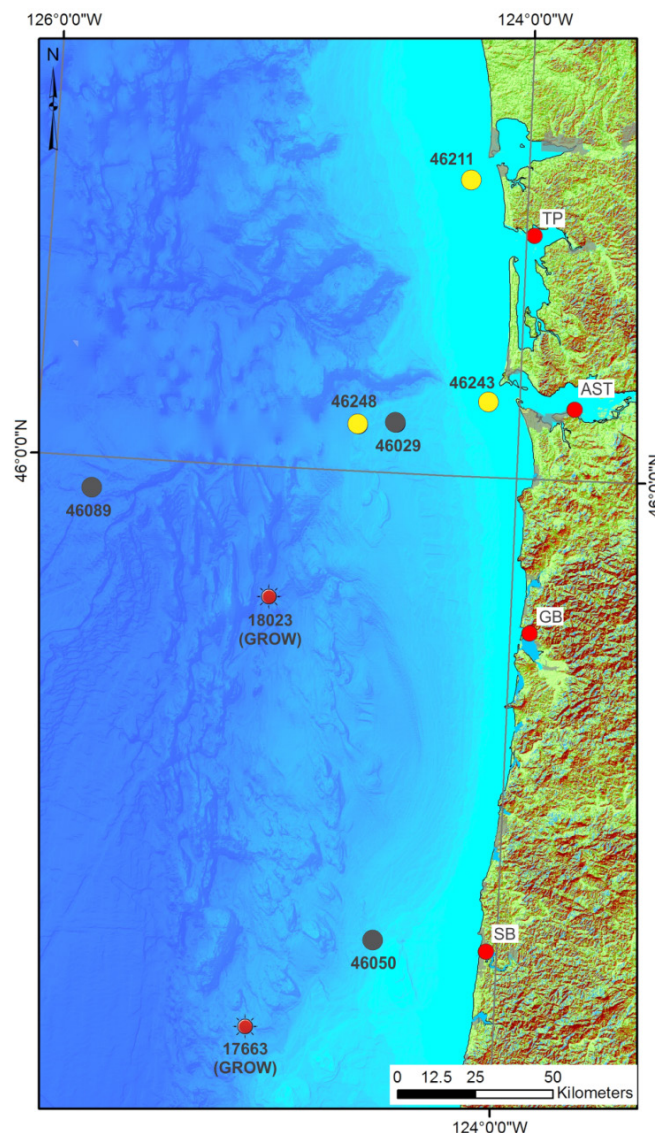


**Figure 3-3.** Location map of NDBC (black) and CDIP (yellow) wave buoys, tide gauges (red), and GROW wave hindcast stations (red suns) (Allan and others, unpub. data, 2014).



3.2.2 Tides

Tides along the Oregon coast are classified as moderate, with a maximum range of up to 4.3 m (14 ft) and an average range of about 1.8 m (6 ft) (Komar, 1997). There are two highs and two lows each day, with successive highs (or lows) usually having markedly different levels. Tidal elevations are given in reference to the mean of the lower low water levels (MLLW) and can be adjusted easily to the NAVD88 vertical datum. As a result, most tidal elevations are positive numbers with only the most extreme lower lows having negative values.

Allan and others (unpub. data, 2014) used a combined time series that encompassed tides measured hourly at the Southbeach (SB) gauge (#9435380) in

Yaquina Bay (1967–2005) and from the Garibaldi (GB) tide gauge (#9437540) in Tillamook Bay (2005-2011) for a combined time series of 1967–2011 (Figure 3-3). Figure 3-4 shows the tidal elevation statistics derived from the South Beach tide gauge (the longest temporal record), with a mean range of 1.91 m (6.3 ft) and a diurnal range of 2.54 m (8.3 ft). The highest tide measured from this record reached 3.73 m (12.2 ft), recorded in December 1969 during a major storm. These values are comparable to those measured at the Garibaldi site (mean = 1.9 m [6.2 ft], diurnal = 2.53 m [8.30 ft]), with the only real difference being that the Garibaldi gauge recorded a peak water level of 3.64 m (11.9 ft) in December 2005.

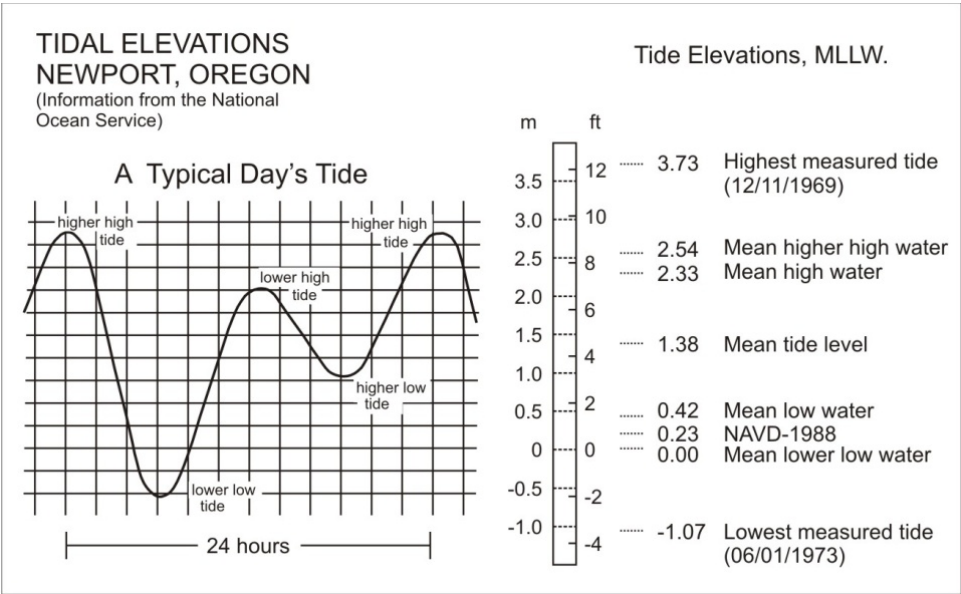


**Figure 3-4.** Daily tidal elevations measured at Southbeach, Newport on the central Oregon coast. Data from NOS (<http://www.co-ops.nos.noaa.gov/waterlevels.html?id=9435380>).

Tides on the Oregon coast tend to be enhanced during the winter months due to warmer water temperatures and the presence of northward flowing ocean currents that raise water levels along the shore, persisting throughout the winter rather than lasting for only a couple of days as is the case for a storm surge. This effect can be seen in the monthly averaged water levels derived from the combined time series (Figure 3-5) but where the averaging process has removed the water-level variations of the tides to yield a mean water level for the entire month. Based on 45 years of data, the results in Figure 3-5 show that on average monthly-mean water levels during the winter are nearly 25 cm (0.8 ft) higher than in the summer.

### 3.2.3 El Niño

The PNW coast is periodically influenced by the El Niño Southern Oscillation phenomenon, which causes mean sea levels along the U.S. West Coast to increase beyond the typical seasonal cycle characteristic of the PNW coast (Komar and others, 2011). This response is due to an intensification of the processes that tend to raise mean sea levels, particularly enhanced ocean sea surface temperatures offshore from the Oregon coast. This occurred during the unusually strong 1982-1983 and 1997-1998 El Niños. As seen in Figure 3-5, water levels during El Niño climate events were approximately 25–30 cm (0.8–1 ft) higher than the seasonal peak, and as much as 56 cm (1.8 ft) higher than during the preceding summer, enabling wave swash processes to reach much higher elevations on the beach during the winter months, with storm surges potentially raising the water levels still farther. As a result, under these conditions wave swash processes are able to reach to much higher elevations on the beach, potentially eroding dunes and bluffs. Because these processes are effectively captured in the measured tides, the effect of El Niños is embedded for several of the storms and hence in the final calculated  $T_{WLs}$ .

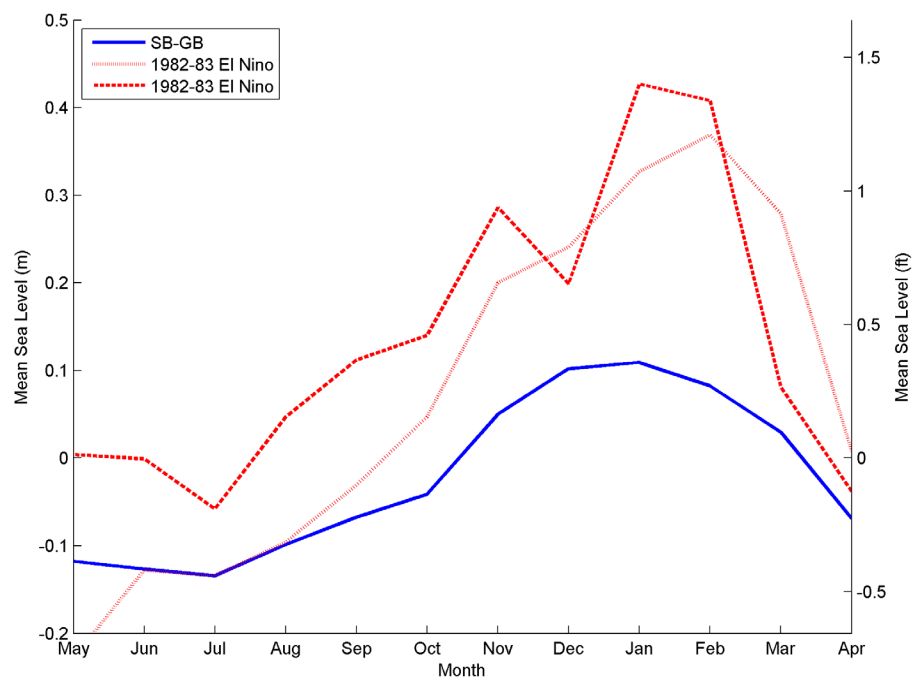


**Figure 3-5.** Seasonal cycles in monthly-mean water levels based on data from the combined Southbeach/Garibaldi measured tides.

### 3.2.4 Storm surge

The actual level of the measured tide can be considerably higher than the predicted tides provided in standard tide tables and is a function of a variety of atmospheric and oceanographic forces, which ultimately combine to raise the mean elevation of the sea. These latter processes also vary over a wide range of time scales and may have quite different effects on the coastal environment. For example, strong onshore winds coupled with the extreme low atmospheric pressures associated with a major storm can cause the water surface to be locally raised along the shore as a storm surge and have been found in tide gauge measurements to be as much as 1.4 m (4.9 ft) on the Oregon coast (Allan and Komar, 2002; Allan and others, 2011). However, during the summer months these processes can be essentially ignored due to the absence of major storm systems. Allan and others (2011) performed an analysis of the nontidal residuals (the difference between the astronomical and measured tide) and, ultimately, the storm surges identified at various tide gauges on the central to northern Oregon coast. The study indicated that Pacific Northwest storm surges are generally small, averaging about 0.4 m (1.3 ft), while 95% of the surges were less than 0.8 m (2.6 ft). The study by Allan and others provided a better understanding of the overall spatial and temporal variability of PNW storms as they track across the North Pacific, the magnitudes (and frequency) of the surges, and the potential differences in the nontidal residuals between the gauges due to variations in the storms tracks, barometric pressures, and winds. Because the effects of storm surges are effectively captured in the measured tides, the effect of storm surges is embedded in the final calculated  $T_{WLS}$ .

### 3.2.5 Sea level rise

Global sea level has risen approximately 20 cm (0.66 ft) during the 20th century at an average rate of  $\sim 1.75$  mm/yr ( $\sim 0.07$  in/yr) (Holgate, 2007). The rate of sea level rise (SLR) has accelerated over the last few decades, reaching rates of 2.8 to 3.4 mm/yr (0.11 to 0.13 in/yr), determined from satellite altimetry (Cazenave and Llovel, 2010), although some of this probably reflects steric (temperature and salinity) variations due to interdecadal ocean cycles. SLR must be considered when predicting future coastal change.

On the Oregon coast, historic rates of relative sea level change vary from a decrease of  $-0.62 \pm 0.35$  mm/yr ( $-0.024 \pm 0.014$  in/yr) at Astoria on the northern Oregon coast, to an increase of  $+1.33$  mm/yr  $\pm 0.79$  mm/yr ( $+0.05 \pm 0.03$  in/yr) on the central coast (Figure 3-6), and a decrease of  $-1.10$  mm/yr  $\pm 0.5$  mm/yr ( $-0.04 \pm 0.02$  in/yr) on the northern California coast at Crescent City (Komar and others, 2011). Differences in the responses at these sites (and others) reflect the effects of regional tectonics, such that the southern Oregon coast (south of about Coos Bay) is presently an emergent coast as tectonic uplift outpaces sea level rise, while the central to northern Oregon coast (including Tillamook County) is gradually being submerged (i.e., sea level rise exceeds tectonic uplift).



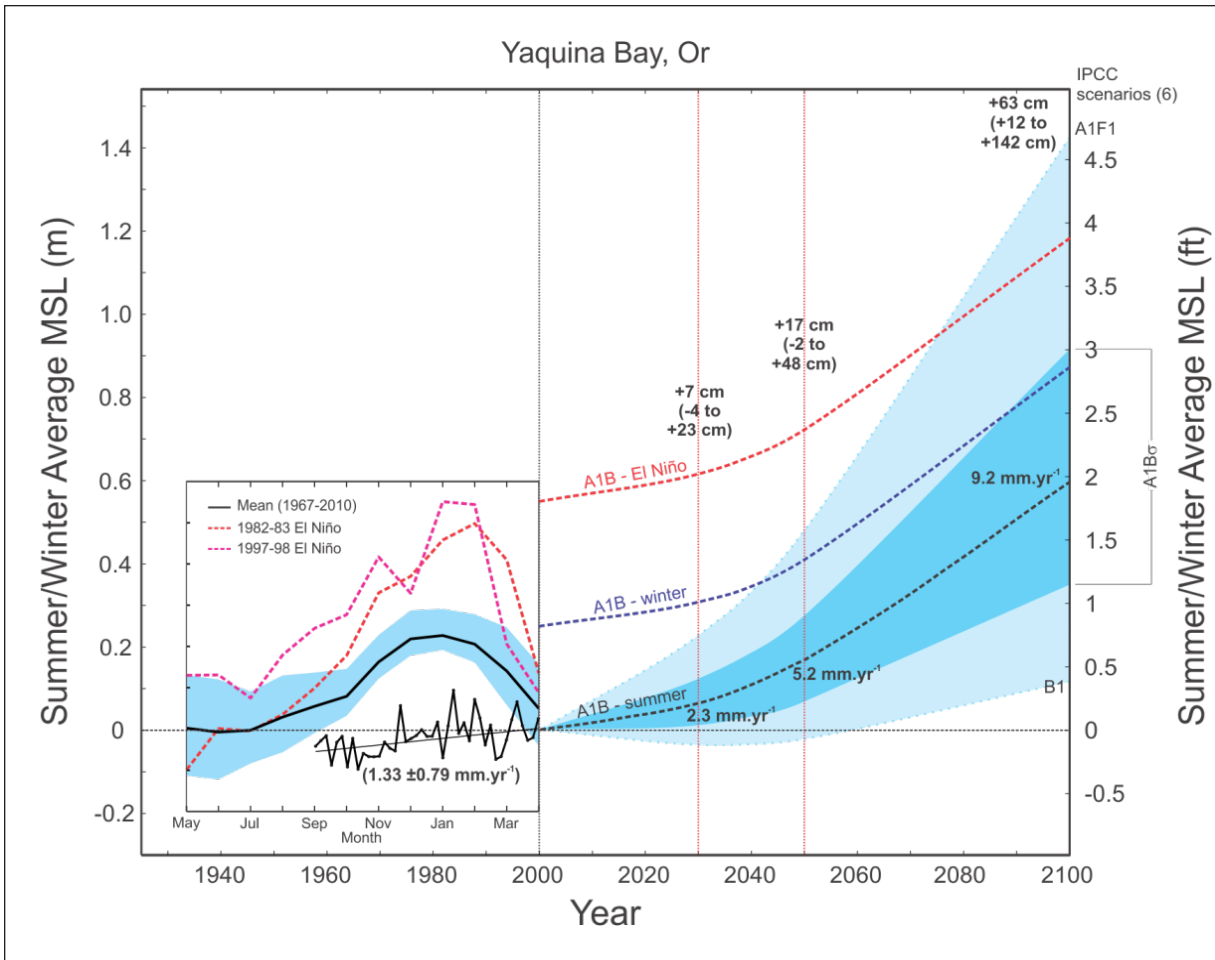


**Figure 3-6.** Projections of future sea level rise for the central Oregon coast. Dashed lines reflect the mid-range (A1B) estimate. Darker shading depicts the uncertainty for the A1B scenarios, while lighter shading reflects the uncertainty for all global climate models. Inset figure depicts the seasonal and El Niño cycle in monthly mean sea levels along with the historical rate of sea level rise determined for the Newport tide gauge.

In December 2010, state and federal agencies on the U.S. West Coast commissioned a sea level change study by the National Academy of Sciences with the expressed purpose of deriving future projections of SLR for the years 2030, 2050, and 2100. Importantly, a major component of the study was to incorporate such factors as regional tectonics, glacial isostatic adjustments, and tide gauge information in order to constrain the estimates to the regional level (NRC, 2012). For the central Oregon coast the results of the report indicate that mean sea level is projected to increase as follows (NRC, 2012):

- by 2030: +7 cm (2.8 in)  
(-4 to +23 cm range [-1.6 to +9.1 in range])
- by 2050: +17 cm (6.7 in)  
(-2 to +48 cm range [-0.8 to +18.9 in range])
- by 2100: +63 cm ( 2.1 ft)  
(+12 to +142 cm range [+0.4 to +4.7 ft range])

These projections are presented conceptually in Figure 3-6, which demonstrates the effect of these increases under a range of mean sea level conditions (summer, winter, and El Niño effects) typical of the Oregon coast, forecast for the next 85 years.

For the purposes of this study, we considered three (low, medium, and high) SLR scenarios shown in Table 3-1 for the 2030, 2050, and 2100 time frames. The low range values for 2030 and 2050 are based on the historical rate of change identified for the Newport tide gauge (Komar and others, 2011), *not* the low range values from the NRC (2012) study. This is because there is no physical reason for this pattern to gradually reverse itself in the foreseeable future.

**Table 3-1.** Relative sea level rise values for the north-central Oregon coast for low, medium, and high hazard zone scenarios (after NRC, 2012; Komar and others, 2011).

	Sea Level Rise Scenario					
	Low		Medium		High	
	(m)	(ft)	(m)	(ft)	(m)	(ft)
Year 2030	0.02	0.07	0.07	0.23	0.23	0.75
Year 2050	0.05	0.16	0.17	0.56	0.48	1.57
Year 2100	0.12	0.39	0.63	2.07	1.42	4.66

To estimate how beaches and dunes might respond to SLR, we used the widely cited Bruun (1962) method:

$$R = \frac{L_*}{B + h_*} S \quad (3-6)$$

where  $R$  is the shoreline retreat rate,  $L_*$  is the cross-shore distance to the water depth  $h_*$ ,  $B$  is the vertical dune elevation that may be eroded, and  $S$  is the expected amount of sea level rise as presented in Table 3-1. This two-dimensional mass conservation principle assumes that as a dune profile becomes inundated with water levels caused by a rising sea, the dune profile will translate landward and up in elevation until a new equilibrium is established while the shape of the dune profile is unchanged. Table 3-2 summarizes estimated erosion distances associated with SLR across the county. A complete list of SLR erosion at each transect is provided in a digital spreadsheet that accompanies this report.

**Table 3-2.** Summary of the estimated erosion associated with sea level rise. Three erosion estimates are calculated for each time period (high, medium, and low). The three time periods equate to our proposed High, Medium, and Low hazard zones.

Estimates vary at individual sites based on beach characteristics. This table reports the maximum, mean, and standard deviation of all nine erosion estimates across all Tillamook County transects.

Hazard Zone	Estimated Erosional Distance								
	Year 2030			Year 2050			Year 2100		
	Low	Medium	High	Low	Medium	High	Low	Medium	High
Maximum (m)	3.3	11.7	38.3	8.3	28.3	80.0	20.0	105.0	236.7
Mean (m)	1.4	5.0	16.3	3.6	12.1	34.0	8.5	44.7	100.7
Standard deviation (m)	0.3	1.0	3.3	0.7	2.4	6.8	1.7	8.9	20.08
Maximum (ft)	10.9	38.3	125.8	27.3	93.0	262.5	65.6	344.5	776.5
Mean (ft)	4.7	16.3	53.5	11.6	39.5	111.7	27.9	146.6	330.4
Standard deviation (ft)	0.9	3.2	10.7	2.3	7.9	22.3	5.6	29.2	65.9

### 3.3 Wave runup and total water levels

Wave runup is the culmination of the wave breaking process whereby the swash of the wave above the mean sea level is able to run up the beach face, where the wave may encounter a dune, structure, or bluff, potentially resulting in the erosion, or overtopping and flooding of adjacent land.

A variety of models have been proposed for calculating wave runup on beaches. Detailed studies of wave runup under a range of wave conditions and beach slopes (Ruggiero and others, 1996; Ruggiero and others, 2001; Stockdon and others, 2006) have yielded the following relationship for estimating the 2% exceedance runup elevation ( $R_{2\%}$ ):

$$R_{2\%} = 1.1 \left( 0.35 \tan \beta (H_o L_o)^{\frac{1}{2}} + \frac{[H_o L_o (0.563 \tan \beta^2 + 0.004)]^{\frac{1}{2}}}{2} \right) \quad (3-7)$$

where  $\tan \beta$  is the foreshore beach slope,  $H_o$  is the deepwater wave height, and  $L_o$  is the deepwater wave length given by  $L_o = (g/2\pi)T^2$ , where  $T$  is the wave period and  $g$  is acceleration due to gravity ( $9.81 \text{ m/s}^2$ ).

Combining the calculated wave runup (Equation 3-7) with the measured water level at tide gages produces the total water level at the shore. Importantly, having been originally developed using quantitative measurements from PNW beaches, the model is valid for the range of slopes and conditions observed along the Tillamook County coastline and elsewhere on the Oregon coast.

In summary, the development of storm-induced total water levels ( $T_{WL}$ s) by Allan and others (unpub. data, 2014) proceeded in the following order:

1. A long (~30 year) time series of hourly measured wave conditions was developed at approximately the shelf edge offshore of the study area;
2. The SWAN model was run with a full range of input conditions, using constant offshore boundary conditions, to compute bathymetric induced wave transformations up to wave breaking; 2,184 simulations of potential wave conditions were run using SWAN;
3. A “lookup table” approach from the suite of SWAN simulations was implemented to adjust the deepwater wave data;
4. Storm wave data were transformed by using the “lookup table” approach in order to generate an alongshore varying time series of waves at approximately the 20-m depth contour along the length of the study area;
5. Wave height data were shoaled back linearly into deepwater to derive a refracted deepwater equivalent wave parameterization (wave height and peak period) that could be used ultimately to calculate the wave runup;
6. Approximately 150 discrete storms that have impacted the Tillamook County coast during the past 30 years were identified;
7. Using the deepwater equivalent alongshore varying wave conditions and the appropriate measured tides from the combined Yaquina Bay/Garibaldi time series, a time series of  $T_{WL}$ s for 178 study reaches, characterized by beach profile sentinel stations, along the Tillamook County coast was computed. These included sentinel transects established on Nehalem Spit/Manzanita (21 sites), Twin Rocks/Rockaway/Nedonna Beach (40 sites), Bayocean Spit (11 sites), Short Sand beach (3 sites), Netarts Spit/Oceanside (29 sites), Tierra Del Mar/Sand Lake (32 sites), Nestucca Spit/Pacific City (14 sites) and Neskowin (28 sites).
8. The 10, 50, 100, and 500-year  $T_{WL}$  elevations were computed by using a Poisson-Generalized Pareto Distribution with a peak-over-threshold (POT) approach (e.g., Coles, 2001; Ruggiero and others, 2010).

For this study we calculated erosion distances using the 10%, 2%, and 1% (10-, 50- and 100-year, respectively)  $T_{WL}$  elevations derived from the study by Allan and others (unpub. data, 2014). This approaches spans the spectrum of significant events that the County could experience in any given year and for different storm event magnitudes.



### 3.4 Beach and shoreline morphology

Changes in the morphology of the dune-backed beaches along the Tillamook County coast were derived from an analysis of high-resolution lidar data as well as from up-to-date GPS surveys of the beaches. These data sets allow us to document the spatial and temporal variability of the shore and provide the starting point on which to base the erosion hazard modeling. Lidar data were acquired in 1997, 1998, and 2002 by the U.S. Geological Survey (USGS), the National Aeronautics and Space Administration (NASA), and the National Oceanic and Atmospheric Association (NOAA). In particular, the 1998 lidar data measured at the end of the major 1997-1998 El Niño provide the only measurements (other than from site-specific GPS measurements) of the beach in an eroded state, as the beach was measured at the end of the 1997-1998 El Niño winter. The 1997, 1998, and 2002 lidar data were downloaded from NOAA's Coastal Service Center, gridded in Esri® ArcGIS® using a triangulated irregular network (TIN) algorithm. Distance and elevation data were extracted from the grid lidar digital elevation models (DEMs) (Allan and

Harris, 2012). Lidar data measured by Watershed Sciences, Inc. (WSI) in 2009 and 2011 for DOGAMI were also integrated into the beach profile data set (Allan and Harris, 2012). Lidar data collected in 2010 by the U.S. Army Corps of Engineers (USACE) were not used in this study due to problems with the data.

Beach-dune junctures and beach slopes were extracted from the four lidar data sets (1998, 2002, 2009, and 2011) at transects spaced 25 m (82 ft) apart. Beach-dune junctures were visually identified from a graphical representation of the data much like the example shown in Figure 3-7. Features used to distinguish the beach-dune juncture included erosion scarps, major breaks in slope, or some combination. Beach slopes were estimated using standard linear regression techniques and included those data seaward from the beach-dune juncture down to the 2.0-m (6.6-ft) contour elevation relative to the NAVD88 datum. Approximately 2,000 transects were included in this study, providing a detailed analysis of morphology along the dune-backed shoreline. Beach morphology values can be found in the geodatabase and spreadsheet files included with this publication.

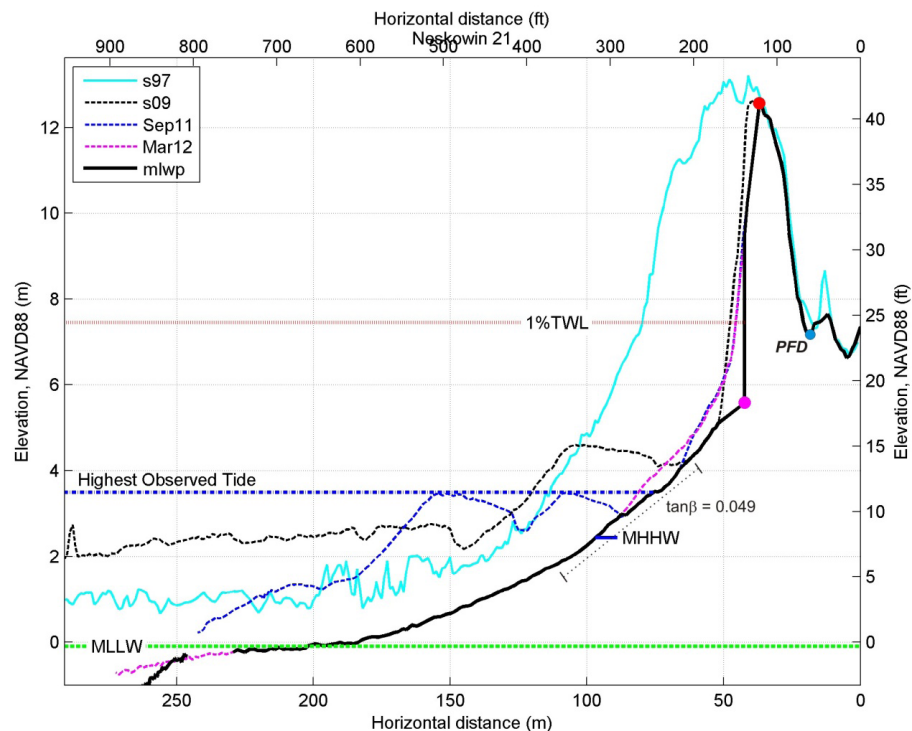


**Figure 3-7.** An example cross-section established adjacent to Camp Winema in the Neskowin cell showing both recent RTK-DGPS surveys and measurements from 1997, 1998, and 2009 lidar data. Beach morphological features (dune crest [red circle], beach-dune junction [magenta circle], and beach slope) are indicated in the plot.

Our initial focus was to perform sensitivity testing in order to better understand the relative effects of both the local beach slope and beach-dune juncture elevations on the calculated erosion distances. To accomplish this, preliminary erosion distances were calculated using arbitrary oceanographic conditions and the actual local beach morphology parameters (i.e., slope and beach-dune juncture elevation). The results clearly demonstrated that the calculated erosion distances are highly sensitive to the unique values at each transect, especially the beach slope. In general, beaches characterized with lower beach slopes and lower beach-dune juncture elevations produced the widest erosion hazard zones. Conversely, steeper beaches with higher beach-dune juncture elevations produced the narrowest zones. Furthermore, in a number of locations such as adjacent to creek outlets or dune blowouts, the erosion hazard calculations tended to substantially under- (or over-) estimate the width of the erosion distances. Because the processes causing these latter perturbations tend to be highly variable both spatially and temporally, such patterns may not necessarily reflect the broader regional patterns characteristic along a particular cell or subcell. As a result, basing the final calculated hazard zones on the original slopes and beach-dune juncture elevations may not necessarily be appropriate. Accordingly, the decision was made to smooth the beach-dune juncture elevations and slopes within each littoral subcell by using a moving average of 100 m (328 ft), effectively removing much of the alongshore noise associated with such morphologic perturbations. Final erosion distances were subsequently calculated using the maximum and minimum smoothed beach-dune juncture elevations (at every transect location) to evaluate the uncertainty in the calculated erosion distances due to morphologic variations. A third morphologic variation, the beach-dune juncture calculated by Allan and others (unpub. data, 2014), was also considered in an effort to maintain consistency with their study.

Erosion distances are measured landward from a baseline beach-dune juncture. For each transect there four beach-dune junctures derived from each of the four lidar data sets reflect four different beach conditions. For the purposes of the Tillamook County maps,

we used the most landward of the four locations (at each transect) as the baseline  $E_j$  and hence the starting point on which to base the final erosion hazard zones. This approach is conservative in that it ignores the fact that there may have been some accretion between 1998 and 2011 (e.g., in areas such as along Bayocean or Nehalem spits) while accounting for the erosion that has occurred along much of the county coastline (e.g., Neskowin and Rockaway); note that the mapping does not reflect any additional erosion that has occurred post 2011.

Roughly 12% of the dune-backed beaches in Tillamook County are fronted by riprap coastal engineering structures. The majority of these structures occur along three communities: Neskowin, Tierra Del Mar, and Rockaway (~250 individual transects span these discrete areas). The presence of the riprap highlights the effects of recent erosion in these areas, which accelerated in the late 1990s. The erosion distances calculated in this report rely upon the assumption that the beach is backed by a sandy dune which erodes in response to ocean waves. In the case of riprap, the dune is essentially replaced by a “fixed” structure, such that no additional foredune erosion is likely to take place. However, as sea level continues to increase into the future and because many of these structures are already subject to increasing wave attack, the structures themselves can periodically fail, potentially affecting the viability of homes built immediately adjacent to the eroding coast and in some cases the entire community (Figure 3-8). To that end, we have mapped areas backed by a structure according to two assumptions:

- Erosion occurs in the absence of a structure and the entire shoreline shifts landward; and,
- The shoreline is fixed to the structure and no additional retreat takes place. Thus the erosion hazard zones converge to the landward edge of the structure.

Using this approach, we have separately mapped erosion zones for areas backed by coastal engineering structures, depicting the hazard zones in a different color in order to highlight these two potential responses.



**Figure 3-8.** (left) Storm waves damage a riprap structure during a moderate storm in January 2008 in the community of Neskowin (Photo: A. Thibault, 2008); (Right) A rip embayment sets up immediately in front of the Shorewood RV park, Twin Rocks, enabling waves to attack the structure during storms. (Photo: D. Best, 2007)

### 3.5 Cascadia subduction zone

As discussed in Section 2.3, an earthquake on the Cascadia subduction zone will result in a nearly instantaneous lowering of the coast, which equates to raising sea level by the same amount. This will result in extensive erosion of the coast as the beaches and shorelines adjust to a new equilibrium condition.

A key component to the tsunami modeling was numerical modeling of the fault zone (Wang, 2007) including a grid depicting the post-earthquake (i.e., deformed) North American plate (Witter and others, 2011). It is this deformation that is responsible for subsidence along the Oregon coast. We extracted the Mean Higher High Water shoreline contour located at an elevation of 2.3 m (7.6 ft) (NAVD88 vertical datum) from pre- and post-earthquake modeled topography. Having extracted the pre- and post earthquake shoreline, we then calculated the change in shoreline position and applied this change to all the lidar transects, to approximate the sudden landward shift in the beach profile. This assumption is consistent with the general principles of the geometric, K&D, and Bruun models, which propose an upward and landward shift of the entire profile as a result of an increase in ocean water levels along a particular coast.

This latter scenario is meant to depict a potentially worst-case response and is intended to provide an understanding of the dramatic coastal erosion effects that will take place along the Tillamook County coast following a CSZ earthquake.

### 3.6 Scenarios of coastal change in Tillamook County

For the purposes of mapping coastal erosion hazard zones in Tillamook County, we have made a number of assumptions concerning potential future climate effects. First, we assumed that the magnitude of future storms is unlikely to be significantly different from those that have occurred in the recent past. As a result, we do not account for any potential changes in the frequency or magnitudes of major storms and hence any increase (or decrease) in the associated storm-induced wave heights. Second, we assumed that the magnitude of past El Niños will remain much the same as in the future. Because the effects of these events are already integrated in the measured tides, no further changes were implemented here. Third, we assumed that the magnitude of storm surges on the Oregon coast will remain much the same. Fourth, on the basis of the regional sea level study by the NRC (2012), we assumed that regional sea levels will increase in the future and, further, that the rise in sea level will accelerate out to 2100. With these assumptions in mind, we modeled a total of 81 potential scenarios of shoreline erosion hazard zones for the dune-backed beaches of Tillamook County using the Komar and others (1999) geometric model in order to generate the most reasonably conservative hazard zones. The scenarios reflected the following range of conditions:

- Three total water level ( $T_{wLs}$ ) scenarios associated with 10%, 2%, and 1% storm events;



- Three beach-dune juncture elevations. These included the lowest smoothed  $E_j$ , values of  $E_j$  derived from an analysis of the winter beach conditions (Allan and others, unpub. data, 2014), and the highest smoothed  $E_j$ ; and,
- Three sea level rise conditions (low, middle, and high ranges) determined for 2030, 2050, and 2100.

The complete suite of erosion hazard scenarios (81) have been further categorized into the same general hazard zones originally developed by Allan and Priest (2001), each of which accounts for various combinations (27 in each) of extreme  $T_{WL}$ s, beach conditions, and future projections of SLR (3  $T_{WL}$   $\times$  3 beach-dune junctures  $\times$  3 SLR). Thus, modeled erosion hazards that encompass a rise in sea level projected for 2030 (16 years from now) will be incorporated into the *High hazard zone* (Hhz) scenarios; SLR projections for 2050 will be incorporated into the *Medium hazard zone* (Mhz) scenarios, and 2100 predictions into the *Low hazard zone* (Lhz) scenarios. The suite of scenarios represents uncertainty in the calculated erosion distances due to variations in the  $T_{WL}$ s and beach conditions. Appendix A describes the parameters used for each scenario; erosion distances for each scenario are provided in the attached geodatabase and spreadsheet files for the individual transects used.

Two additional scenarios are included as part of this work. The first is the duration-limited erosion hazard zone determined using the K&D approach (these results are described in Section 4.3). Finally, we include a worst-case scenario that reflects the landward shift in the entire beach profile immediately following a CSZ earthquake. This latter scenario is analogous to instantaneously raising mean sea level by as much as 3 m (10 ft) along the Oregon coast, resulting in widespread erosion.

## 4.0 RESULTS

This section presents the modeled erosion hazard zones. Calculations of erosion for the dune-backed beaches in Tillamook County were determined, first, by applying the geometric model to assess the storm-induced erosion and, second, by applying the Bruun model to account for the gradual retreat of the beaches

due to the projected future rise in sea level at 2030, 2050, and 2100. Combined, the two calculations yield the maximum potential erosion distances ( $DE_{MAX}$ ) shown conceptually in Figure 3-1B. As described in Section 3.6, the erosion hazard zones are based on a total of 83 possible scenarios. These zones have been overlaid on a Google Maps™ digitally rectified orthophoto of the study area with the results shown in Figures 4-1 for the Neskowin community; the final maps for the entire coastline are included in Appendix B. The complete suite of calculated erosion distances (as point data), and modeled hazard lines are available in a digital form, accompanying this report.

### 4.1 Projected coastal erosion hazard zones

Each of the coastal erosion hazard zones (High, Medium, and Low) consists of 27 potential erosion scenarios that account for a broad spectrum of forcing conditions including variations in the magnitudes of the storms, changing beach conditions (i.e., summer versus winter), and projected future increases in sea level. The key factor that largely differentiates the relative widths of the hazard zones is the erosion response due to sea level rise (Table 3-2), especially when considering the potential for high rates of sea level rise late this century. This contrasts with the calculated erosion determined for the storms (Table 4-1). The large standard deviations presented in Table 4-1 are entirely due to variations in the local beach morphology (i.e., the beach slope and beach-dune juncture elevations). In all cases, the erosion distances are relative to the most landward beach-dune juncture locations as described in Section 3.4 and shown in Figure 4-1.

**Table 4-1.** Calculated erosion distances determined for Tillamook County using the geometric model. Values presented in the table were derived by using 10%, 2%, and 1% total water levels ( $T_{WL}$ s) and the local beach morphology and exclude sea level rise.

	Erosion Distance					
	10% $T_{WL}$		2% $T_{WL}$		1% $T_{WL}$	
	(m)	(ft)	(m)	(ft)	(m)	(ft)
Average width	33.1	108.6	45.1	148.0	50	164.1
Standard deviation	22.9	75.1	26.8	87.9	28.7	94.2



**Figure 4-1.** Modeled erosion hazard zones for Neskowin showing all 83 scenarios of change (lines). In all cases, the hazard lines are relative to the location of the landward  $E_j$  line. White circles depict actual locations of the  $E_j$ /structure toe defined from lidar transects spaced 25 m (82 ft) apart.

Table 4-2 provides a summary of the calculated erosion distances based on the mean (and standard deviation) of all 27 scenarios within the three broad hazard zone classes. As can be seen from the table, the High hazard zone (Hhz) has an average width of 44 m (143 ft), while the standard deviation is 13 m (43 ft), giving a potential range of 30 to 58 m (98 to 190 ft). On average, these results reflect about a 47% reduction in the width of the Hhz, when compared to Allan and Priest (2001); in general the Medium hazard zone (Mhz) and Low hazard zone (Lhz) decreased by ~61% and 41% respectively.

The overall decrease in the width of the calculated erosion hazard zones is largely due to the updated coastal hydraulic modeling undertaken for the Tillamook County coastline (Allan and others, unpub. data, 2014), which involved a probabilistic analysis of the total water level ( $T_{WL}$ ) derived from over 30 years of combined wave and tide data. This contrasts with the approach used by Allan and Priest (2001), which involved three scenarios of future storm-induced erosion that were based on two combinations of wave heights (2% wave height at 17-sec peak period [high

hazard zone] and 1% wave height at 25-sec peak period [low hazard zone]) superimposed on a MHHW tide and combined with a seasonal increase in the water level that included an El Niño effect and a storm surge (1 m [3.3 ft, high hazard zone] and 1.7 m [5.6 ft, high hazard zone]), producing the high  $T_{WL}$ s shown in Figure 4-2. Figure 4-2 highlights the relative differences between the two approaches. The top plot shows the calculated  $T_{WL}$ s using the same deterministic approach for the High (black) and Moderate (red) hazard zone scenarios, modeled for a range of beach slopes. The blue lines show the same overall effect but defined using the combined wave and tide time series. As shown in Figure 4-2 (bottom), differences in the two approaches are even more apparent when modeling the calculated erosion distances. For example, erosion differences range from as much as 30 m (85 ft) for a low sloping beach ( $\tan \beta = 0.04$ ) to ~14 m (41 ft) for a steeper beach slope ( $\tan \beta = 0.11$ ) under the High (Moderate) hazard scenario, when compared with calculations using the probabilistic approach. In both cases this comparison is based on the upper range of the hourly calculated  $T_{WL}$ s shown in Figure 4-2.

**Table 4-2.** Summary statistics of the width of the calculated hazard zones based on all Tillamook profiles. Values outside the 98th percentile have been removed. Erosion distances are with respect to the most landward beach-dune juncture locations as described in Section 3.4.

	Calculated Erosion Distance							
	High Hazard Zone (Hhz)		Medium Hazard Zone (Mhz)		Low Hazard Zone (Lhz)		Lhz + Cascadia Subduction Zone Earthquake	
	(m)	(ft)	(m)	(ft)	(m)	(ft)	(m)	(ft)
Max erosion distance	105	344.5	124.2	407.5	204	669.3	301.4	988.9
Average width	43.5	142.7	52.4	171.9	86.7	284.5	144.2	473.1
Standard deviation	13.2	43.3	13.4	44.0	15	49.2	24.5	80.4



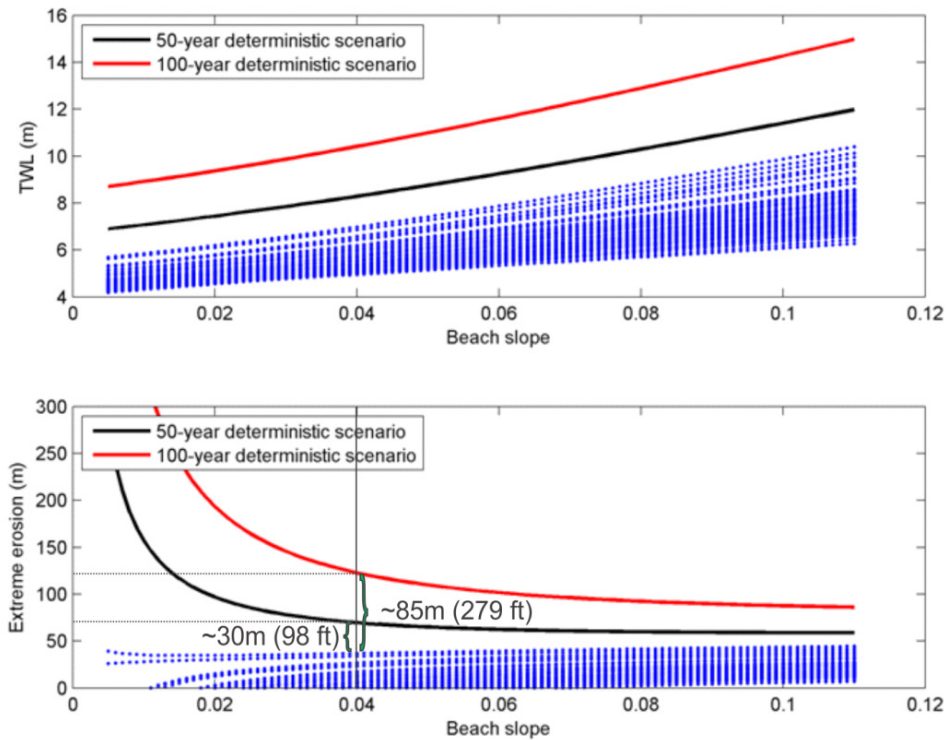


**Figure 4-2.** (top) Plot showing the difference between calculating total water levels, using the Allan and Priest (2001) deterministic approach (solid lines) versus total water levels calculated using a combined wave/tide time series approach for a range of beach slopes. (bottom) Plot showing the calculated erosion that would take place using the deterministic approach versus a combined wave/tide time series approach for a range of beach slopes.

Table 4-3 provides information relating to the widths of the coastal erosion hazard zones but now divided according to each littoral cell. The latter highlights the variability in erosion hazard zones among the various littoral cells along the Tillamook County coast. As can be seen in Table 4-3, calculated erosion distances along the Neskowin shore were generally higher than the county average, with the hazard zones ranging from 47 m (154 ft) to 86 m (282 ft) in width (standard deviation = ~8 m [~27 ft]). These results are not overly surprising given the degree of erosion that has occurred in this area since the late 1990s, the product of generally steeper beach slopes ( $\tan \beta = \sim 0.04$ ) and lower beach-dune juncture elevations, which tends to increase the calculated  $T_{wL}$ s and hence associated erosion. In Neskowin, erosion reached acute levels as a result of the major storms of the late 1990s and as of 2014 virtually the entire length of the community of Neskowin was hardened with riprap.

Rockaway Beach also has fairly sizeable calculated erosion distances due to its prolonged history of erosion. We calculate an average Hhz erosion distance of 46 m (151 ft) (standard deviation = 7.7 m [25 ft]), while the Lhz increases to 95 m (312 ft) (standard deviation = 9 m [29 ft]). As described in Section 2.2.4, the Rockaway cell has also experienced considerable erosion over the past 15 years (Figures 2-25 and 2-26), which continues to this day. These ongoing changes influence the slopes of the beaches (making them steeper) while maintaining generally lower beach-dune juncture elevations, all of which tends to contribute to the presence of wider hazard zones. Because the erosion problem in the Rockaway cell has reached acute levels over the past 15 years, much of the shoreline is now backed by riprap. It is important to recall that the erosion distances calculated for transects protected by riprap are based on the assumption that the beach is backed by a sandy dune, which erodes in response to ocean waves.

**Table 4-3.** Hazard characteristics calculated for each subcell.

Subcell	Calculated Erosion Distance					
	High Hazard Zone (Hhz)		Medium Hazard Zone (Mhz)		Low Hazard Zone (Lhz)	
	Mean	Standard Deviation	Mean	Standard Deviation	Mean	Standard Deviation
	(m)	(m)	(m)	(m)	(m)	(m)
Neskowin	47.1	8.2	54.3	8.4	85.9	9.5
Nestucca	41.6	7.4	48.9	7.4	80.9	8.0
Sand Lake/Tierra Del Mar	41.4	8.3	49.9	8.2	86.8	8.5
Netarts	54.9	10.3	64.9	10.3	107.7	10.1
Bayocean	36.0	14.2	45.8	14.1	88.5	14.3
Rockaway	46.0	7.7	55.1	7.7	95.2	8.9
Nehalem	35.3	12.3	44.6	12.3	85.2	12.6
	(ft)	(ft)	(ft)	(ft)	(ft)	(ft)
Neskowin	154.5	26.9	178.2	27.6	281.8	31.2
Nestucca	136.5	24.3	160.4	24.3	265.4	26.2
Sand Lake/Tierra Del Mar	135.8	27.2	163.7	26.9	284.8	27.9
Netarts	180.1	33.8	212.9	33.8	353.4	33.1
Bayocean	118.1	46.6	150.3	46.3	290.4	46.9
Rockaway	150.9	25.3	180.8	25.3	312.4	29.2
Nehalem	115.8	40.4	146.3	40.4	279.5	41.3

However, as noted previously riprap essentially “fixes” the coast to its present position, effectively mitigating the erosion problem. Nevertheless, because many of these structures are already subject to large ocean waves under conditions today, let alone in the future under higher sea levels, such that they already require periodic maintenance or at worse have failed, it is prudent to consider erosion distances that may be experienced in the absence of riprap. It is also important to acknowledge that the presence of the riprap may be responsible for some of the beach characteristics that facilitate larger erosion distances (e.g., lowered beach-dune junctures, steeper beach slopes, and higher runup and hence  $T_{wls}$ ).

Erosion distances calculated for Nestucca Spit and the Sand Lake/Tierra Del Mar sublittoral cells average about 41 m (135 ft) for the Hhz and 81 to 87 m (265 to 285 ft) for the Lhz (standard deviation = ~8 m [26 ft]). Nestucca Spit is somewhat unique in that the spit has gained large volumes of sediment along much of its northern half. This is probably as a result of the persistent El Niño conditions that have characterized the Oregon coast since the 1980s as well as the extreme winter storms of the late 1990s (Section 2.2.1), which moved a tremendous volume of sand offshore and to the north feeding Nestucca Spit. As a result, the beach-dune juncture elevations along Nestucca Spit are generally located at a higher elevations, while the beach slopes are milder, effectively reducing the calculated wave runup and hence the total water levels in this area. As described in Section 2.2.2, the mouth of the sand lake estuary has also experienced repeated episodes of erosion, while much of the community of Tierra Del Mar, which resides along the south-central end of the cell, is now protected with riprap. Because much of the beach is characterized with generally lower beach slopes, which effectively reduce the wave runup,

the hazard zones in the Tierra Del Mar area tend to be generally narrower.

Bayocean spit and Nehalem Spit have the smallest erosion distances with an average of 36 m (standard deviation = 14 m and 12 m, respectively) for the Hhz. These areas have experienced substantial accumulations of sand over the past few decades, leading to generally much higher beach-dune junctures.

4.2 Cascadia subduction zone hazard

As discussed in Sections 2.3 and 3.5, a CSZ earthquake will result in significant changes to the Tillamook County coastline, primarily in the form of a permanently elevated sea level and ensuing erosion. Using deformation models extracted from the DOGAMI tsunami mapping project (Witter and others, 2011), the worst-case shoreline retreat was determined at every transect location and was used as a proxy for the landward retreat of the beach-dune juncture. These amounts were incorporated into the suite of Low hazard zone scenarios, which also included the same three morphology,  $T_{wL}$ , and SLR parameters. Table 4-4 provides a summary of erosion widths for a worst-case scenario that includes the effect of a CSZ earthquake, coupled with the storm-induced and SLR responses. The average amount of erosion (i.e., the subsidence effect) calculated to occur after a CSZ earthquake is ~60 m (196 ft) (standard deviation = 25 m [82 ft]). The average erosion distance for the worst-case storm-induced erosion scenario is 149 m (489 ft) (standard deviation = 17 m [55 ft]), while the combined worst-case erosion distance averages 206 m (677 ft) (standard deviation = 25 m [81 ft]) with roughly 60% of that due to extreme storm events, SLR, and beach conditions and 40% due to the sudden submergence of the shoreline and rapid rise in sea level associated with a CSZ earthquake.

**Table 4-4.** Worst-case erosion distances calculated using the geometric model assuming a sudden land level drop after a Cascadia subduction zone (CSZ) earthquake causing relative sea level (aka  $T_{wL}$ ) to rise along with a worst-case storm-induced erosion (geometric foredune erosion) and SLR rise.

	CSZ Erosion	Low Hazard Zone Storm-Induced Erosion	Total Worst-Case Erosion Estimate
	(Pre-EQ – Post-EQ Land Level)	(100-yr $T_{wL}$ + High 2100 SLR)	(CSZ + Low)
Average erosion distance (m)	59.6	149	206.3
Standard deviation (m)	25.1	16.8	24.7
Average erosion distance (ft)	195.5	488.9	676.9
Standard deviation (ft)	82.4	55.1	81.0



### 4.3 Kreibel and Dean model

As discussed in Section 3.1.2, the Kreibel and Dean (1993) (K&D) model takes into account the duration of a storm event in order to derive a duration-limited recession value ( $DE_m$ ) based on an extreme winter storm. K&D estimates of the duration-limited erosion were originally derived as a part of the FEMA coastal flood study (Allan and others, unpub. data, 2014) with the maximum value for each subcell used in this study to represent a likely worst case event based response. Table 4-5 lists the K&D erosion distances calculated for each subcell containing dune-backed beaches in Tillamook County. These data are included as overlays in Figures 5-1 to 5-3 for three representative sites along the Tillamook County shoreline. As can be seen in Table 4-5, the calculated duration-limited erosion ranges from 14.5 m to as much as 22 m (48 to 73 ft), with the greatest erosion distances occurring along Netarts Spit; the narrowest K&D erosion value is identified along Nestucca Spit. These latter results are entirely consistent with the erosion responses described in Table 4-3.

**Table 4-5.** Maximum Kreibel and Dean (1993) erosion distance calculated for each subcell from Allan and others (unpub. data, 2014) as described in Section 3.2.2.

	Maximum K&D Erosion Distance	
	(m)	(ft)
Neskowin	20.6	67.6
Nestucca	14.5	47.6
Sand Lake	18.7	61.4
Netarts Spit	22.2	72.8
Bayocean	17.6	57.7
Rockaway	19.9	65.3
Nehalem	19.3	63.3

#### 4.1.1 Estimates of hazard zone uncertainty

As noted previously, the locations of the hazard lines are strongly dependent on the morphology of the beach, particularly the beach slope and to a lesser extent the beach-dune juncture elevation, as well as on the event forcing (i.e., the storm wave runup superimposed on the tides). To assess the relative effects of such factors, we examined the variations in the measured beach slopes determined from repeat RTK-DGPS surveys of 40 beach profile sites located along the Tillamook County shoreline; 15 sites in the Neskowin cell and 25 in the Rockaway cell. These surveys have been undertaken seasonally by DOGAMI staff since 2004 and have been integrated with lidar data flown in 1997, 1998, and 2002. By using these 11 years of monitoring data, we were able to define a seasonal variation in beach slopes (summer versus winter) for each of the 40 transect sites. For areas backed by coastal engineering structures, new  $T_{wLS}$  were calculated using the local beach slope. These data were then subjected to an extreme value analysis in order to yield updated 10%, 2%, and 1%  $T_{wLS}$ ; the original  $T_{wLS}$  defined as part of the study by Allan and others (unpub. data, 2014) were used for the remaining un-engineered beach sites in Tillamook County.

Having defined the seasonal beach slopes, we calculated geometric erosion distances for the dune-backed beaches on the basis of the following conditions:

- The smoothed minimum beach-dune juncture elevation ( $MinE_j$ ) defined for all lidar transects, the mean winter beach slope  $\pm 1\sigma$ , and the calculated 10%, 2%, and 1%  $T_{wLS}$ ;
- The smoothed maximum beach-dune juncture elevation ( $MaxE_j$ ) defined for all lidar transects, the mean winter beach slope  $\pm 1\sigma$ , and the calculated 10%, 2%, and 1%  $T_{wLS}$ ; and,
- The beach-dune juncture elevation defined from the Tillamook County FEMA study (Allan and others, unpub. data, 2014), the mean winter beach slope  $\pm 1\sigma$ , and the calculated 10%, 2%, and 1%  $T_{wLS}$ .

In all cases we used the winter beach slope, as this is when erosion hazards are prevalent.

Table 4-6 presents the results of this analysis, averaged for all possible combinations. As can be seen from the table, the uncertainty associated with the hazard lines ranges from 6 to 9 m (20 to 30 ft) for a 10% storm  $T_{WL}$ , increasing to as much as 9 to 12 m (30 to 39 ft) for a 1% storm event; factoring in the standard deviation of the uncertainty demonstrates the potential for large erosion excursions associated with a major storm, assuming high storm total water levels, steeper beach slopes and generally lower beach-dune juncture elevations. Similar analyses were performed to assess the

relative effects of varying the beach-dune juncture elevation (mean elevation  $\pm 1\sigma$ ). In general, we find that the beach-dune juncture elevations tend to be more consistent along the littoral cell, varying by no more than  $\pm 0.3$  m (1 ft). As a result, the effect of variations in the beach-dune juncture elevations on the hazard zone widths tends to be lower (ranging from 3 to 8 m [10 to 26 ft]), when compared with the effect of slope. These results highlight the challenges faced when trying to model future coastal erosion responses.

**Table 4-6.** Estimates of uncertainty due to variations in the beach slope and its effect on the calculated widths of the erosion hazard zones. The FEMA study is that of Allan and others (unpub. data, 2014).

$T_{WL}$ Event	Minimum Beach-Dune Juncture Elevation (Min $E_j$ )		Maximum Beach-Dune Juncture Elevation (Max $E_j$ )		FEMA Study Beach-Dune Juncture Elevation ( $E_j$ )	
	Mean	Standard Deviation	Mean	Standard Deviation	Mean	Standard Deviation
	(m)	(m)	(m)	(m)	(m)	(m)
10%	8.8	5.2	6.4	4.3	6.3	4.8
2%	11.4	6.3	8.4	5.6	8.2	6.1
1%	12.5	6.7	9.4	6.0	9.2	6.6
	(ft)	(ft)	(ft)	(ft)	(ft)	(ft)
10%	28.9	17.1	21.0	14.1	20.7	15.7
2%	37.4	20.7	27.6	18.4	26.9	20.0
1%	41.0	22.0	30.8	19.7	30.2	21.7

## 5.0 DISCUSSION AND CONCLUSION

The purpose of hazard mitigation planning is to identify policies and actions that can be implemented over the long term to reduce risk and future losses due to natural hazards. This coastal erosion analysis and maps include the most current and comprehensive information on potential coastal erosion risk in Tillamook County. Therefore, it is appropriate to utilize this information to revise and update Tillamook County, and Tillamook County Cities, hazard information within such documents as their Comprehensive land use plans and hazard Mitigation Plans to further address coastal erosion hazards.

Beginning nearest to the beach-dune juncture line, the K&D duration-limited erosion hazard zone reflects the calculated erosion associated with the largest single storm on record, after accounting for the duration of the storm (Allan and others, unpub. data, 2014). As indicated previously, these data were found to range from 14.5 m to as much as 22 m (48 to 72 ft) along Tillamook County. Given that documented storm-induced erosion of beaches and dunes by DOGAMI staff over the past 14 years indicate a minimum of at least 10 m of erosion for a single event (the magnitude of the storm is estimated to have been ~10%), the K&D results are certainly reasonable. Nevertheless, the effects associated with a single storm clearly do not necessarily equate to a worst-case erosion scenario. For example, it is important to appreciate that rarely does the Oregon coast experience a single event over an entire winter season. Instead, beaches and dunes on the Oregon coast (and hence properties built atop the dune) are typically subject to multiple storms over a winter season that may contribute toward the loss of several tens of meters (many tens of feet) of dune retreat. Thus, the K&D duration-limited recession response ( $DE_m$ ) potentially will be significantly less than the cumulative response associated with these multiple events. As a result, *the actual degree of erosion associated with a major storm(s) is likely to span the spectrum between the K&D duration-limited erosion response ( $DE_m$ ) and the maximum potential erosion ( $DE_{MAX}$ )* discussed above in Section 4. Irrespective of these issues, the K&D model results provide a robust estimate for the actual storm-induced risks to properties located immediately adjacent to the active beach and dune, and as a result we believe these data are suitable for assisting

with defining the minimum width of a coastal erosion setback zone for Tillamook County. Furthermore, assuming that the intensity and duration of future storms remain unchanged, we recommend that as the beach-dune juncture continues to retreat landward into the future, the K&D erosion hazard zone would similarly shift landward with it. This would essentially result in a buffer always being maintained between the active beach and properties built adjacent to the coast. Furthermore, were the reverse to occur such that the beach and dunes build seaward, agencies and planning departments could adopt the policy that the K&D erosion line remain relative to the original beach-dune juncture locations as defined in this study. This approach has merit since it is analogous in concept to the approach taken by the Oregon Parks and Recreation Department (OPRD) who manages the public beach up to the vegetation line. By law, its position reflects the mapped line as defined in 1967 or the position of the vegetation line today, whichever is located the farthest landward.

Of the 83 scenarios modeled for Tillamook County, we recommend focusing on six for future planning purposes. The six lines are shown for three discrete sections of the Tillamook County coastline (Figures 5-1 to 5-3), while the maps for the entire coast is provided in Appendix B. For the High hazard zone (Hhz) we recommend adopting the mid-range 2030 sea level rise (0.07 m [0.2 ft]) along with the 2% storm total water level scenario. For the Medium hazard zone (Mhz), we recommend using the 2% storm total water level scenario coupled with a medium-range 2050 SLR estimate of 0.17 m (0.6 ft). Large uncertainties inevitably arise when determining potential erosion hazard distances far into the future. In an effort to acknowledge those uncertainties including the amount of sea level rise expected by 2100 and the possibility of a CSZ earthquake in that time frame, we recommend three versions of the Low hazard zone: Low 1, Low 2, and Low 3. In each of these cases we adopted the 1% storm total water level, making it entirely consistent with the FEMA flood maps that are similarly based on the effects of the 1% storm. Low 1 adopts a mid-range sea level rise at 2100 (0.63 m [2 ft]) while Low 2 adopts the more extreme high SLR estimate (1.42 m [4.66 ft]). Low 3 represents a worst-case scenario: high SLR along with an estimate of the extent of erosion due to a CSZ event. All recommended scenarios are relative to the location of the



beach-dune juncture line defined in this study, since this line reflects the most conservative beach-condition yielding the largest erosion hazard zones. Tables 5-1

and 5-2 provide a summary of erosion distance characteristics for each recommended hazard zone.

**Table 5-1.** Summary of erosion distance characteristics for Tillamook County. In all cases, the width of the hazard zone is relative to the location of the landward  $E_j$ . Maximum zone width serves as a proxy for the uncertainty in predicting erosion through the given time period. A broader zone represents greater uncertainty than a narrow zone. Erosion distances are with respect to the most landward beach-dune juncture locations as described in Section 3.4.

	High Hazard Zone	Medium Hazard Zone	Low1* (Medium Sea Level Rise)	Low2* (High Sea Level Rise)	Low3* (High Sea Level Rise + Cascadia Subduction Zone Earthquake)
Average width (m)	50.1	61.5	93.6	148.9	206.3
Standard deviation (m)	10.2	10.5	12.1	16.8	24.7
Average width (ft)	164.4	201.8	307.1	488.5	676.9
Standard deviation (ft)	33.5	34.5	39.7	55.1	81.0

Low 1, Low 2, and Low 3: In each of these cases we adopted the 1% storm total water level, making it entirely consistent with the FEMA flood maps that are similarly based on the effects of the 1% storm. Low 1 adopts a mid-range sea level rise at 2100 (0.63 m [2 ft]). Low 2 adopts the more extreme high SLR estimate (1.42 m [4.66 ft]). Low 3 represents a worst-case scenario: high SLR along with an estimate of the extent of erosion due to a CSZ event.

**Table 5-2.** Summary of erosion distance characteristics for each recommended hazard zone by subcell. In all cases, the width of the hazard zone is relative to the location of the landward  $E_j$ . Maximum zone width serves as a proxy for the uncertainty in predicting erosion through the given time period. A broader zone represents greater uncertainty than a narrow zone. Erosion distances are with respect to the most landward beach-dune juncture locations as described in Section 3.4.

Subcell	High Hazard Zone		Medium Hazard Zone		Low 1* Hazard Zone		Low 2* Hazard Zone		Low 3* Hazard Zone	
	Mean	Standard Deviation	Mean	Standard Deviation	Mean	Standard Deviation	Mean	Standard Deviation	Mean	Standard Deviation
	(m)	(m)	(m)	(m)	(m)	(m)	(m)	(m)	(m)	(m)
Neskowin	55.7	6.9	65.4	7.2	91		135.1	8.1	199.3	25.6
Nestucca	42.8	6.6	52.4	6.6	79.2	6.8	125.1	7.8	174.5	15.7
Sand Lake/ Tierra Del Mar	48.3	4	59.3	3.9	90.1	4.1	143	4.9	195.6	16.8
Netarts	59.6	5.1	71.9	6	108.2	6.6	170.6	8.5	216.7	10.6
Bayocean	44.1	10.1	56.5	10.7	92.2	10.9	153.7	11.8	209	11.1
Rockaway	53.1	5.1	64.4	5.3	97.4	5.5	154	6.8	228.1	28.2
Nehalem	42.6	10.5	54.9	10.5	88.6	10.3	146.4	10.2	210.2	22.8
	(ft)	(ft)	(ft)	(ft)	(ft)	(ft)	(ft)	(ft)	(ft)	(ft)
Neskowin	182.8	22.6	214.6	23.6	298.6	24.6	443.3	26.6	653.9	84.0
Nestucca	140.4	21.7	171.9	21.7	259.9	22.3	410.5	25.6	572.5	51.5
Sand Lake/ Tierra Del Mar	158.5	13.1	194.6	12.8	295.6	13.5	469.2	16.1	641.8	55.1
Netarts	195.5	16.7	235.9	19.7	355.0	21.7	559.7	27.9	711.0	34.8
Bayocean	144.7	33.1	185.4	35.1	302.5	35.8	504.3	38.7	685.7	36.4
Rockaway	174.2	16.7	211.3	17.4	319.6	18.0	505.3	22.3	748.4	92.5
Nehalem	139.8	34.5	180.1	34.5	290.7	33.8	480.3	33.5	689.7	74.8

Low 1, Low 2, and Low 3: In each of these cases we adopted the 1% storm total water level, making it entirely consistent with the FEMA flood maps that are similarly based on the effects of the 1% storm. Low 1 adopts a mid-range sea level rise at 2100 (0.63 m [2 ft]). Low 2 adopts the more extreme high SLR estimate (1.42 m [4.66 ft]). Low 3 represents a worst-case scenario: high SLR along with an estimate of the extent of erosion due to a CSZ event.

A key function of local governments is to provide important information to citizens. The maps and analysis from this report provide the most current and definitive information on coastal erosion hazards in Tillamook County. As such, the report can serve as a valuable information resource for citizens interested in coastal hazards and processes and, in particular, for coastal property owners, both current and prospective. Property owners and citizens typically seek such information and guidance from local planning agencies, so familiarity with and regular use of this report by local planners can provide an important link to the use of this information by local constituents. The County may also find that by providing access through local public information channels (e.g., County web site or other online resource) this report can be a tool to help develop a broader understanding of the risks to coastal development from natural hazards. Finally, at a more general level, this report can help inform both public and private decision makers about the nature, extent, and location of coastal erosion hazards in Tillamook County and thus allow for more informed decision making, at both individual and community levels.

Statewide planning Goal 7 (Natural Hazards) and Goal 18 (Beaches and Dunes) guide how local comprehensive plans and land use ordinances address coastal hazards. In general, the goals direct local governments to adopt comprehensive plan (e.g., inventories and policies) and implementing measures (zoning and subdivision ordinances) to reduce risk to people and property from natural hazards. The maps and analysis in this report can therefore be used in a variety of ways as a resource for land use planning. These applications range from use as a general background information document to use as a basis for more specific regulatory measures. Examples of potential land use applications include:

- Incorporating the report and maps into the comprehensive plan inventory for purposes of Goal 7 and/or Goal 18;
- Using the risk zone maps to identify areas where site specific engineering geologic reports are needed prior to the siting of new development;
- Using the risk zone maps to identify areas where limitations on some types or intensity of new development (e.g., new land divisions or other increases in density) would be imposed. Such limitations could be tiered based on the different levels of risk identified on the maps.

The above examples are among the approaches that local jurisdictions could consider in incorporating or adapting the findings of this study for land use planning purposes. Ultimately, it will be up to each local government to determine how to best use the map products and analysis in their land use planning programs, considering specific local conditions and the requirements of the Statewide Planning Goals.

The information within this study may also be used to update local hazard mitigation plans. The purpose of hazard mitigation planning is to identify policies and actions that can be implemented over the long term to reduce risk and future losses due to natural hazards. This coastal erosion analysis and maps include the most current and comprehensive information on potential coastal erosion risk in Tillamook County. Therefore, it is appropriate to use this information to revise and update the Tillamook County Hazard Mitigation Plan to address coastal erosion hazards. Furthermore, these findings may also be used to assist local public and private service providers in planning for future facility siting and development. In particular, decisions regarding investments in infrastructure or key facilities in areas that may be at risk from either existing or future coastal erosion hazards can be informed by the consideration of the maps and analyses presented as part of this study. Many such decisions involve long-term capital investments, so the use of these findings to consider the chronic nature of coastal erosion and its effects over time may be especially relevant.

In summary, the information and mapping within this report can serve as a valuable information resource for citizens interested in coastal hazards and processes and for Tillamook County local governments as they address the potential for increased erosion along the Tillamook County coast.



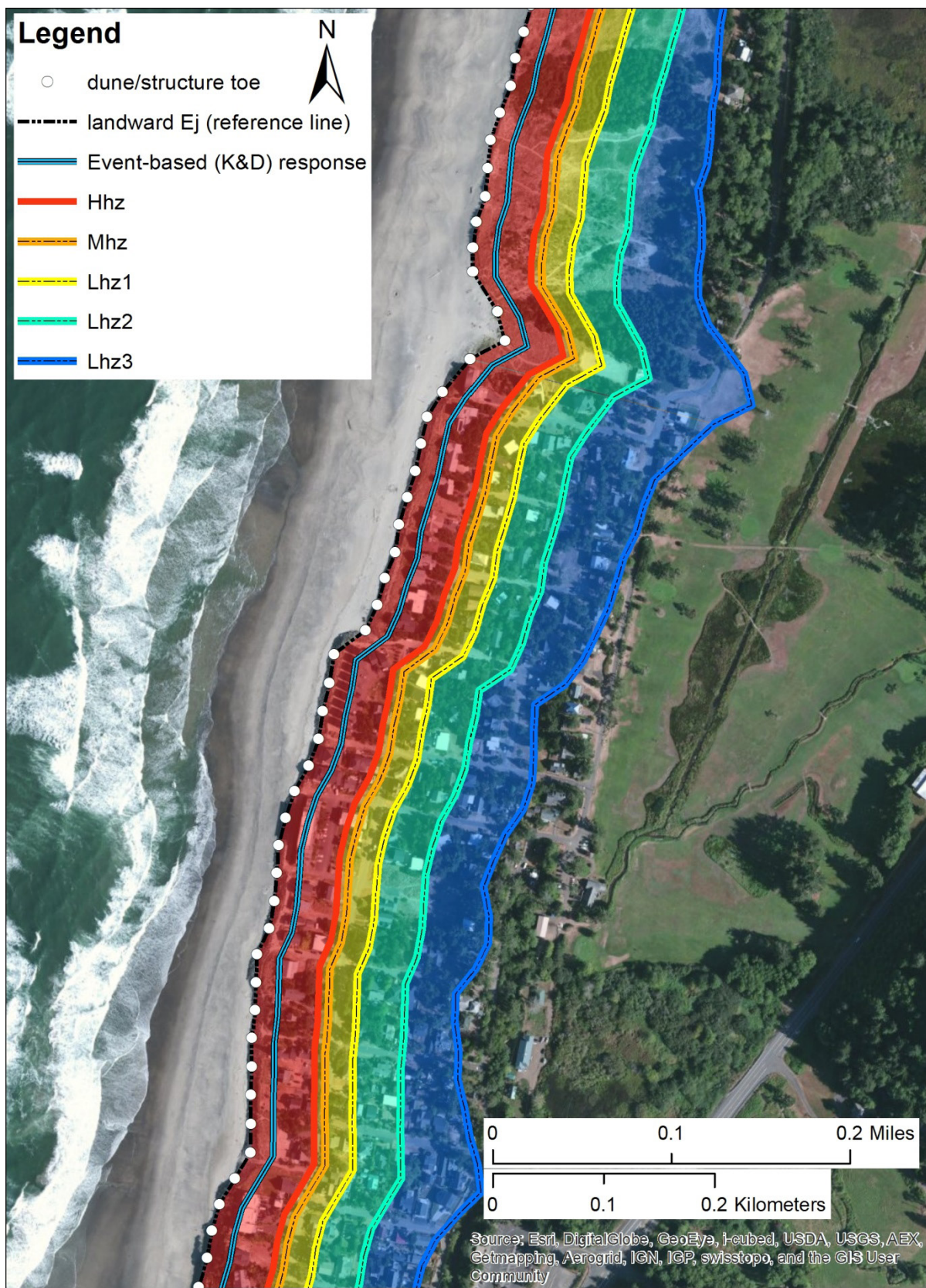


**Figure 5-1.** New dune-backed hazard zones for Neskowin, Tillamook County.



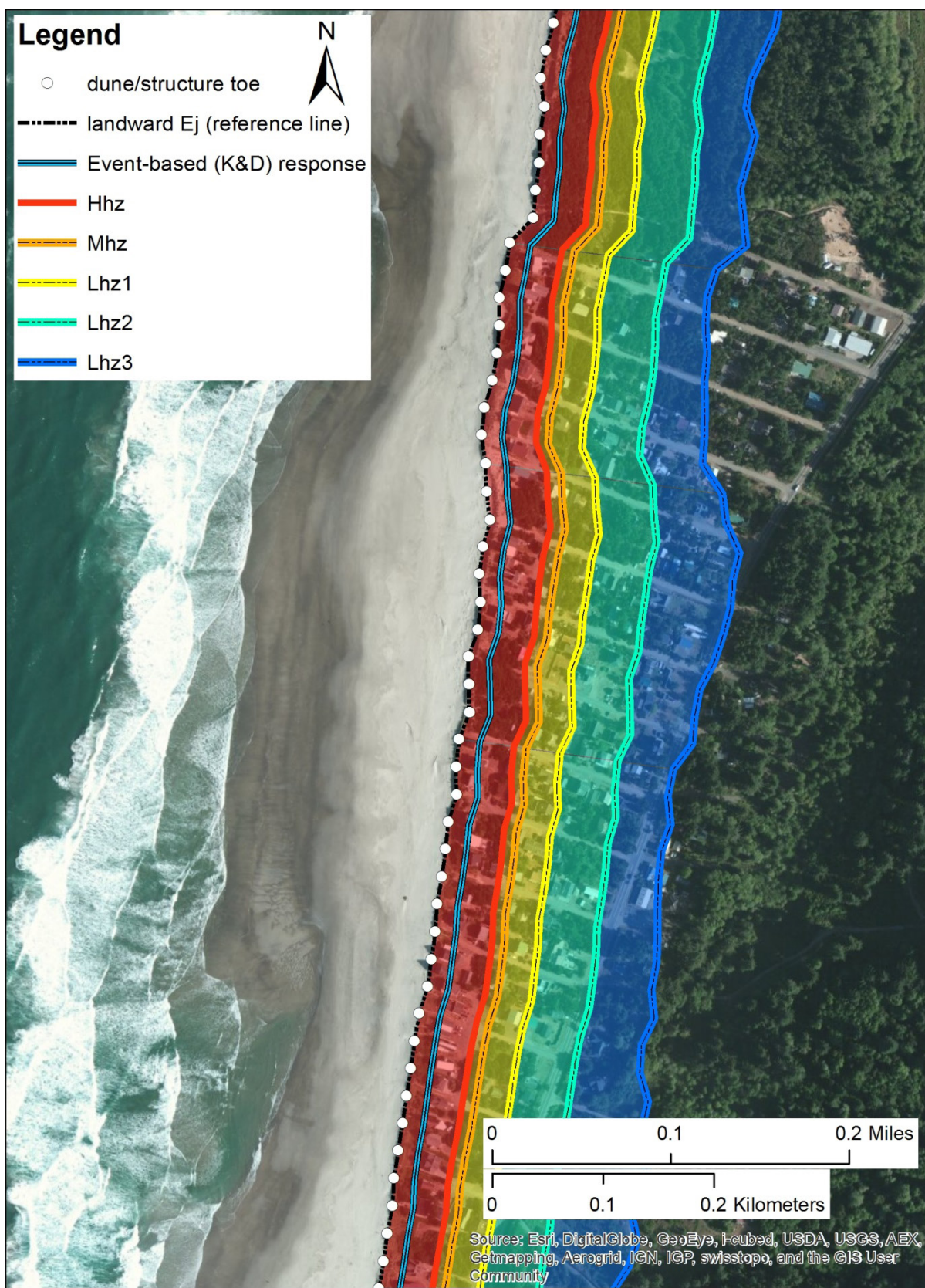


**Figure 5-2.** New dune-backed hazard zones for Tierra Del Mar, Tillamook County.



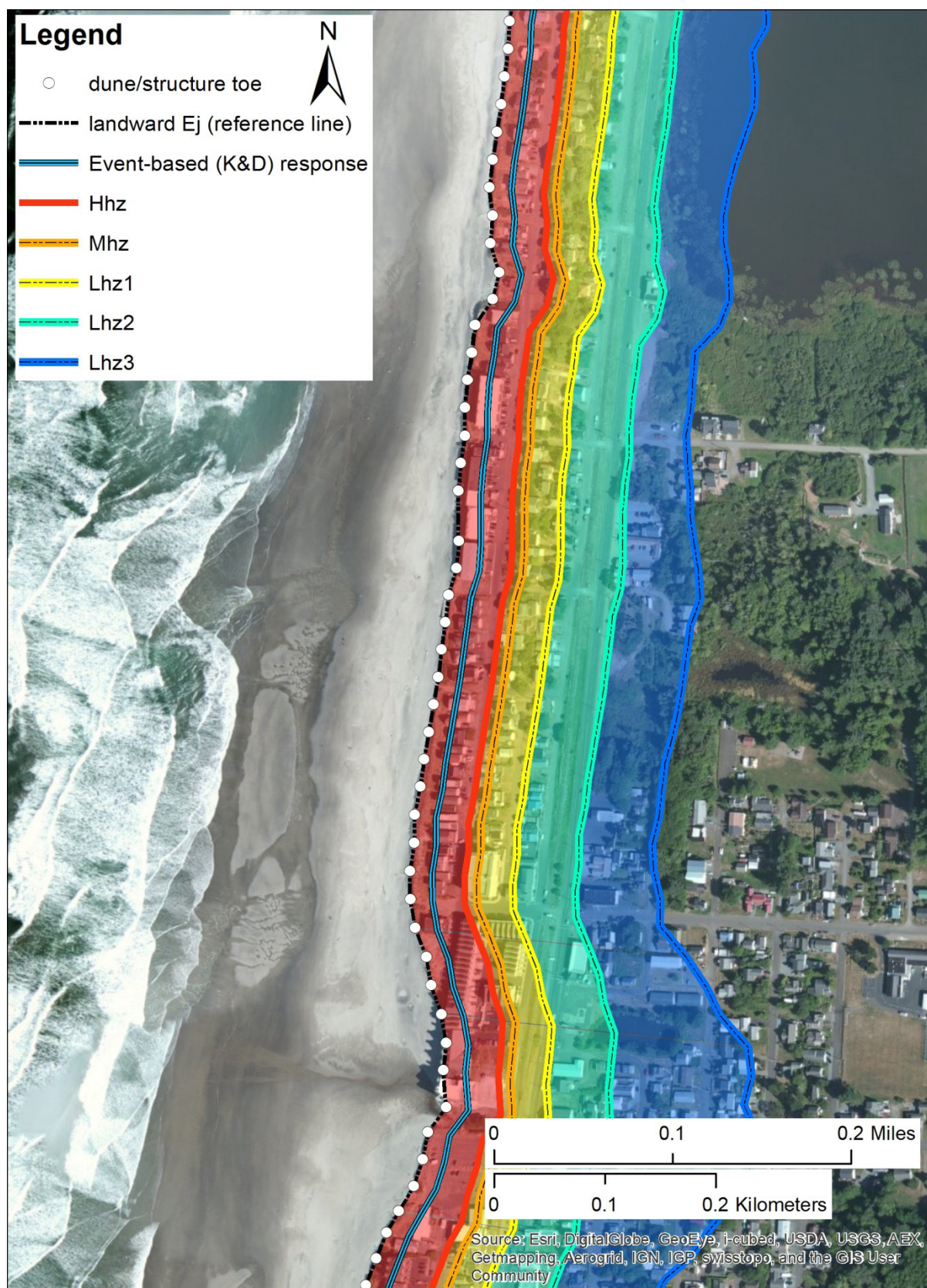


**Figure 5-3.** New dune-backed hazard zones for Rockaway Beach, Tillamook County.

## 6.0 ACKNOWLEDGMENTS

Funding for this study was provided by the Oregon Department of Land Conservation and Development (DLCD) through its Coastal Management Program (#PS09005). We gratefully acknowledge the assistance of Laren Woolley (DLCD) throughout this study. We are also grateful to Dr. Peter Ruggiero, Coastal Engineer in the College of Earth Ocean and Atmospheric Research at Oregon State University, who assisted with the performing additional probabilistic analyses of total water levels for Tillamook County.

## 7.0 REFERENCES

- Allan, J. C., and Harris, E. L., 2012, An “expanded” geospatial database of beach and bluff morphology determined from lidar data collected on the northern Oregon coast, Tillamook to Clatsop County: Oregon Department of Geology and Mineral Industries, Open-File Report O-12-08, 23 p.
- Allan, J. C., and Hart, R., 2007, Assessing the temporal and spatial variability of coastal change in the Neskowin littoral cell: developing a comprehensive monitoring program for Oregon beaches: Oregon Department of Geology and Mineral Industries, Open-File Report O-07-01, 27 p.
- Allan, J. C., and Hart, R., 2008, Oregon beach and shoreline mapping and analysis program: 2007-2008 beach monitoring report: Oregon Department of Geology and Mineral Industries, Open-File Report O-08-15, 60 p.
- Allan, J. C., and Komar, P. D., 2000, Are ocean wave heights increasing in the eastern North Pacific?: Eos, Transactions of the American Geophysical Union, v. 81, no. 47, 561 and 566–567.
- Allan, J. C., and Komar, P. D., 2002, Extreme storms on the Pacific Northwest coast during the 1997-98 El Niño and 1998-99 La Niña: Journal of Coastal Research, v. 18 no. 1, 175-193.
- Allan, J. C., and Priest, G. R., 2001, Evaluation of coastal erosion hazard zones along dune and bluff backed shorelines in Tillamook County, Oregon: Cascade Head to Cape Falcon: Oregon Department of Geology and Mineral Industries, Open-File Report O-01-03, 120 p.
- Allan, J. C., and Stimely, L., 2013, Oregon Beach Shoreline Mapping and Analysis Program: quantifying short to long-term beach and shoreline changes in the Gold Beach, Nesika, and Netarts littoral cells: Oregon Department of Geology and Mineral Industries, Open-File Report O-13-07, 46 p.
- Allan, J. C., Komar, P. D., and Priest, G.R., 2003, Shoreline variability on the high-energy Oregon coast and its usefulness in erosion-hazard assessments, *in* Byrnes, M. R., Crowell, M., and Fowler, C., s., Shoreline mapping and change analysis: technical considerations and management implications: Journal of Coastal Research, Special Issue 38, p. 83–105.
- Allan, J. C., Witter, R. C., Ruggiero, P., and Hawkes, A. D., 2009, Coastal geomorphology, hazards, and management issues along the Pacific Northwest coast of Oregon and Washington, *in* O'Connor, J. E., Dorsey, R. J., and Madin I. P., eds., Volcanoes to vineyards: geologic field trips through the dynamic landscape of the Pacific Northwest: Geological Society of America, Geological Society of America Field Guide 15. p. 495–519.
- Allan, J. C., Komar, P. D., and Ruggiero, P., 2011, Storm surge magnitudes and frequency on the central Oregon coast, *in* Wallendorf, L. A., Jones, C., Ewing, L., and Battalio, B. eds., Proceedings of the 2011 Solutions to Coastal Disasters Conference: American Society of Civil Engineers, p. 53–64.
- Atwater, B. F., Satoko, M. R., Satake, K., Yoshinobu, T., Kazue, U., and Yamaguchi, D. K., 2005, The orphan tsunami of 1700—Japanese clues to a parent earthquake in North America: U.S. Geological Survey Professional Paper 1707, 133 p.
- Baron, H., 2011, Coastal hazards and community exposure in a changing climate: the development of probabilistic coastal change hazard zones: Corvallis, Oreg., Oregon State University, M.S. thesis, 95 p.
- Beaulieu, J. D., 1973, Environmental geology of inland Tillamook and Clatsop counties, Oregon: Oregon Department of Geology and Mineral Industries, Portland, Bulletin 79, 65 p., 14 pl., scale 1:63,000.
- Booij, N., R. C. Ris, and L. H. Holthuijsen, 1999, A third-generation wave model for coastal regions, Part I: Model description and validation: Journal of Geophysical Research, v. 104(C4), 7649–7666.



- Bruun, P., 1962, Sea level rise as a cause of shore erosion: *Journal of the Waterways and Harbors Division, American Society of Civil Engineers*, v. 88, 117–130.
- Cazenave, A., and Llovel, W., 2010, Contemporary sea level rise: *Annual Review of Marine Science*, v. 2, 145–173.
- Coles, S., 2001, *An introduction to statistical modeling of extreme values*: London: Springer-Verlag, 208 p.
- Goldfinger, C., 2009, Paleoseismically derived probabilities for Cascadia great earthquakes, *Geological Society of America Annual Meeting*, Oct. 18–21, 2009, Portland, Oreg.: *Geological Society of America Abstracts with Programs*, v. 41, no. 7, p. 520.
- Goldfinger, C., Nelson, C. H., and Johnson, J. G., 2003, Holocene earthquake records from the Cascadia subduction zone and northern San Andreas fault based on precise dating of offshore turbidites: *Annual Review of Earth and Planetary Sciences*, v. 31, 555–577.
- Goldfinger, C., Nelson, C. H., Morey, A., Johnson, J. G., Gutierrez-Pastor, J., Eriksson, A. T., Karabanov, E., Patton, J., Gracia, E., Enkin, R., Dallimore, A., Dunhill, G., Vallier, T., and The Shipboard Scientific Parties, 2009, Turbidite event history: methods and implications for Holocene paleoseismicity of the Cascadia subduction zone: *U.S. Geological Society Professional Paper 1661-F*, 170 p.
- Holgate, S., 2007, On the decadal rates of sea level change during the twentieth century: *Geophysical Research Letters*, v. 34(L01602), 1–4.
- Jennings, R., and Shulmeister, J., 2002, A field based classification scheme for gravel beaches: *Marine Geology*, v. 186, 211–228.
- Kelsey, H. M., Nelson, A. R., Hemphill-Haley, E., and Witter, R. C., 2005, Tsunami history of an Oregon coastal lake reveals a 4600 yr record of great earthquakes on the Cascadia subduction zone: *Geological Society of America Bulletin*, v. 117, no. 7/8, 1009–1032.
- Komar, P. D., 1986, The 1982–83 El Niño and erosion on the coast of Oregon: *Shore & Beach*, v. 54, no. 2, 3–12.
- Komar, P. D., 1997, *The Pacific Northwest coast: living with the shores of Oregon and Washington*: Durham and London, Duke University Press, 195 p.
- Komar, P. D., 1998, The 1997–98 El Niño and erosion on the Oregon coast: *Shore & Beach*, v. 66, no. 3, 33–41.
- Komar, P. D., Lizarraga-Arciniega, J. R., and Terich, T. A., 1976, Oregon coast shoreline changes due to jetties: *Journal of the Waterways and Harbors Division, American Society of Civil Engineers*, v. 102(WW1), no. 1, 13–30.
- Komar, P. D., Good, J. W., and Shih, S.M., 1989, Erosion of Netarts Spit, Oregon: continued impacts of the 1982–83 El Niño: *Shore & Beach*, v. 57, no. 1, 11–19.
- Komar, P. D., Lanfredi, N., Baba, M., Dean, R. G., Dyer, K., Healy, T., Ibe, A. C., Terwindt, J. H. J., and Thom, B. G., 1991a, The response of beaches to sea-level changes: A review of predictive models: *Journal of Coastal Research*, v. 7, no. 3, 895–921.
- Komar, P. D., Torstenson, R.W., and Shih, S.M., 1991b, Bandon, Oregon: coastal development and the potential for extreme ocean hazards: *Shore & Beach*, v. 59, no. 4, 14–22.
- Komar, P. D., McDougal, W. G., Marra, J. J., and Ruggiero, P., 1999, The rational analysis of setback distances: applications to the Oregon coast: *Shore & Beach*, v. 67, 41–49.
- Komar, P. D., Allan, J. C., and Ruggiero, P., 2011, Sea level variations along the U.S. Pacific Northwest coast: tectonic and climate controls: *Journal of Coastal Research*, v. 27, no. 5, 808–823.
- Kriebel, D. L., and Dean, R. G., 1993, Convolution method for time-dependent beach-profile response: *Journal of Waterway, Port, Coastal, and Ocean Engineering*, v. 119, no. 2, 204–226.
- Moore, L. J., 2000, Shoreline mapping techniques. *Journal of coastal research*, v. 16, no. 1, 111–124.
- NRC (National Research Council), 2012, *Sea-level rise for the coasts of California, Oregon, and Washington: past, present, and future*: Washington, D.C., National Research Council, Division on Earth and Life Studies, Ocean Studies Board, Board on Earth Sciences and Resources, Committee on Sea Level Rise in California, Oregon, and Washington, 250 p.
- Oceanweather, Inc., 2010, *Global Reanalysis of Ocean Waves Fine Northeast Pacific Hindcast (GROW-FINE NEPAC)*, 39 p.

- Priest, G. R., Saul, I., and Diebenow, J., 1993, Pilot erosion rate data study of the central Oregon coast, Lincoln County: Oregon Department of Geology and Mineral Industries, Open-File Report O-93-10, 228 p.
- Priest, G. R., Goldfinger, C., Wang, K., Witter, R. C., Zhang, Y., and Baptista, A.M., 2009, Confidence levels for tsunami-inundation limits in northern Oregon inferred from a 10,000-year history of great earthquakes at the Cascadia subduction zone: *Natural Hazards*, vol. 54, 27–73.
- Revell, D., Komar, P. D., and Sallenger, A.H., 2002, An application of lidar to analyses of El Niño erosion in the Netarts littoral cell, Oregon: *Journal of Coastal Research*, v. 18, no. 4, 792–801.
- Ris, R. C., N. Booij, and L. H. Holthuijsen, 1999, A third-generation wave model for coastal regions, Part II: Verification: *Journal of Geophysical Research*, v. 104(C4), 7667–7681.
- Ruggiero, P., Komar, P. D., McDougal, W. G., and Beach, R. A., 1996, Extreme water levels, wave runup and coastal erosion, *Proceedings of the 25th Conference on Coastal Engineering*: Orlando, Fla., American Society of Civil Engineers, p. 2793–2805.
- Ruggiero, P., Komar, P. D., McDougal, W. G., Marra, J. J., and Beach, R. A., 2001, Wave runup, extreme water levels and the erosion of properties backing beaches: *Journal of Coastal Research*, v. 17, no. 2, 407–419.
- Ruggiero, P., Kaminsky, G. M., and Gelfenbaum, G., 2003, Linking proxy-based and datum-based shorelines on a high-energy coastline: Implications for shoreline change analysis: *Journal of Coastal Research*, Special Issue 38, 57–82.
- Ruggiero, P., Komar, P. D., and Allan, J. C., 2010, Increasing wave heights and extreme value projections: The wave climate of the U.S. Pacific Northwest: *Coastal Engineering*, v. 57, no. 5, 539–552.
- Ruggiero, P., Kratzmann, M. G., Himmelstoss, E. A., Reid, D., Allan, J. C., and Kaminsky, G. M., 2013, National assessment of shoreline change: historical shoreline change along the Pacific Northwest coast: U.S. Geological Survey, Open-File Report 2012-1007, 62 p.
- Satake, K., Shemazaki, K., Yoshinobu, T., and Ueda, K., 1996, Time and size of a giant earthquake in Cascadia inferred from Japanese tsunami records of January 1700: *Nature*, v. 379, no. 6562, 246–249.
- Shoreland Solutions, 1998, Chronic coastal natural hazards model overlay zone, report to the Oregon Department on Land Conservation and Development: Oregon City, Ore., 41 p.
- Stockdon, H. F., Holman, R. A., Howd, P. A., and Sallenger, A. H., 2006, Empirical parameterization of setup, swash, and runup: *Coastal Engineering*, v. 53, no. 7, 573–588.
- Terich, T. A., 1973, Development and erosion history of Bayocean Spit, Tillamook, Oregon: Corvallis, Ore., Oregon State University, Ph.D. dissertation, xx p.
- Terich, T. A., and Komar, P. D., 1973, Development and erosion history of Bayocean Spit, Tillamook, Oregon: Corvallis, Ore.: Oregon State University, School of Oceanography.
- Terich, T. A., and Komar, P. D., 1974, Bayocean Spit, Oregon: history of development and erosional destruction: *Shore & Beach*, v. 42, no. 2, 3–10.
- Tillotson, K., and Komar, P. D., 1997, The wave climate of the Pacific Northwest (Oregon and Washington): A comparison of data sources. *Journal of Coastal Research*, v. 13, no. 2, 440–452.
- Wang, K., 2007, Elastic and viscoelastic models of crustal deformation in subduction earthquake cycles, *in* Dixon, T., and Moore, J. C., eds., *The seismogenic zone of subduction thrust faults*: New York, Columbia University Press, p. 540–575.
- Witter, R. C., Kelsey, H. M. and Hemphill-Haley, E., 2003, Great Cascadia earthquakes and tsunamis of the past 6700 years, Coquille River estuary, southern coastal Oregon: *Geological Society of America Bulletin*, v. 115, 1289–1306.
- Witter, R. C., Zhang, Y., Goldfinger, C., Priest, G. R. and Wang, K., 2010, Validating numerical tsunami simulations in southern Oregon using late Holocene records of great Cascadia earthquakes and tsunamis, *in* Letters, S. R., ed., *Seismological Society of America 2010 Annual Meeting Abstracts*, April 21-23, Portland, Ore., *Seismological Research Letters*, v. 81, no. 2, 290.
- Witter, R. C., Zhang, Y., Wang, K., Priest, G. R., Goldfinger, C., Stimely, L. L., English, J. T., and Ferro, P., 2011, Simulating tsunami inundation at Bandon, Coos County, Oregon, using hypothetical Cascadia and Alaska earthquake scenarios: Oregon Department of Geology and Mineral Industries, Special Paper 43, 57 p.,

## APPENDIX A: EROSION SCENARIOS

The table below presents a list of all erosion scenarios calculated for this study. The High, Medium, and Low hazard zones contain 27 scenarios that represent all unique combinations of beach-dune junctures,  $T_{WL}$ s, and SLR rates. Bold entries are the scenarios we have chosen to represent each hazard zone. Maximum and minimum beach-dune junctures were derived from the analysis as described in Section 3.4; the FEMA  $E_j$  was calculated as part of the 2012 FEMA flood study (Allan and others, unpub. data, 2014) in an effort to maintain consistency with the FEMA methodology. Storm-induced total water levels (10, 50, 100-year storms) were also calculated as part of the 2012 FEMA flood study by Allan and others (unpub. data, 2014). Three SLR ranges

were used for the 2030, 2050, and 2100 time frames. The low range values for 2030 and 2050 are based on the historical rate of change identified for the Newport tide gauge (Komar and others, 2011), *not* the low range values from the NRC (2012) study. This is because there is no physical reason for this pattern to gradually reverse itself in the foreseeable future. Two additional scenarios are included as part of this work. The first is the duration-limited erosion hazard zone derived using the K&D approach (Table 4-5). The second is a worst-case scenario that reflects the landward shift in the entire beach profile immediately following a Cascadia subduction zone (CSZ) earthquake. This scenario is analogous to instantaneously raising mean sea level by as much as 3 m (10 ft) along the Oregon coast, resulting in widespread erosion.

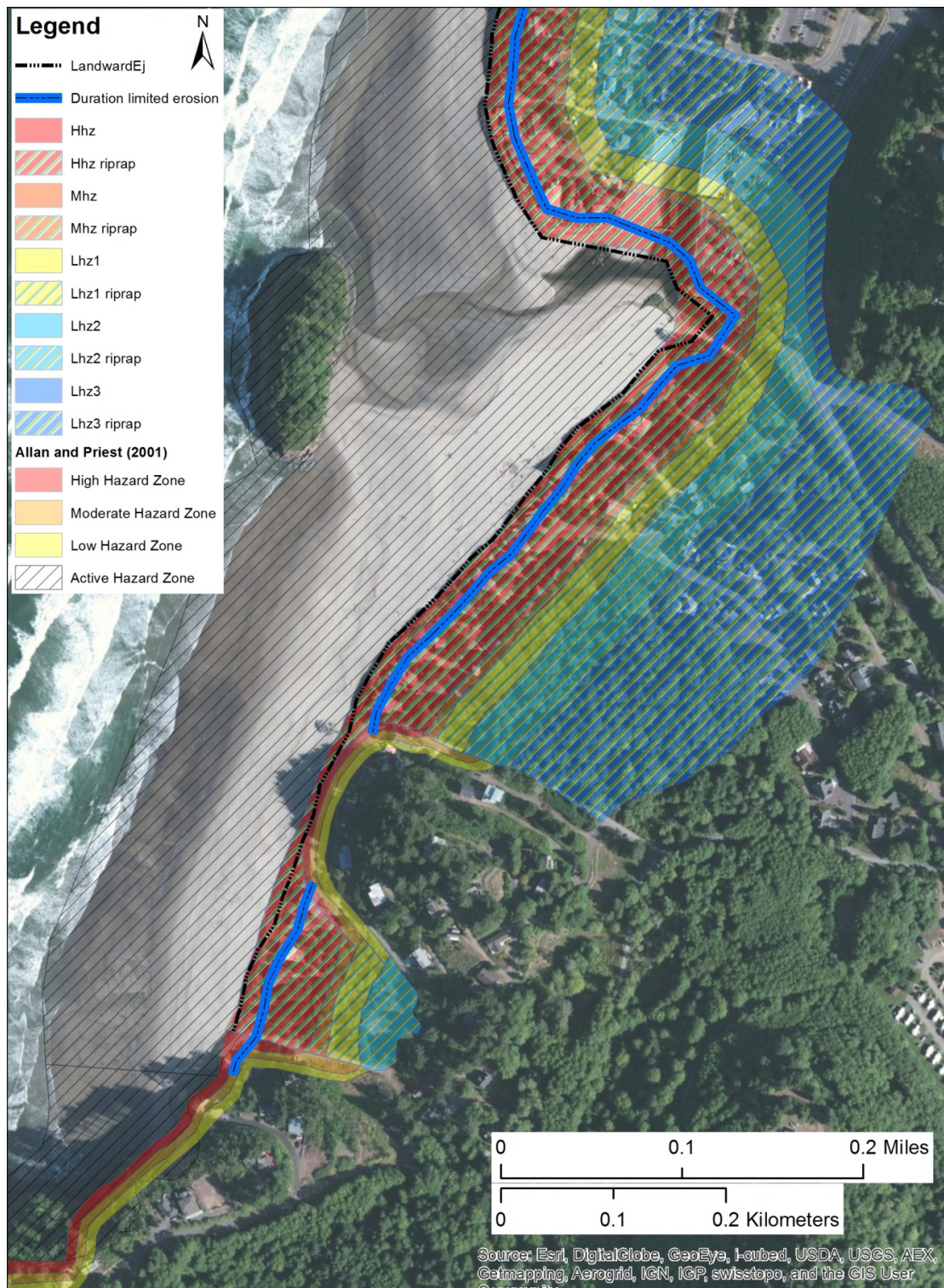
Scenario	Erosion Scenario											
	High Hazard Zone			Medium Hazard Zone			Low Hazard Zone			Low Hazard Zone + CSZ EQ		
	$E_j$	$T_{WL}$	SLR	$E_j$	$T_{WL}$	SLR	$E_j$	$T_{WL}$	SLR	$E_j$	$T_{WL}$	SLR
1	$E_{jMin}$	10	Low 2030	$E_{jMin}$	10	Low 2050	$E_{jMin}$	10	Low 2100	$E_{jMin}$	10	Low 2100
2			Med 2030			Med 2050			Med 2100			Med 2100
3			High 2030			High 2050			High 2100			High 2100
4	<b>50</b>	Low 2030		50	Low 2050		50	Low 2100		50	Low 2100	
5		<b>Med 2030</b>			Med 2050			Med 2100			Med 2100	
6		High 2030			High 2050			High 2100			High 2100	
7	100	Low 2030		<b>100</b>	Low 2050		<b>100</b>	Low 2100		<b>100</b>	Low 2100	
8		Med 2030			<b>Med 2050</b>			<b>Med 2100</b>			Med 2100	
9		High 2030			High 2050			High 2100			High 2100	
10	$E_{jMax}$	10	Low 2030	$E_{jMax}$	10	Low 2050	$E_{jMax}$	10	Low 2100			
11			Med 2030			Med 2050			Med 2100			
12			High 2030			High 2050			High 2100			
13	50	Low 2030		50	Low 2050		50	Low 2100				
14		Med 2030			Med 2050			Med 2100				
15		High 2030			High 2050			High 2100				
16	100	Low 2030		100	Low 2050		100	Low 2100				
17		Med 2030			Med 2050			Med 2100				
18		High 2030			High 2050			High 2100				
19	FEMA	10	Low 2030	FEMA	10	Low 2050	FEMA	10	Low 2100			
20			Med 2030			Med 2050			Med 2100			
21			High 2030			High 2050			High 2100			
22	50	Low 2030		50	Low 2050		50	Low 2100				
23		Med 2030			Med 2050			Med 2100				
24		High 2030			High 2050			High 2100				
25	100	Low 2030		100	Low 2050		100	Low 2100				
26		Med 2030			Med 2050			Med 2100				
27		High 2030			High 2050			High 2100				

Kreibel and Dean

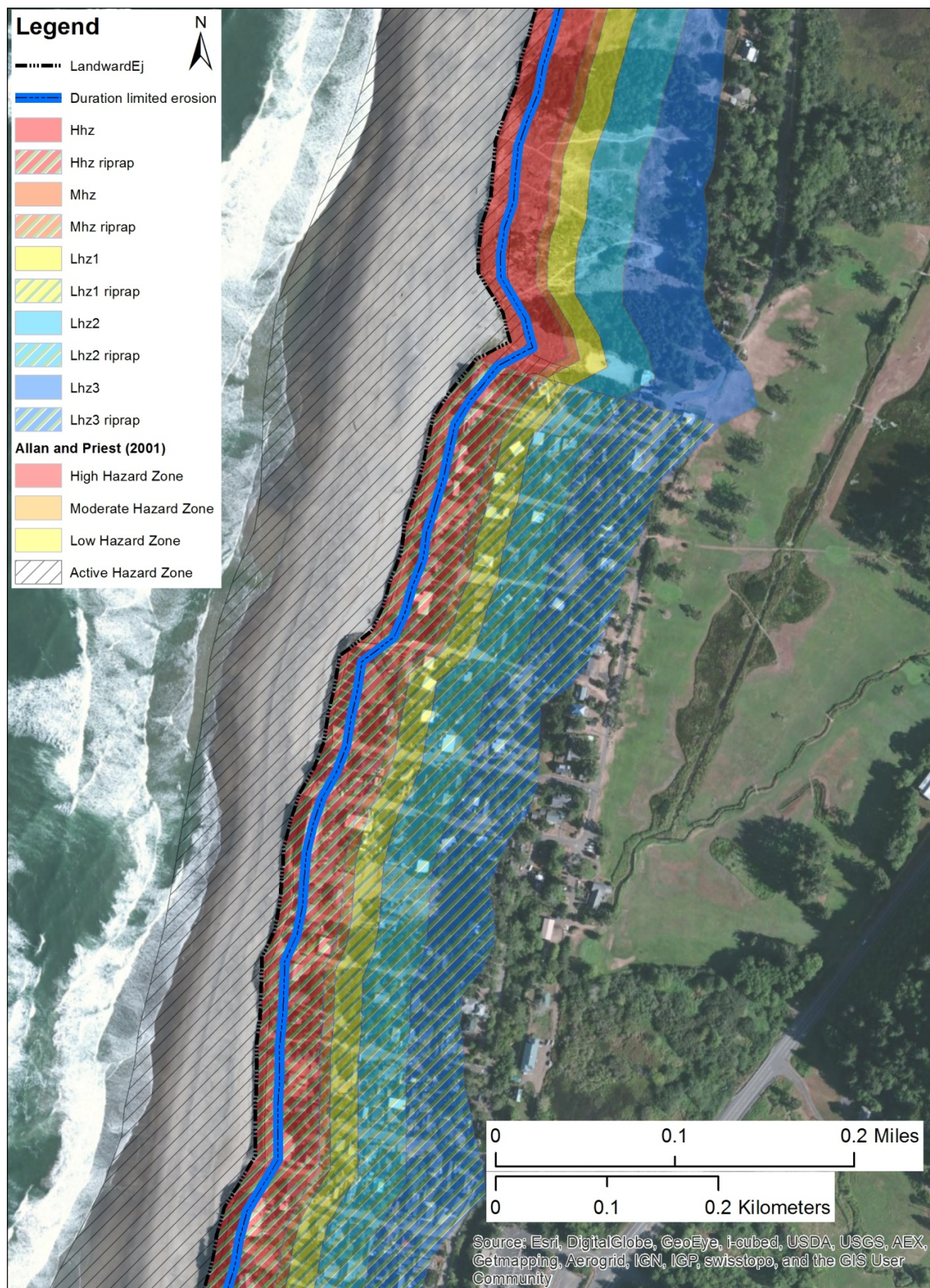


## APPENDIX B: MAPS OF MODELED EROSION HAZARD ZONES

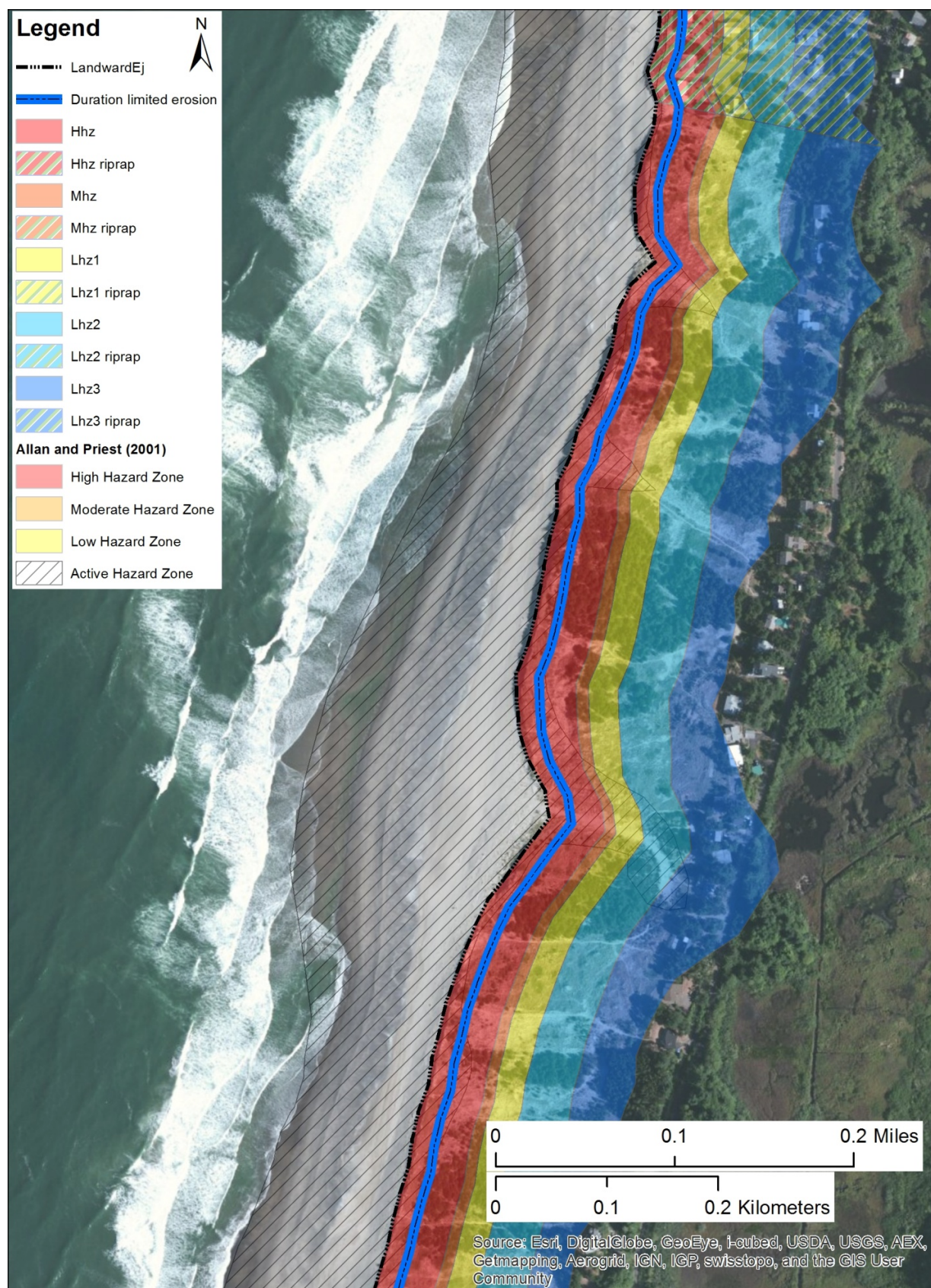
### Neskowin



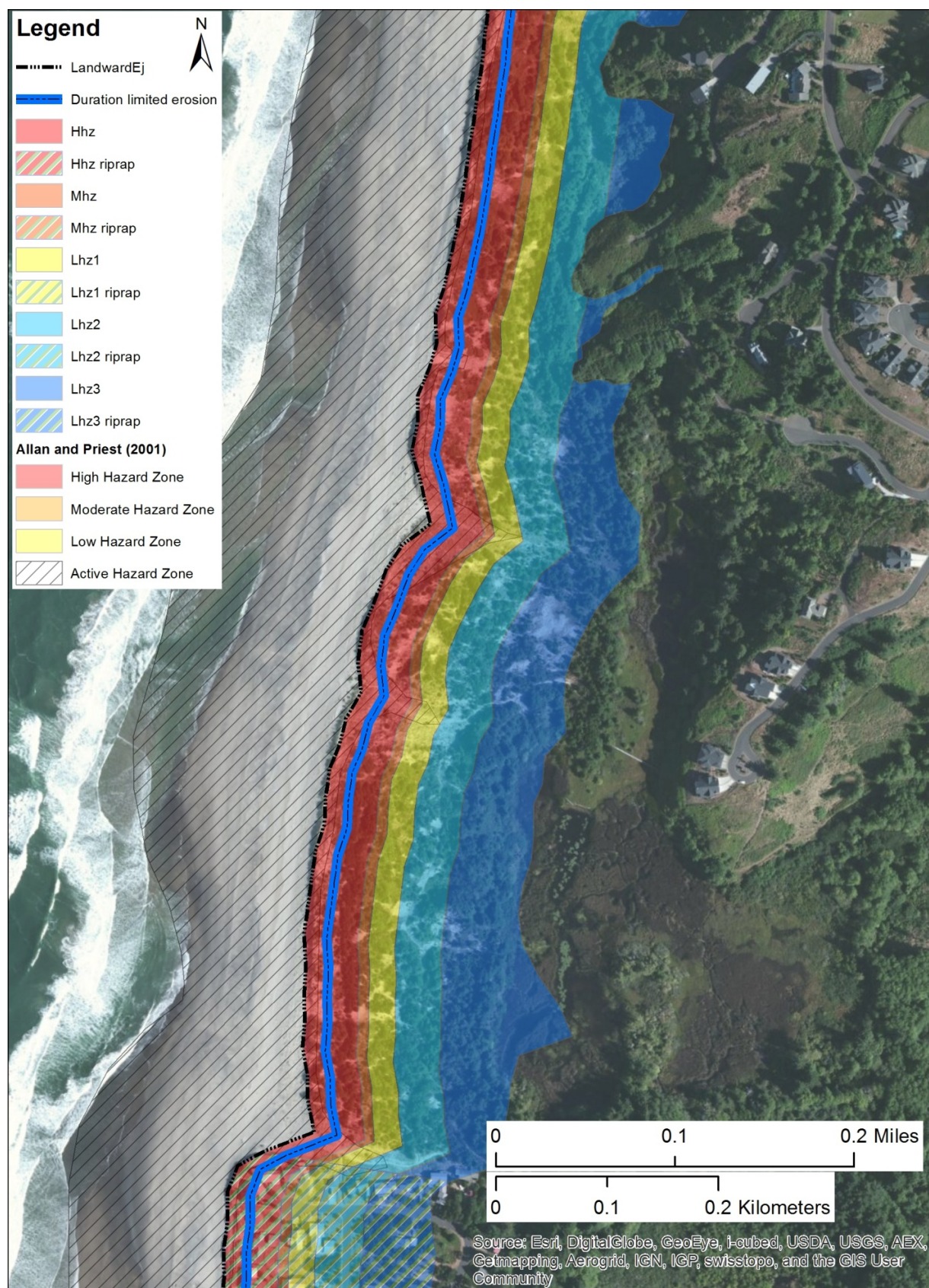




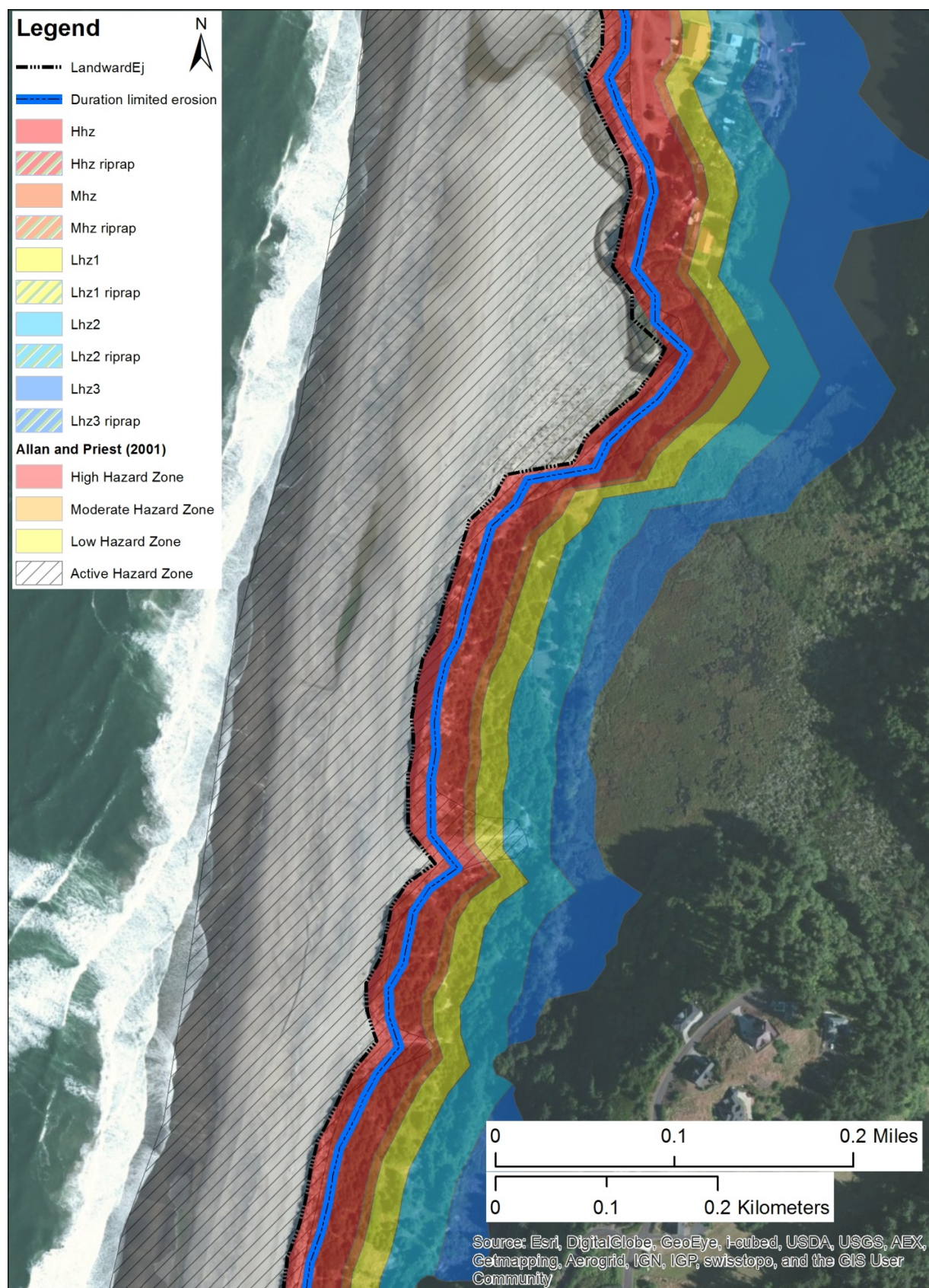




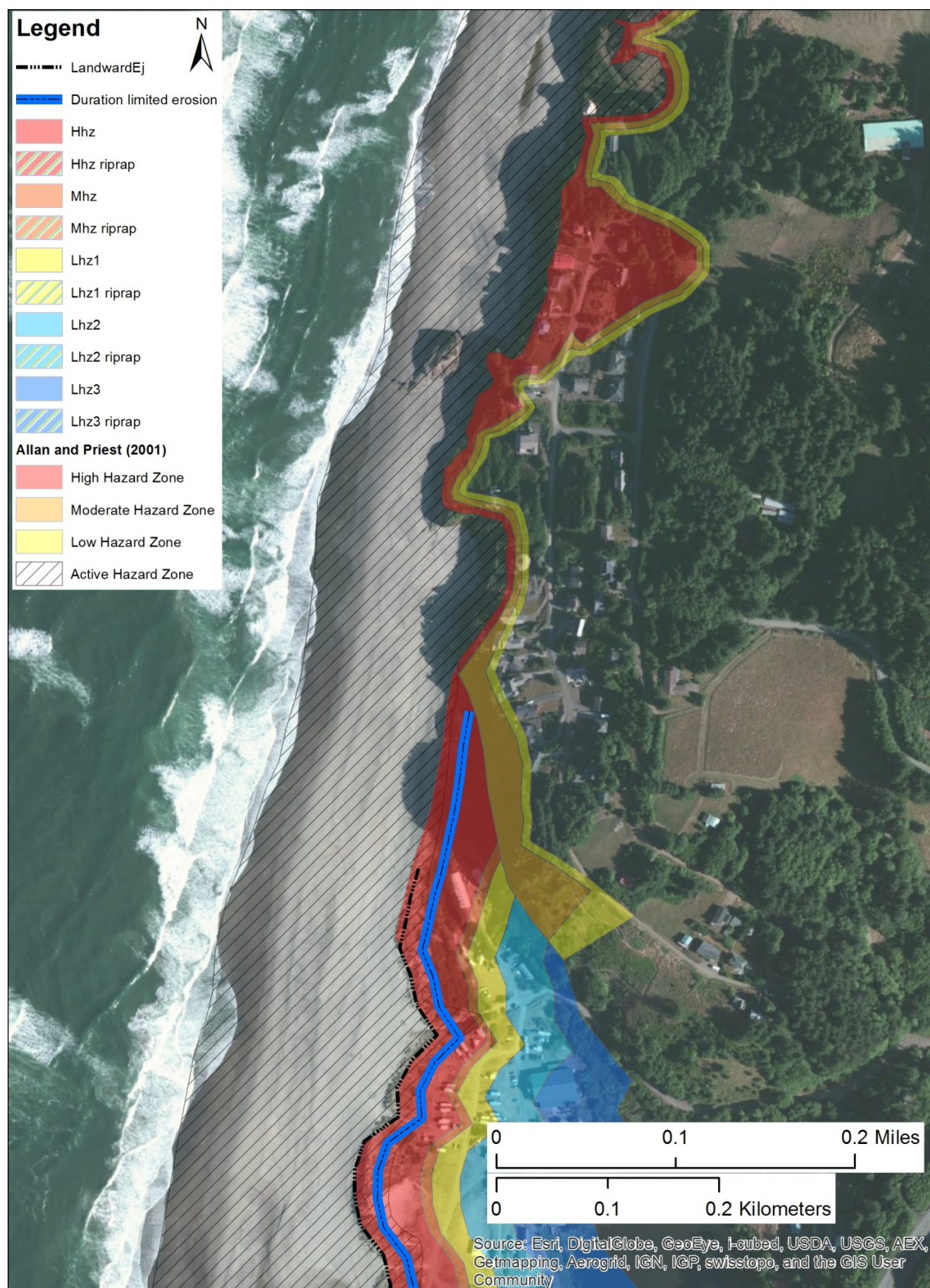




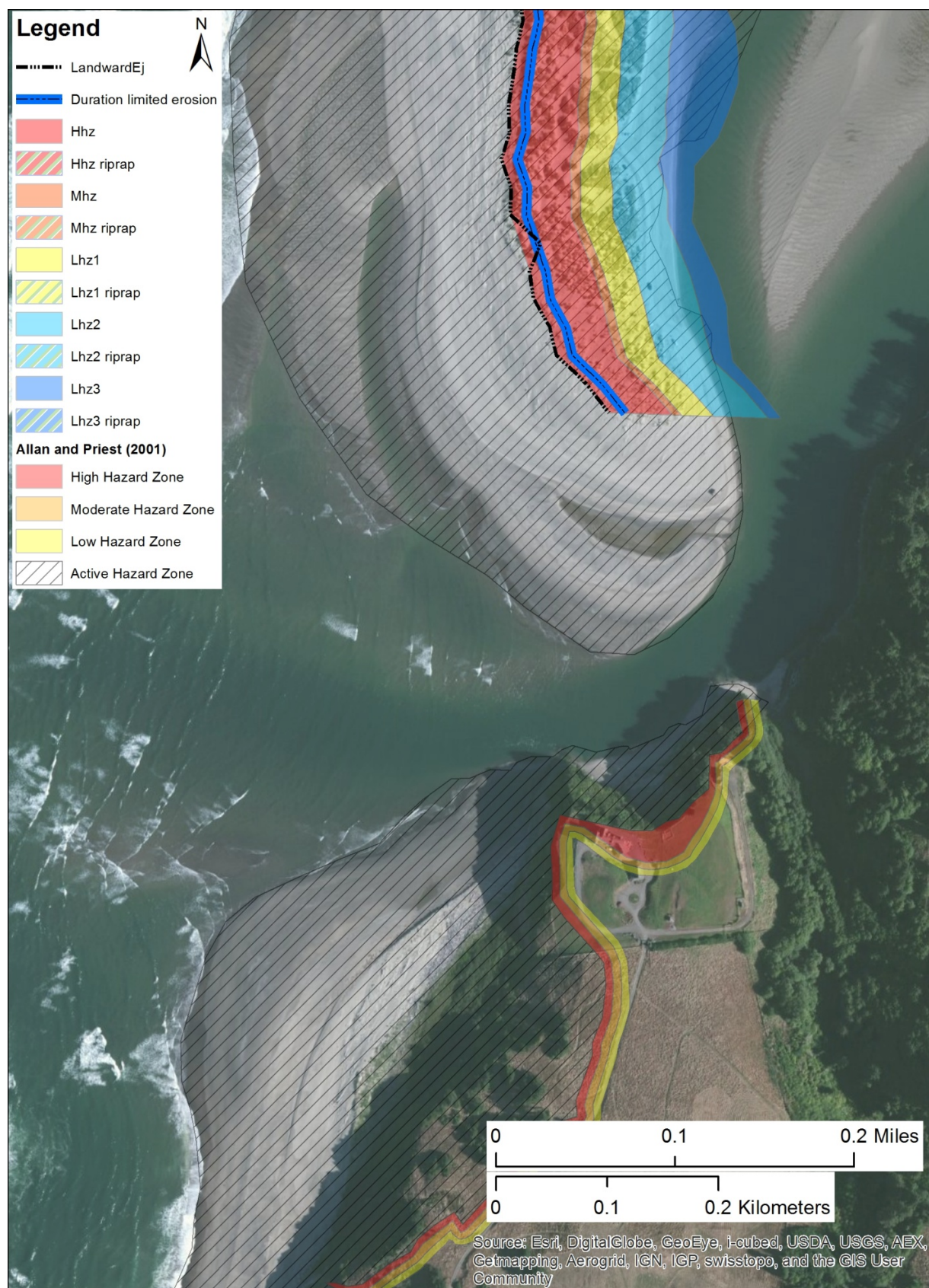




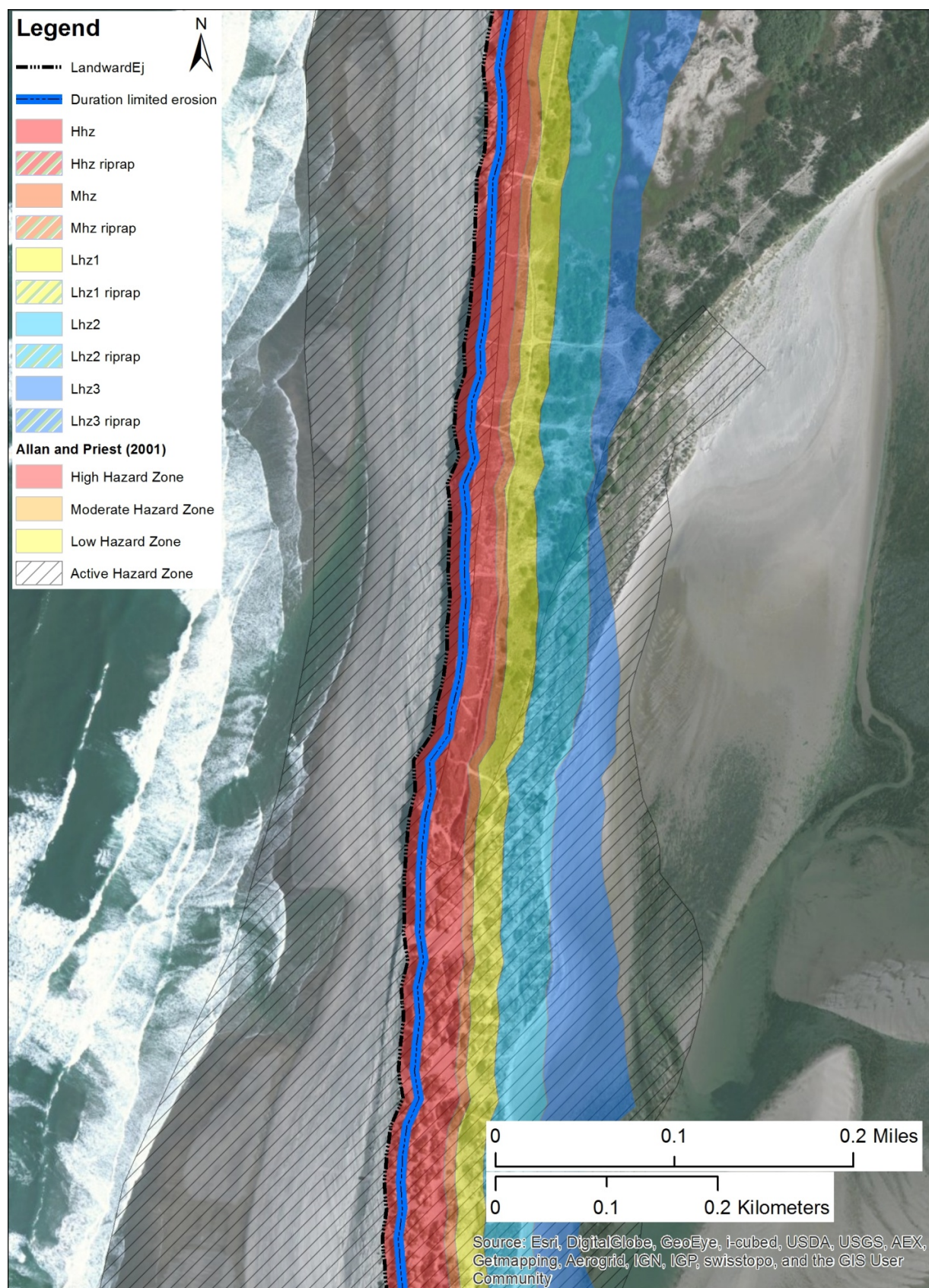




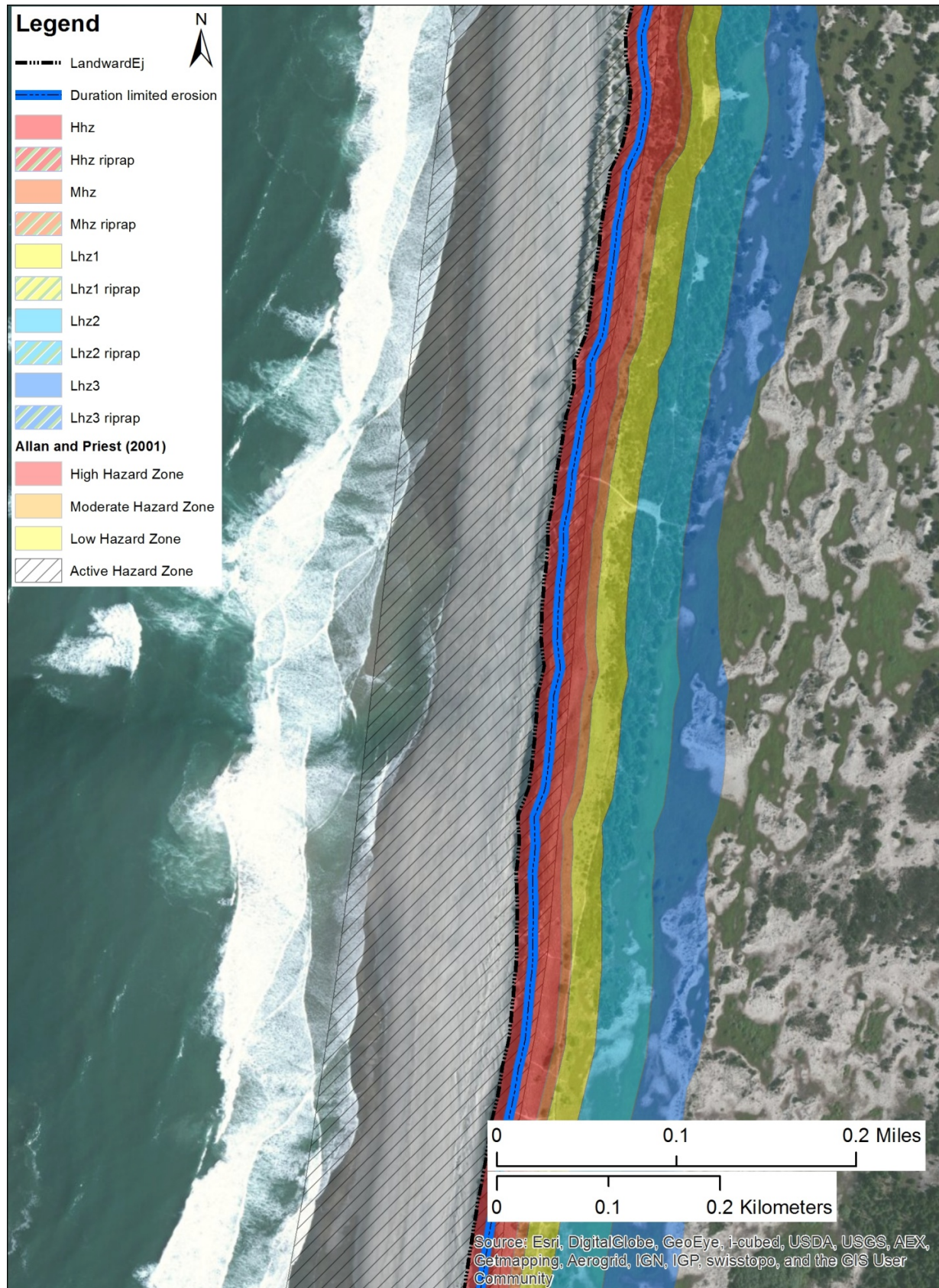




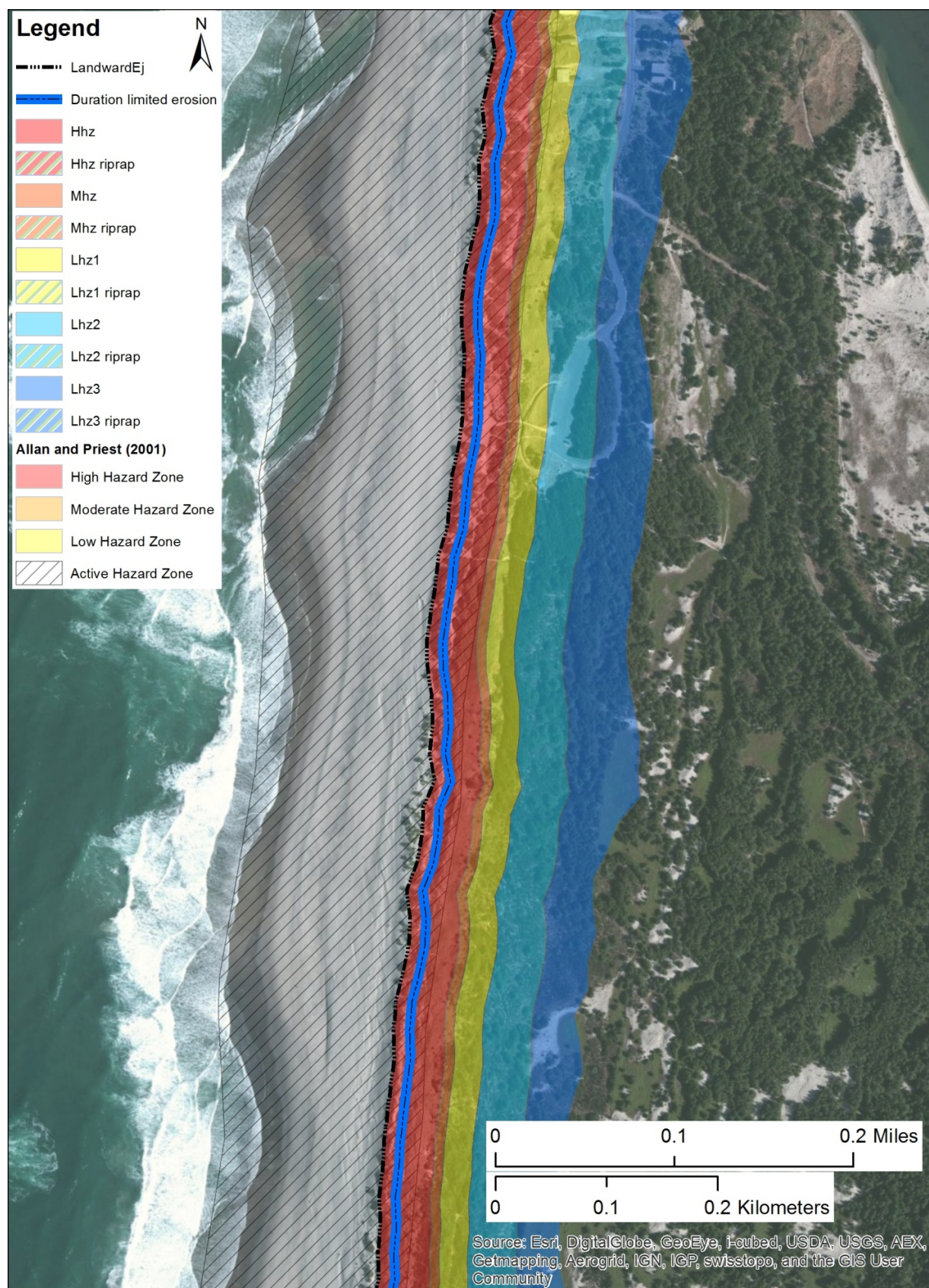






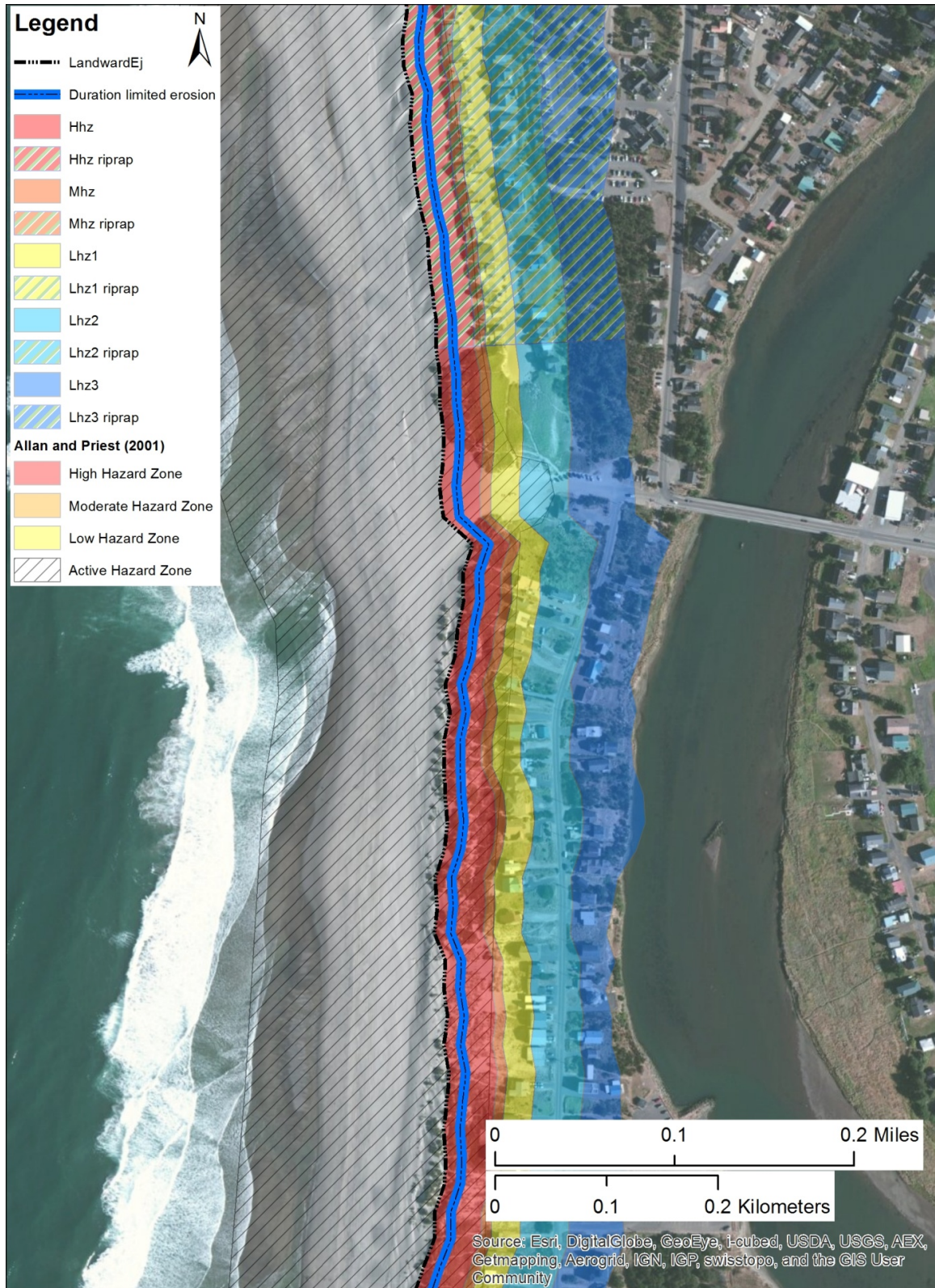




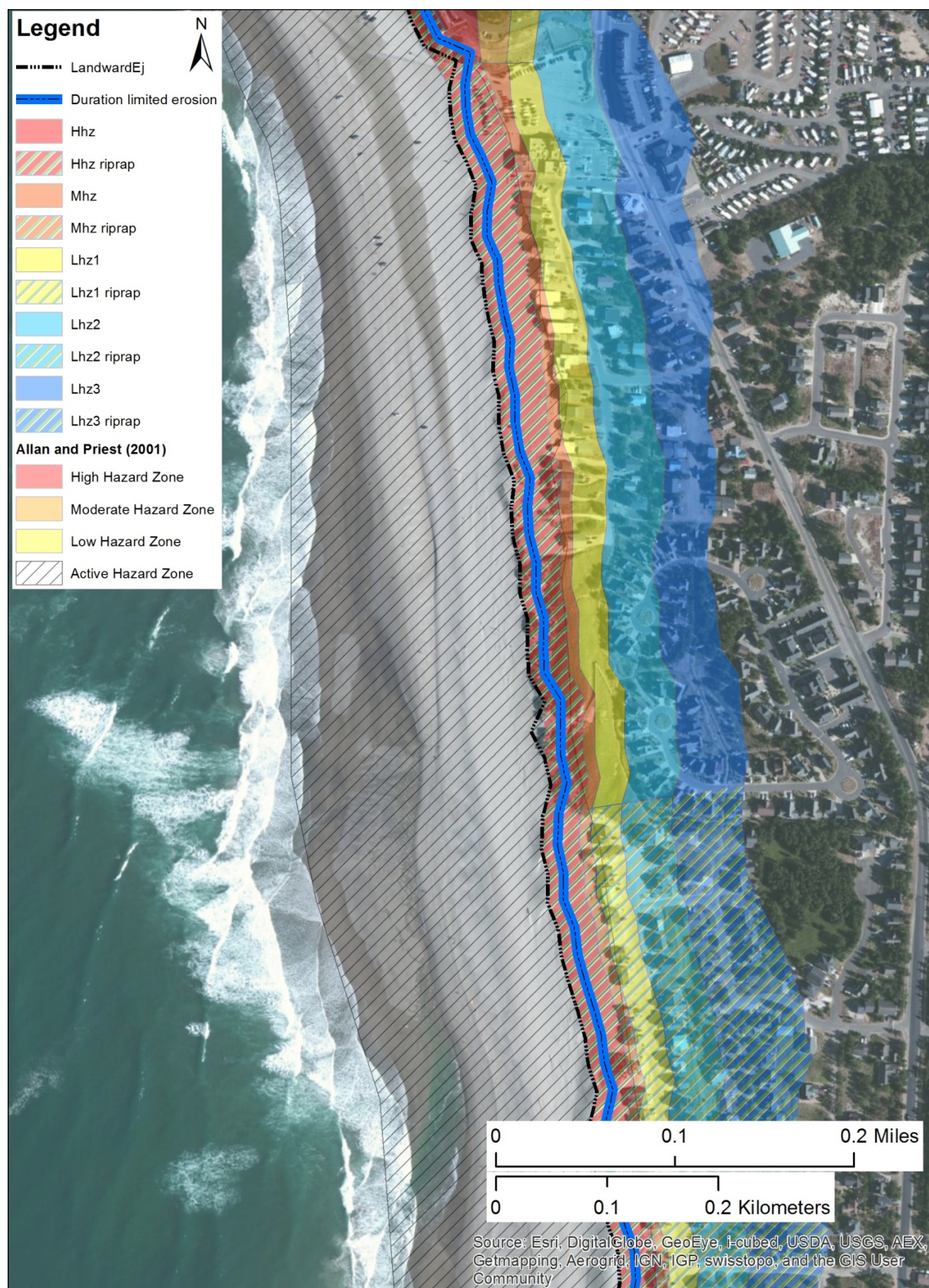




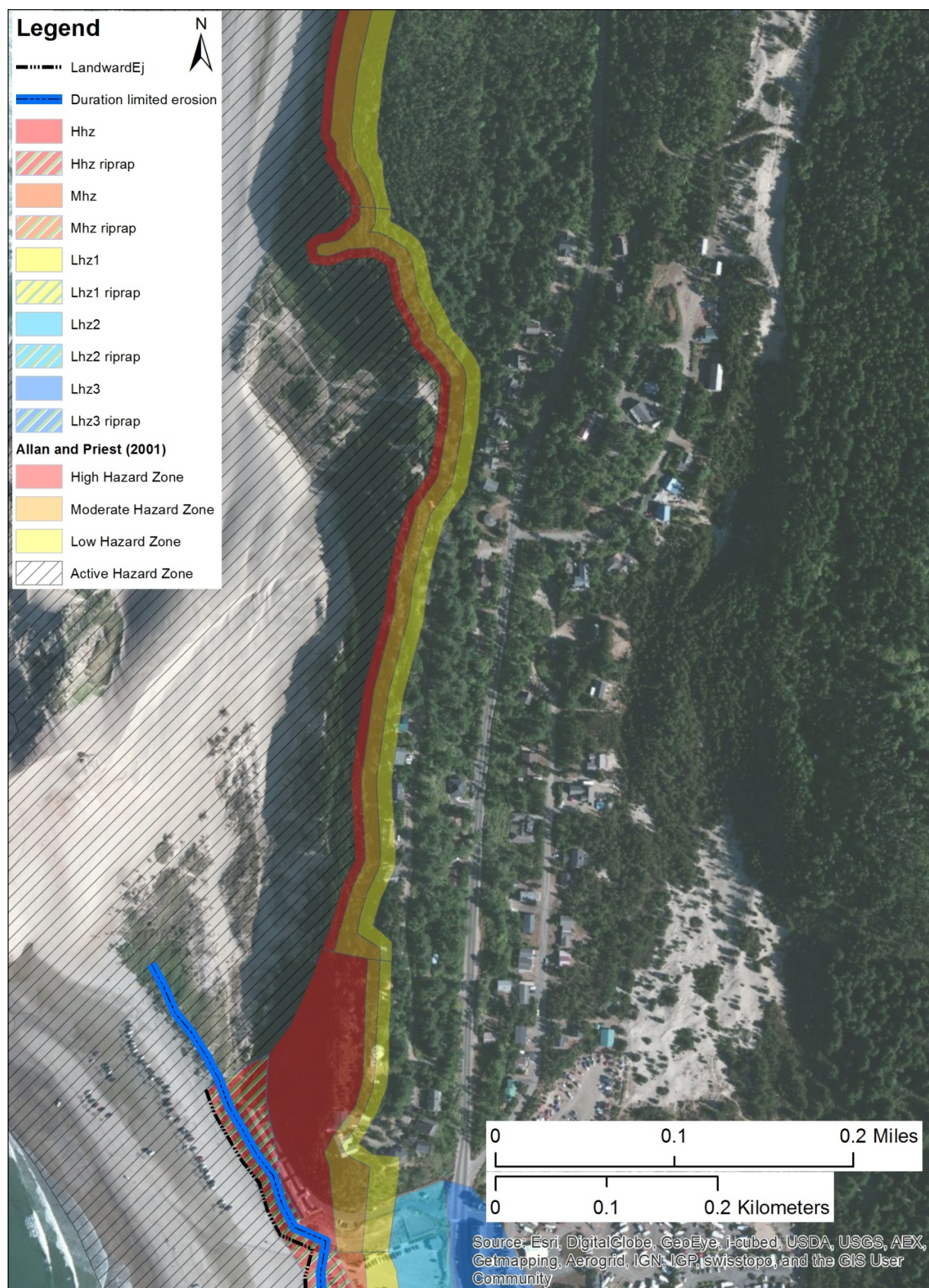
## Pacific City





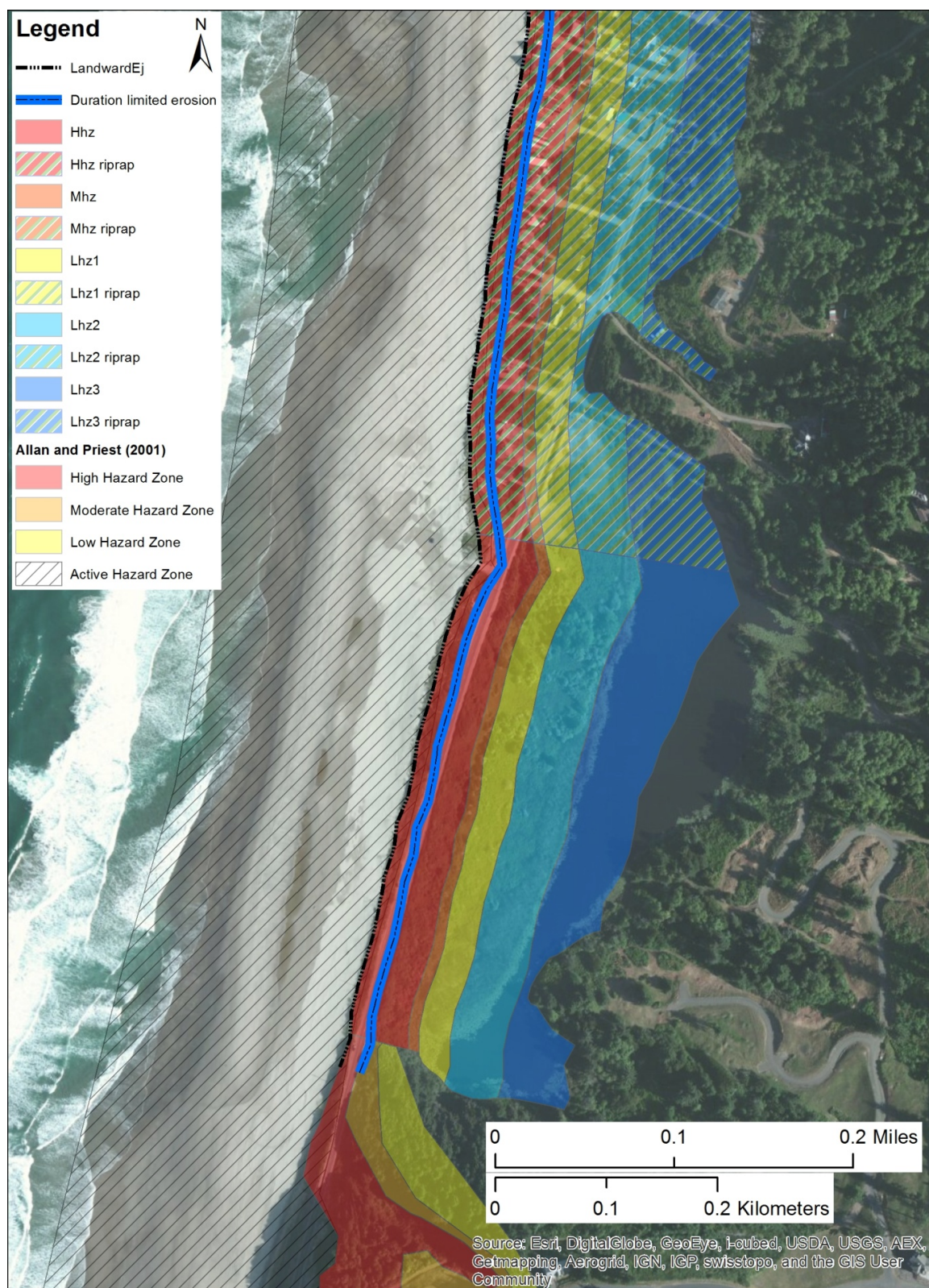




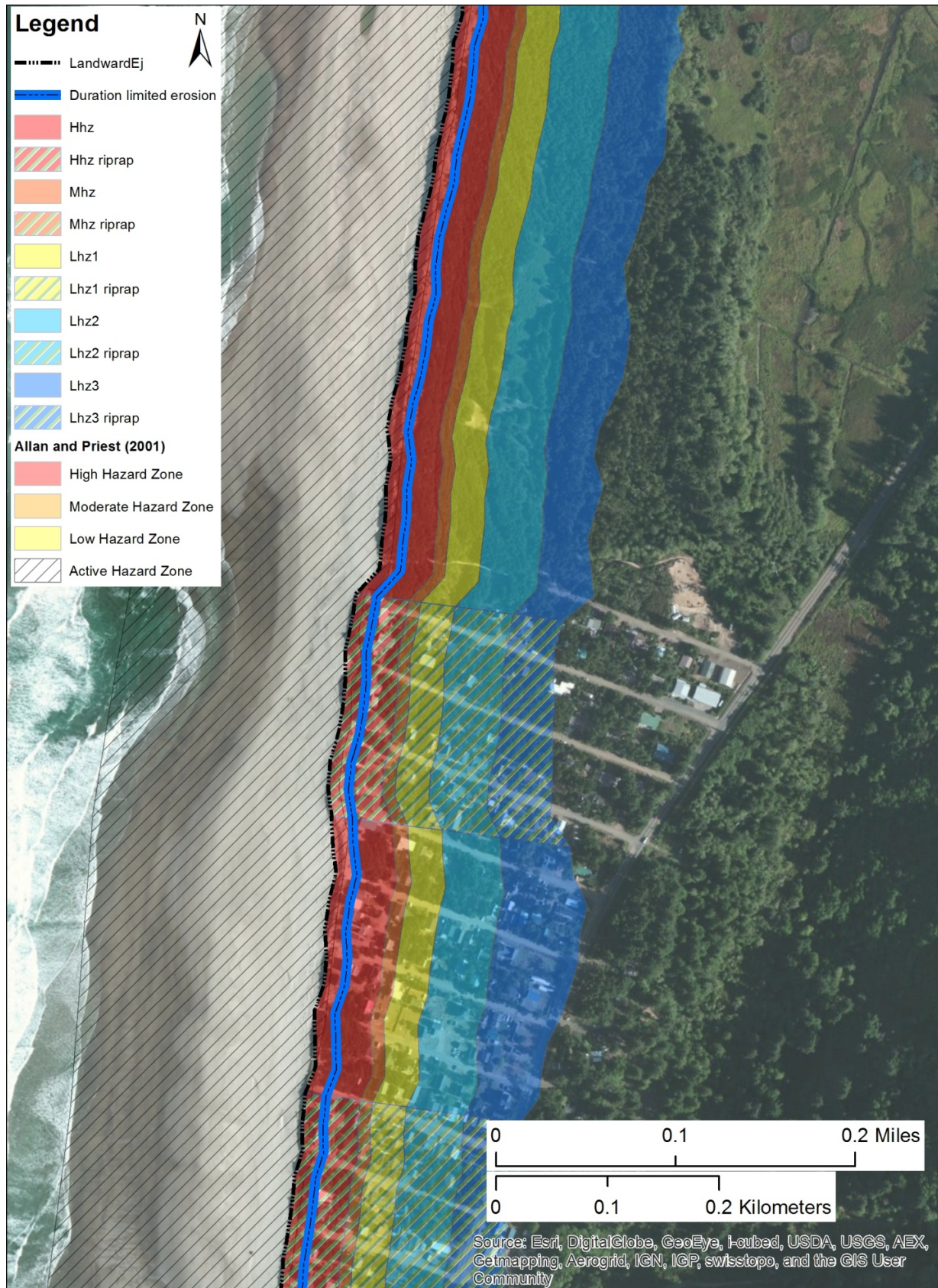




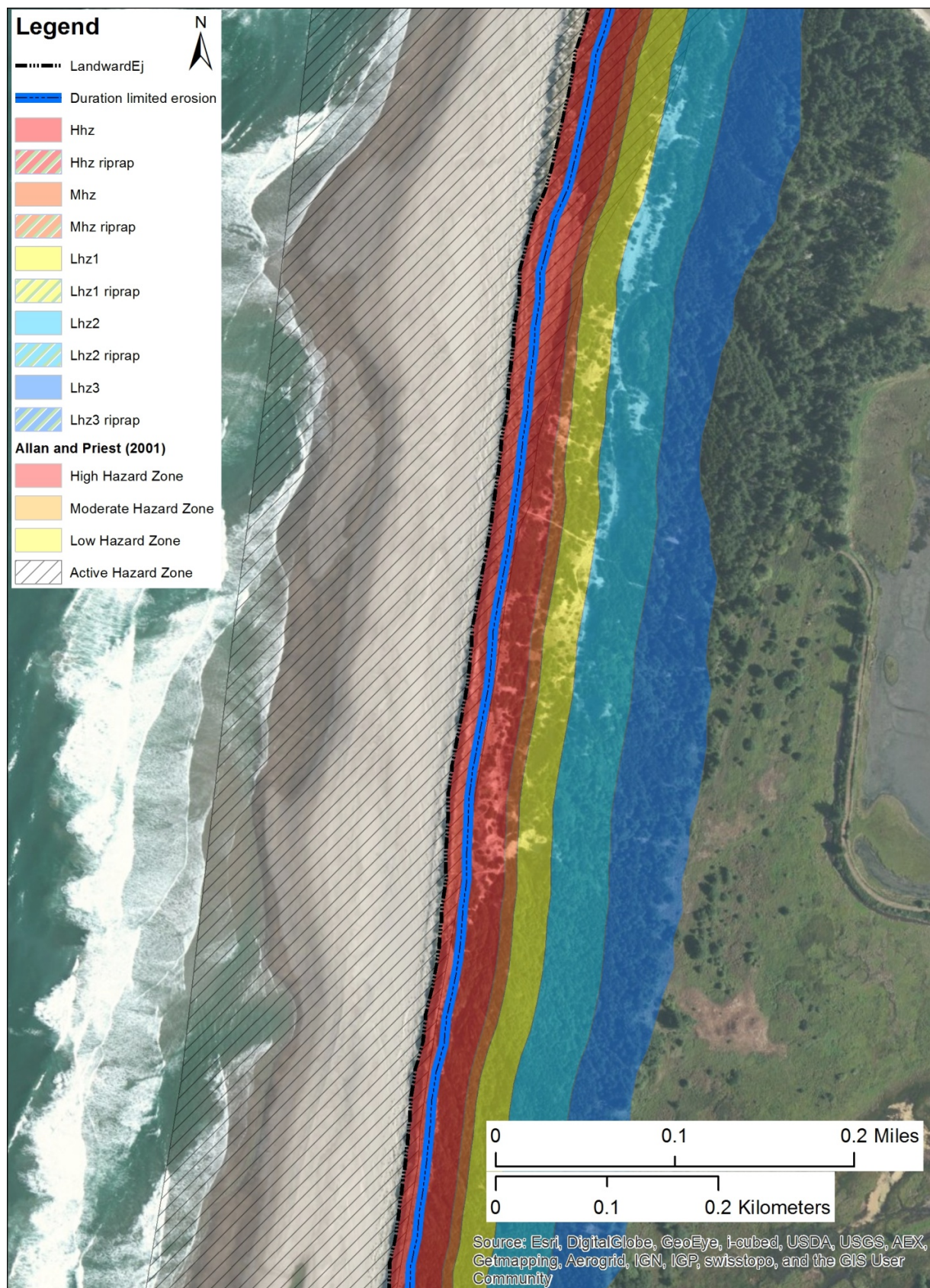
## Tierra Del Mar/Sand Lake



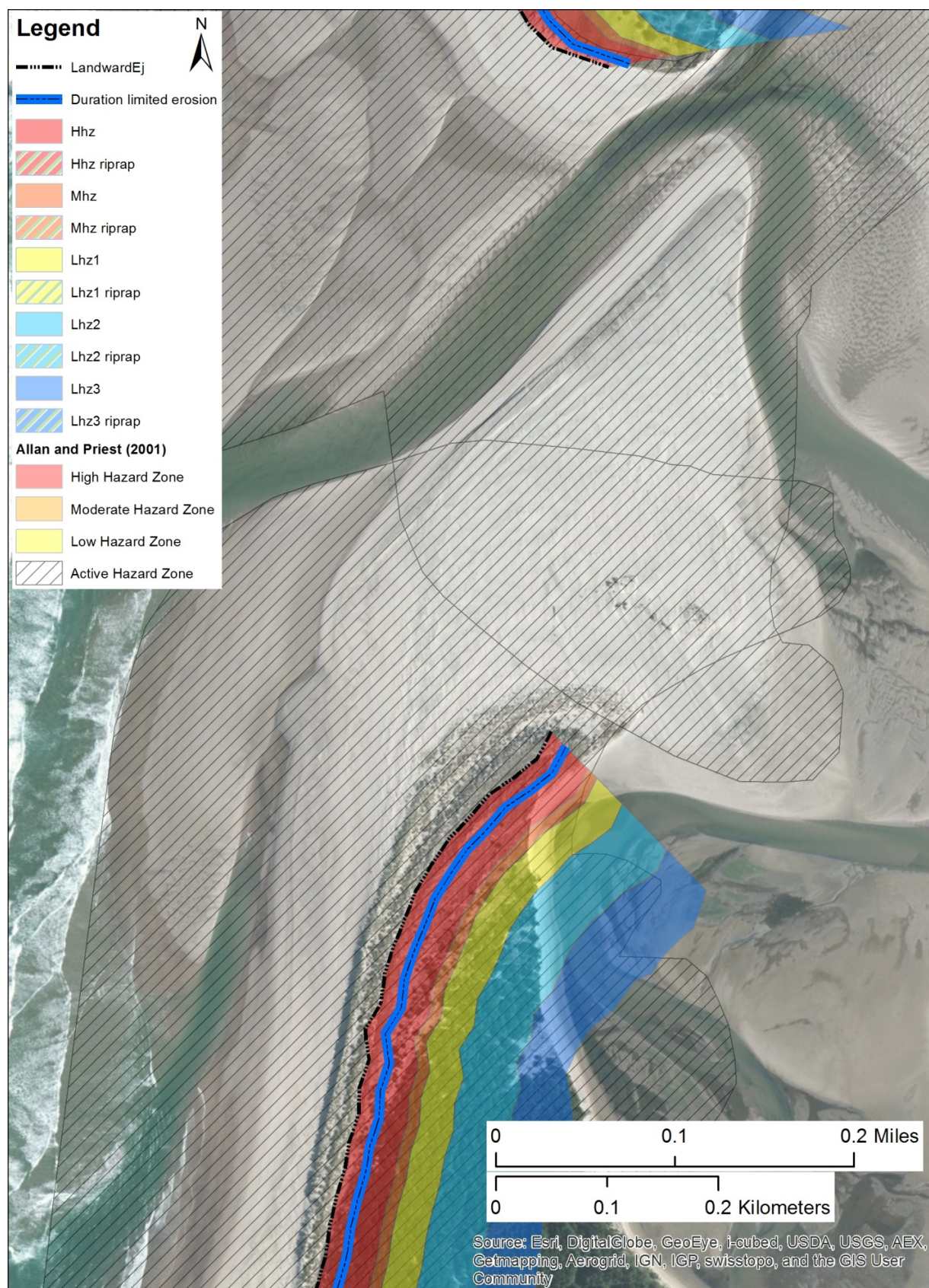




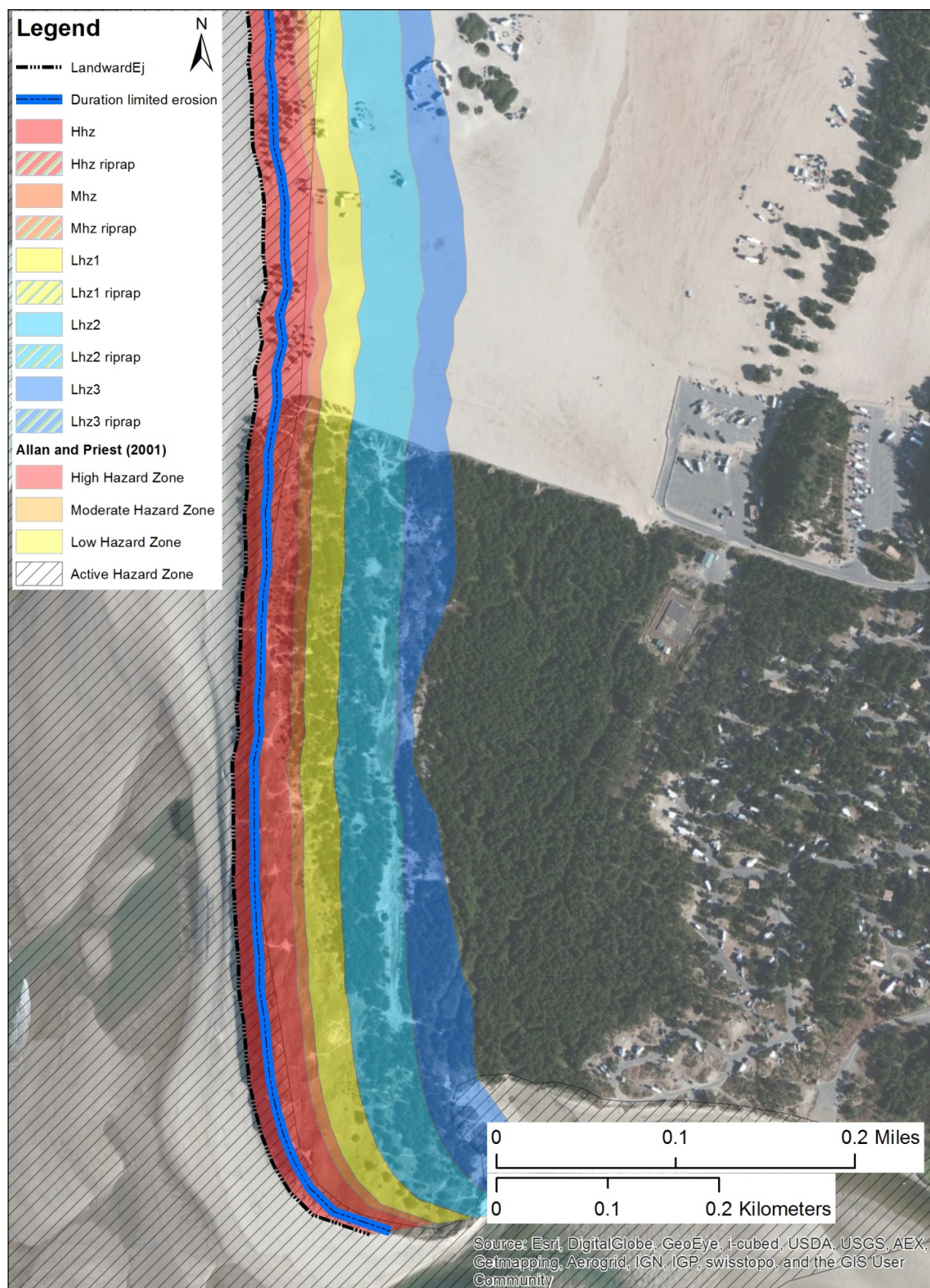




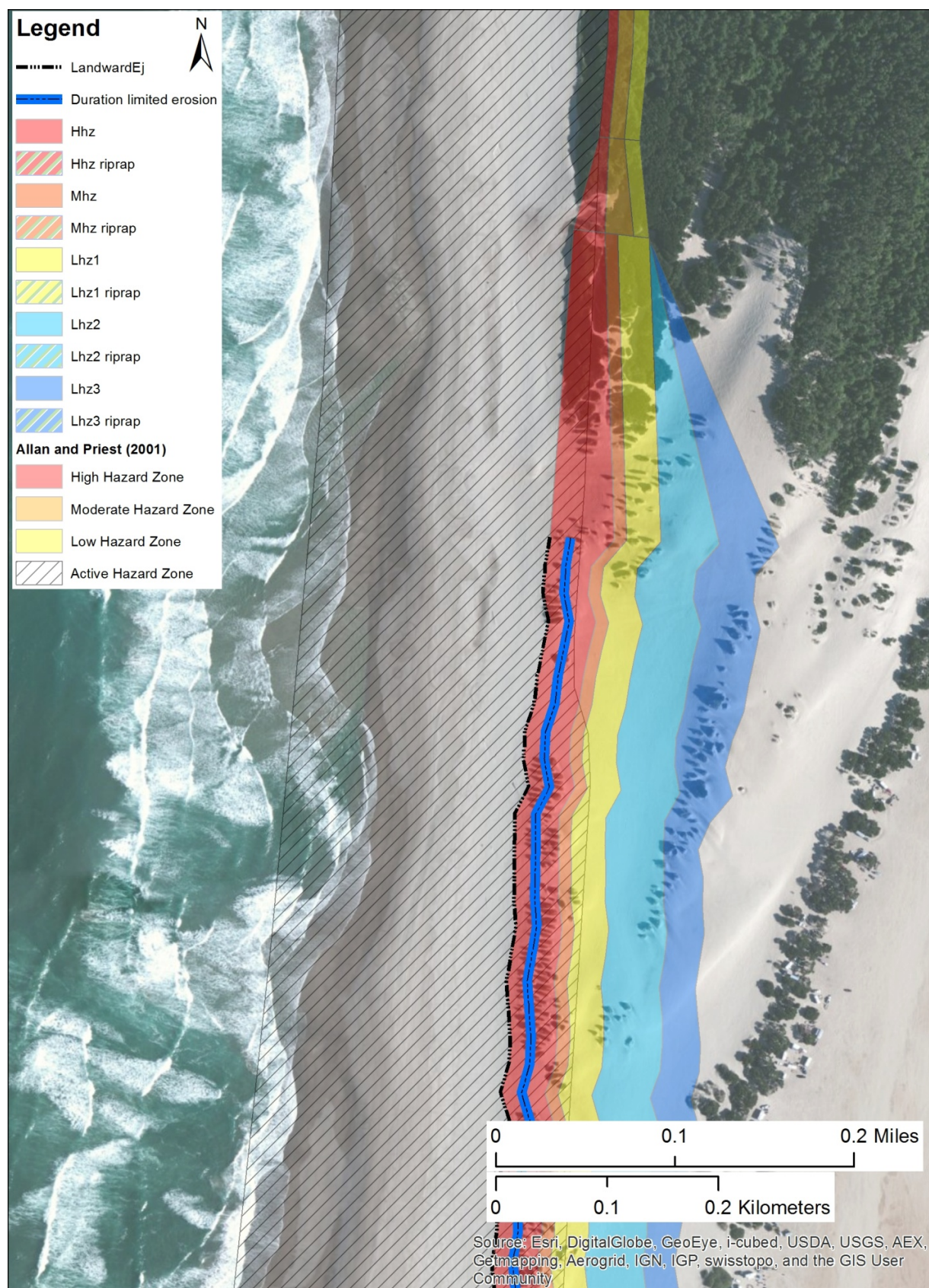






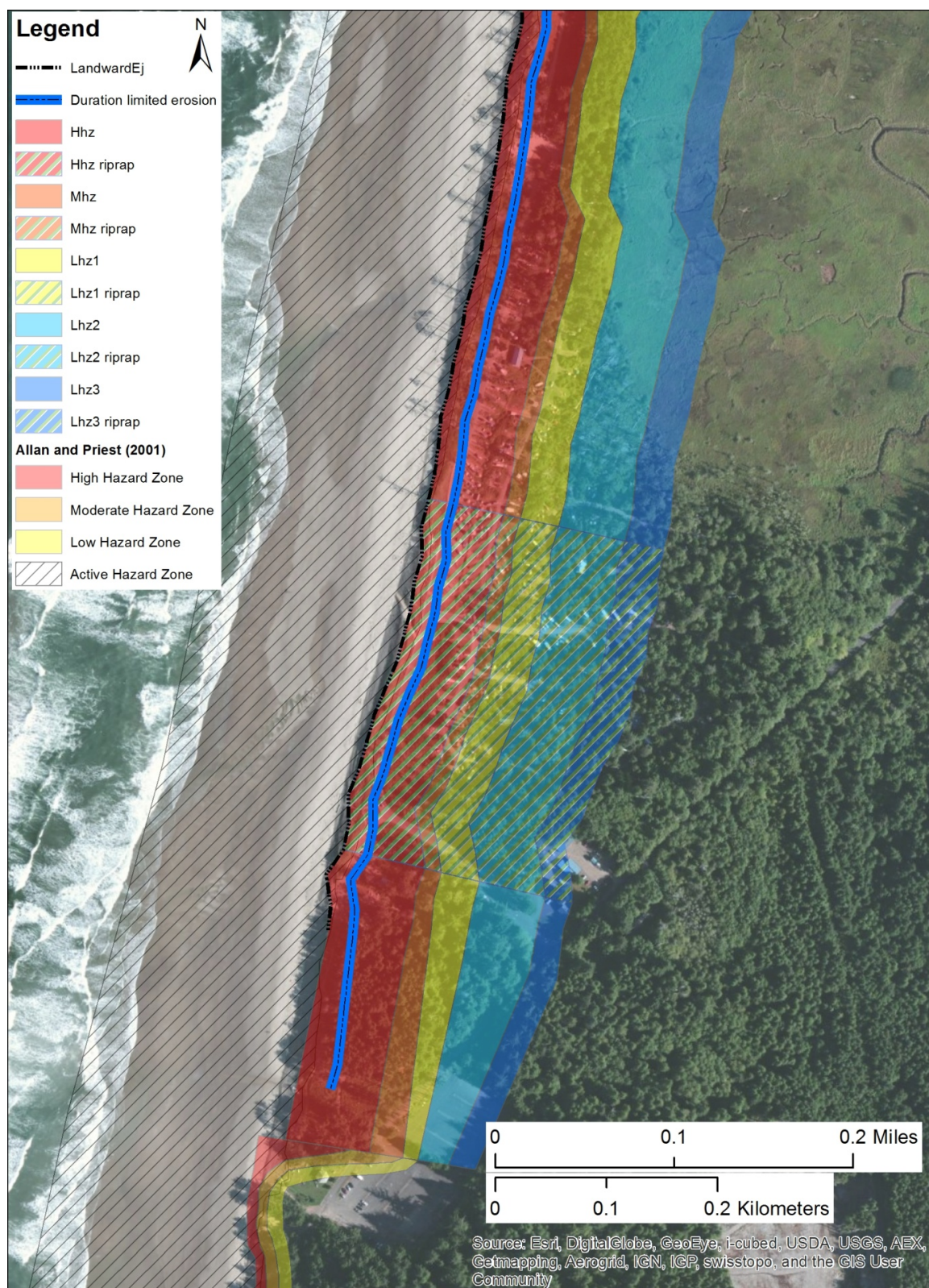




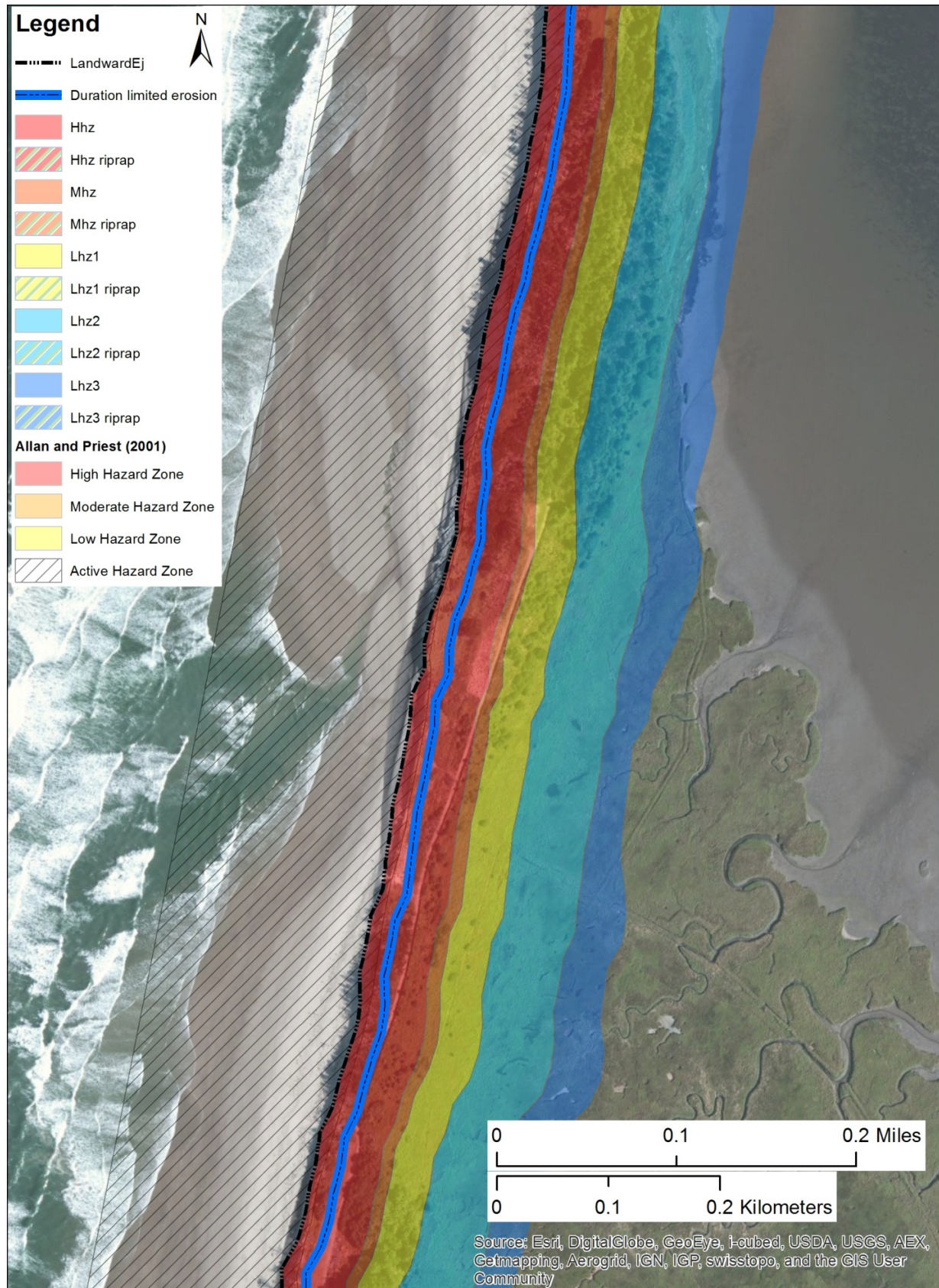




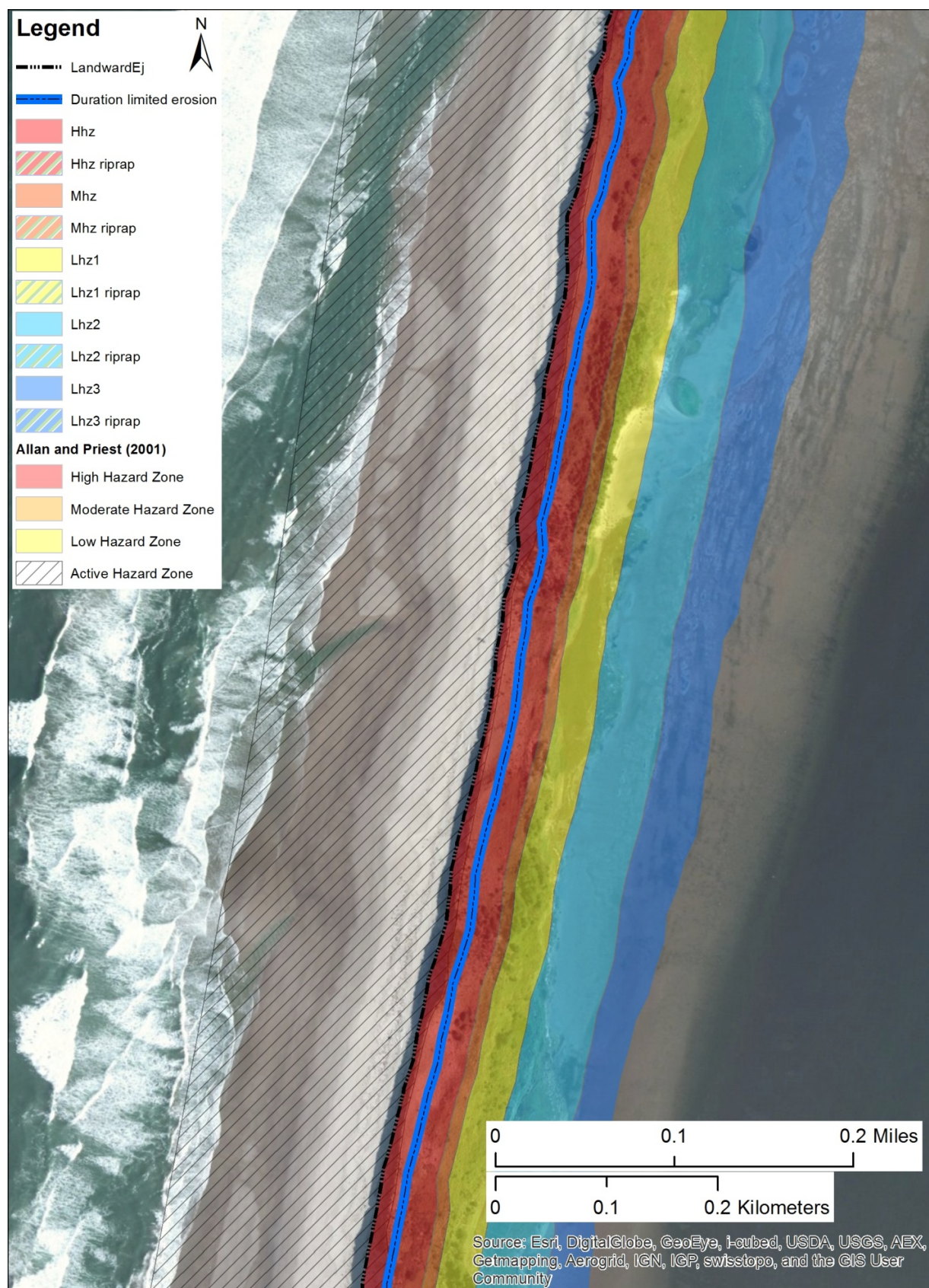
## Netarts



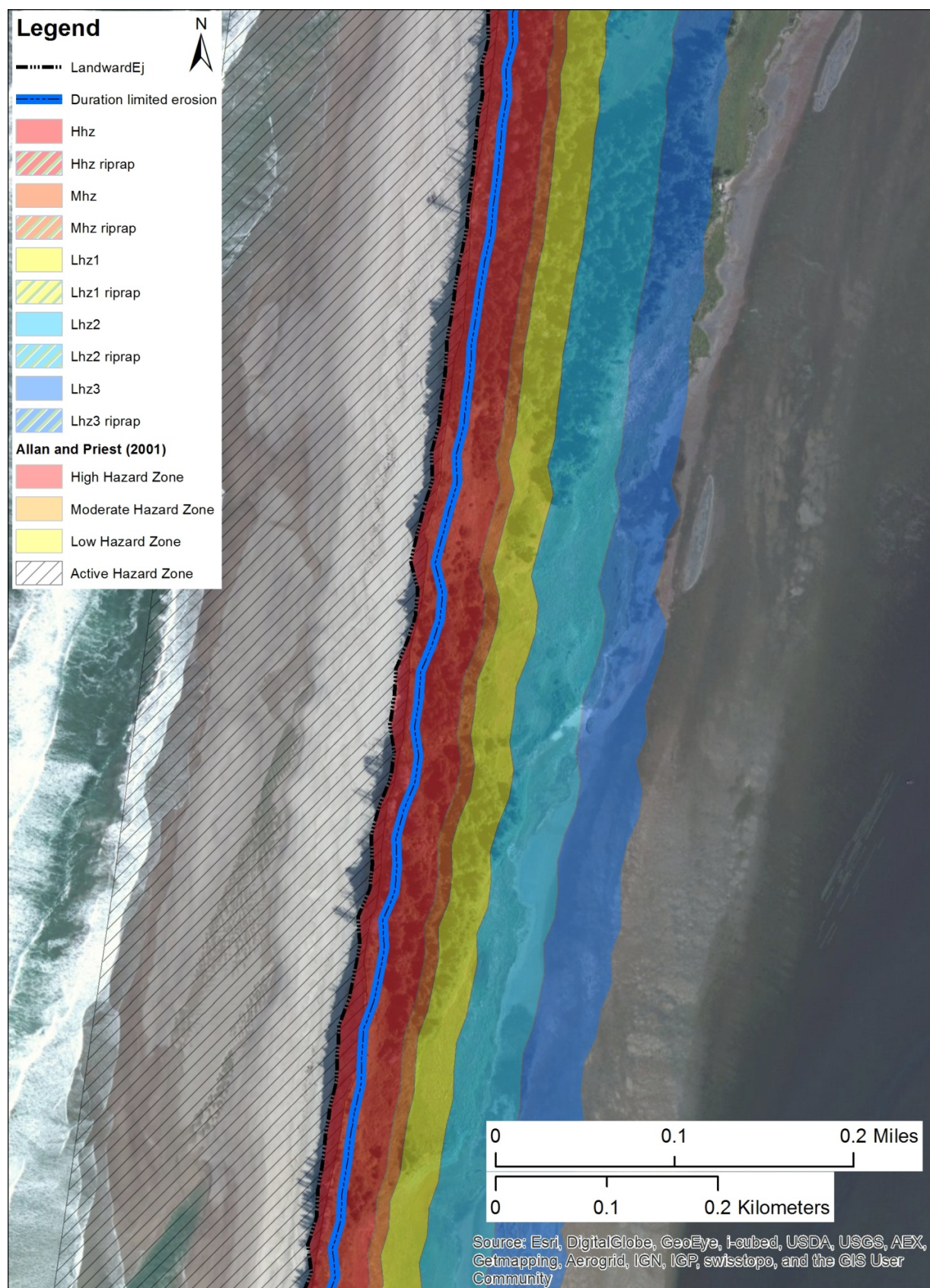




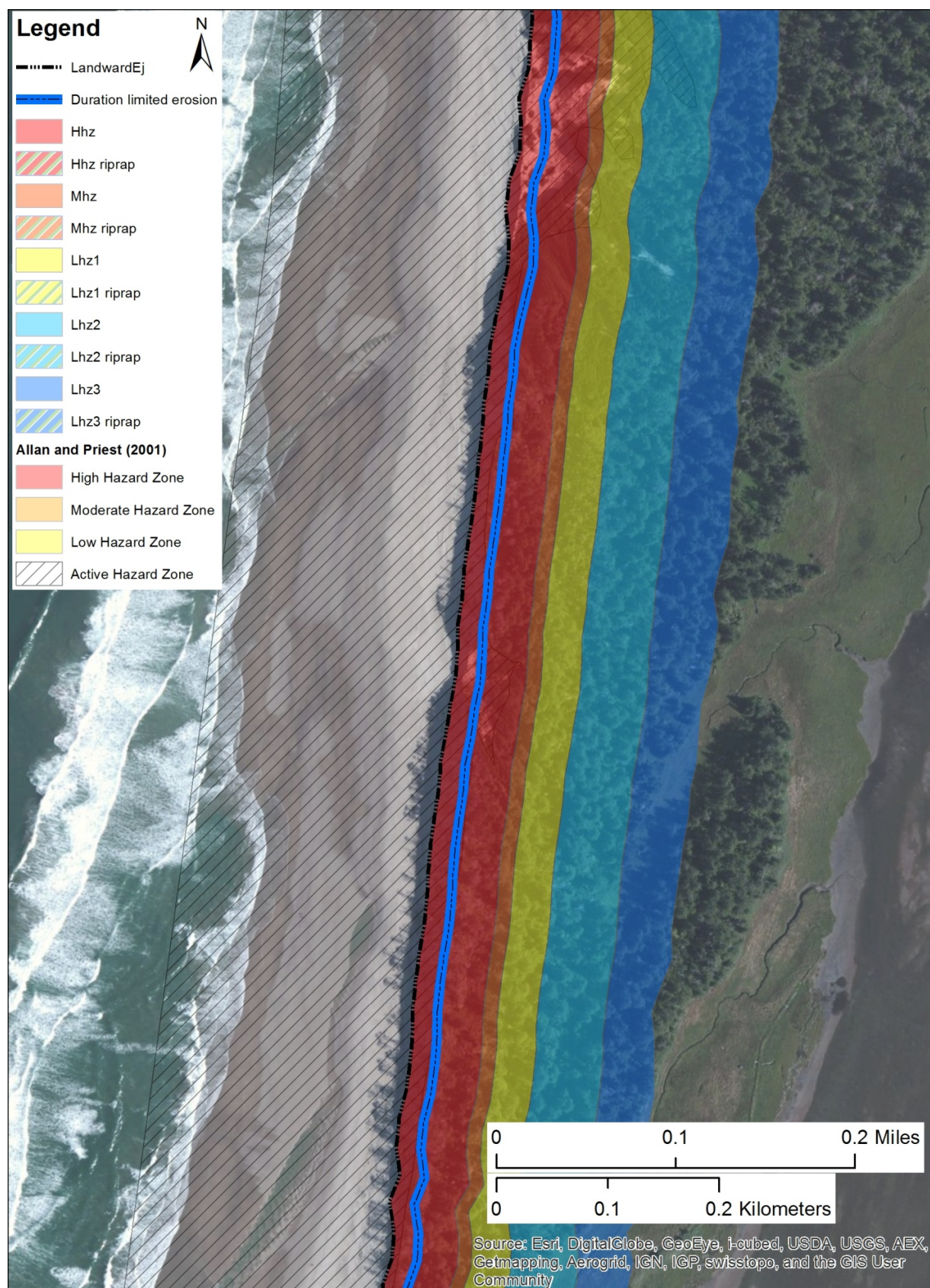




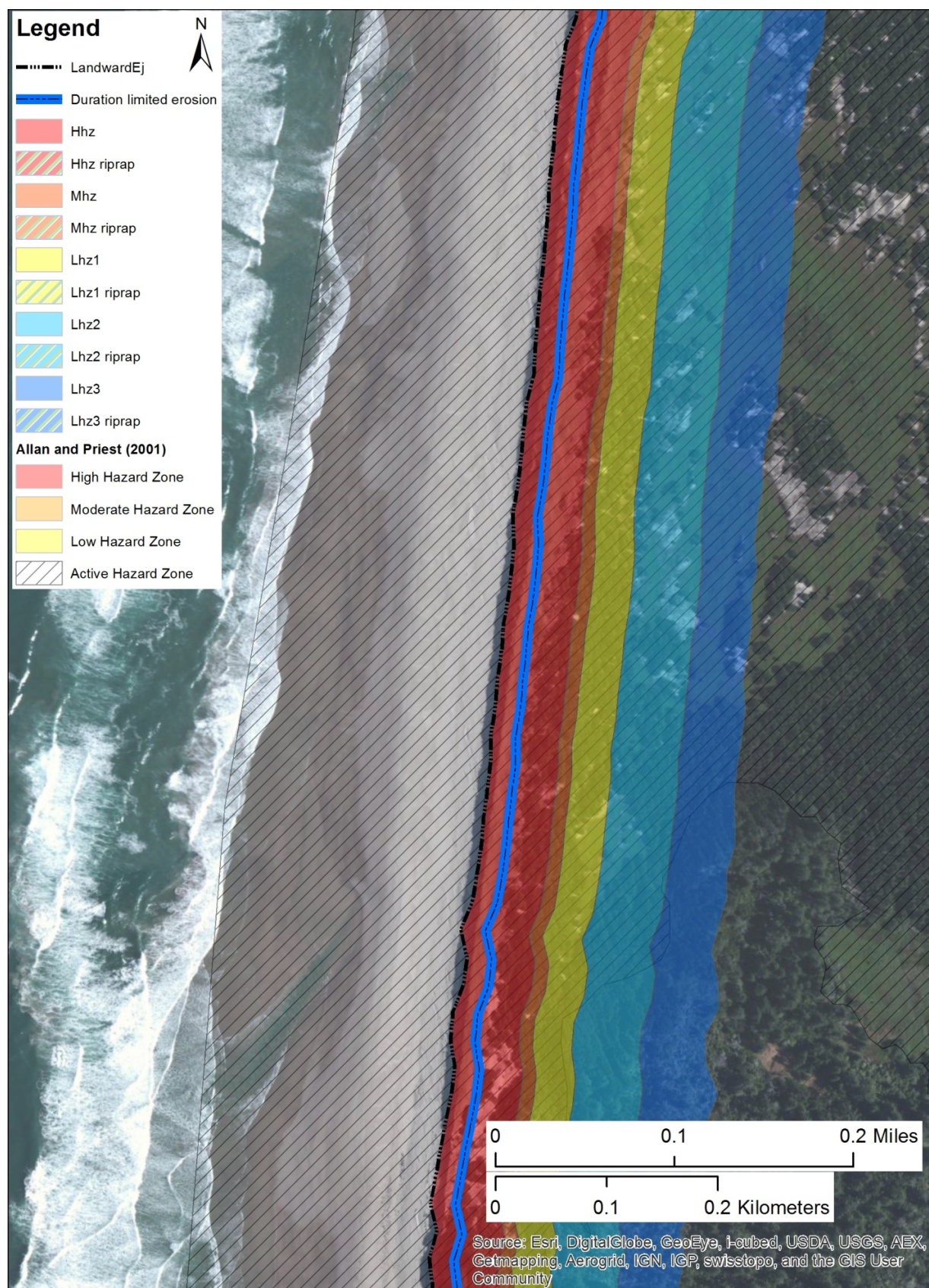




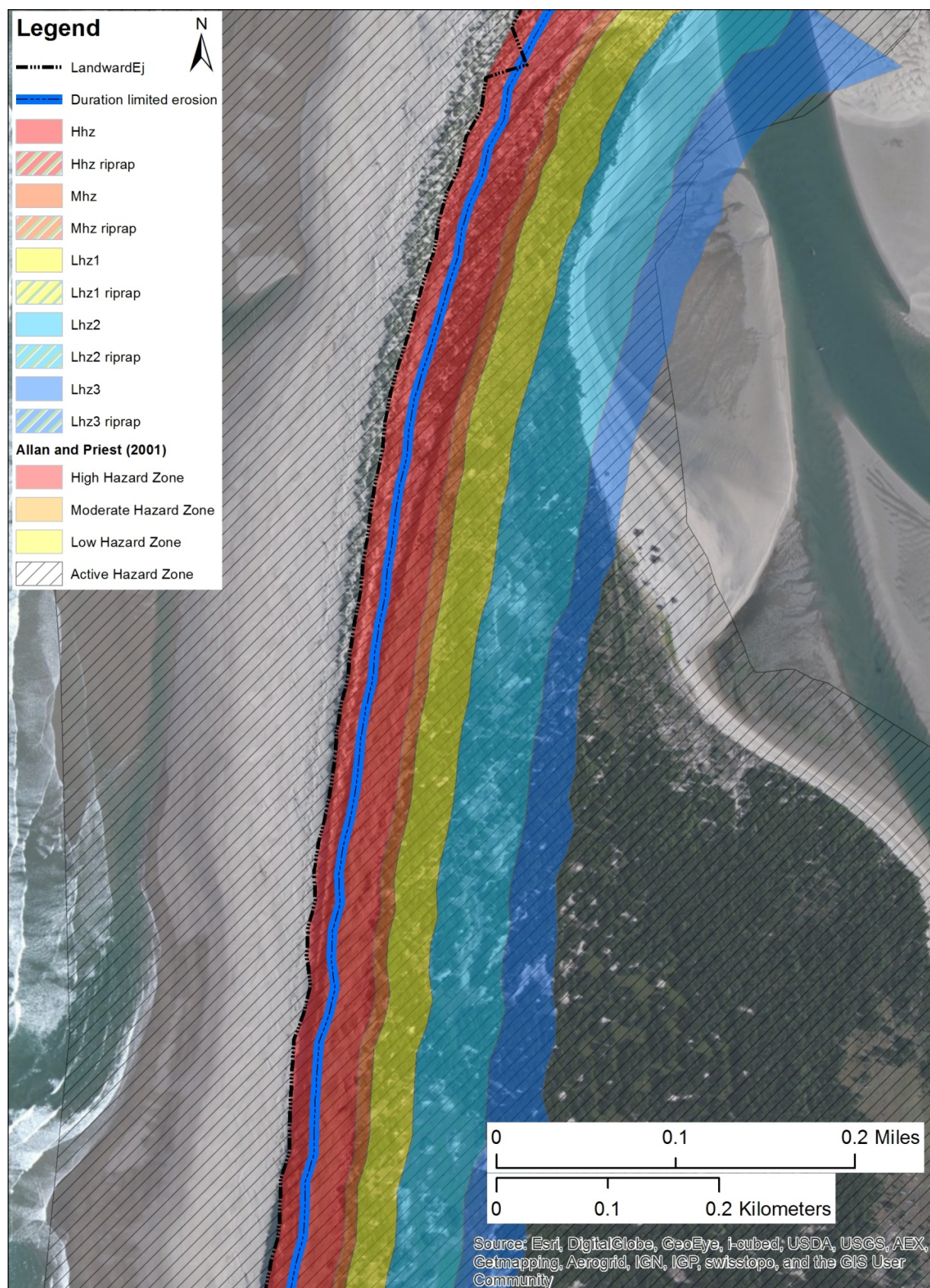










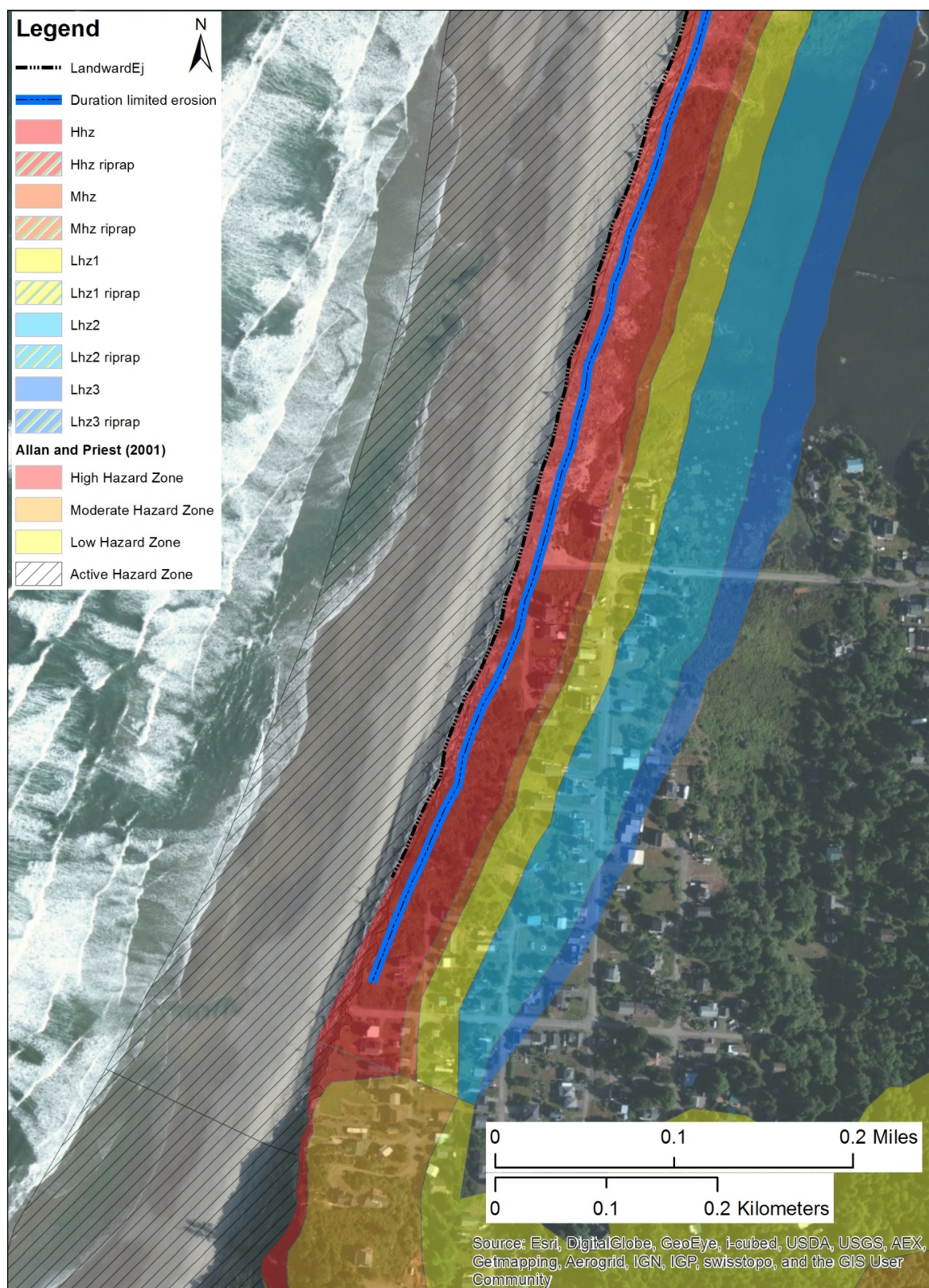




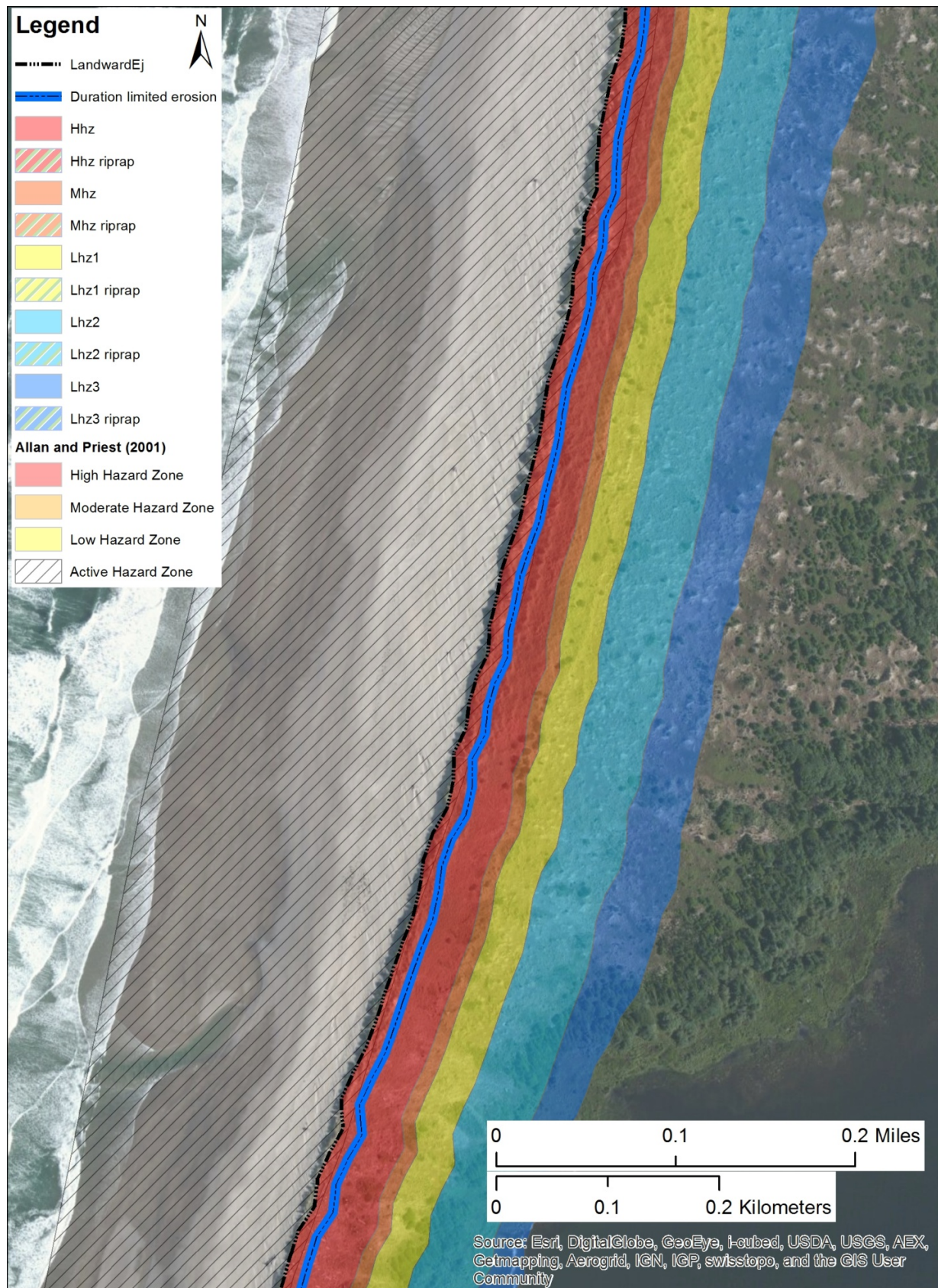




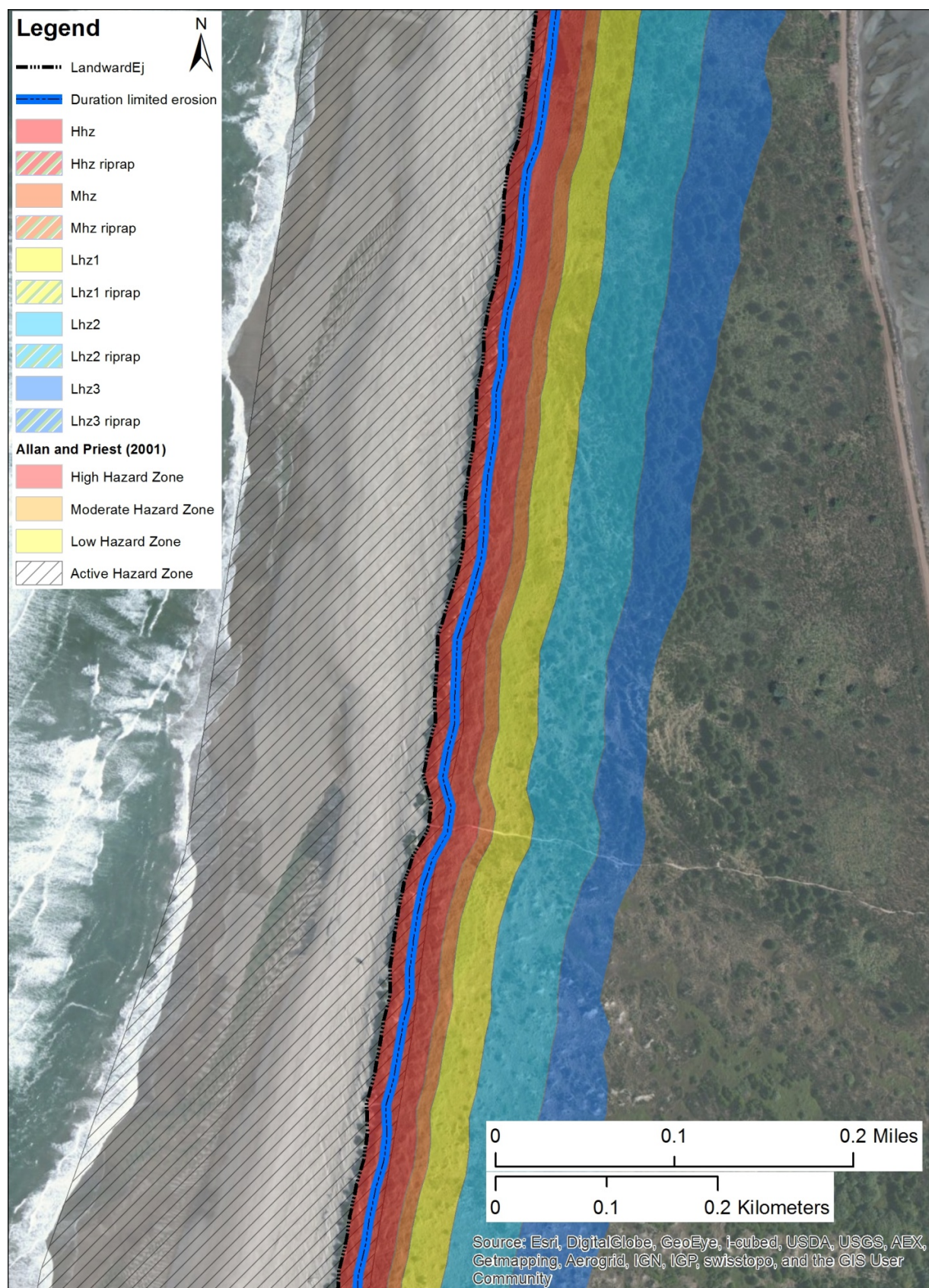
## Cape Meares/Bayocean Spit



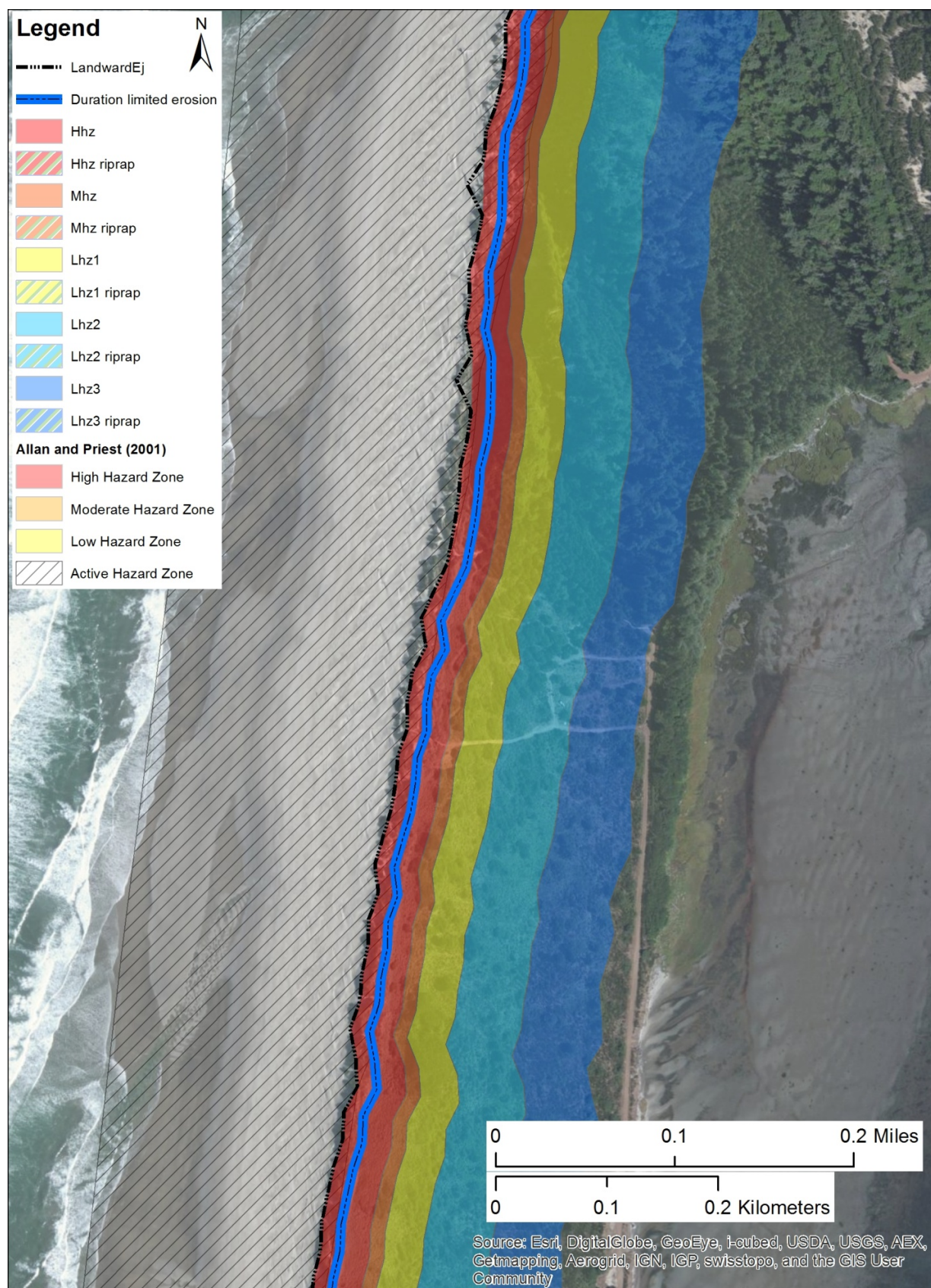




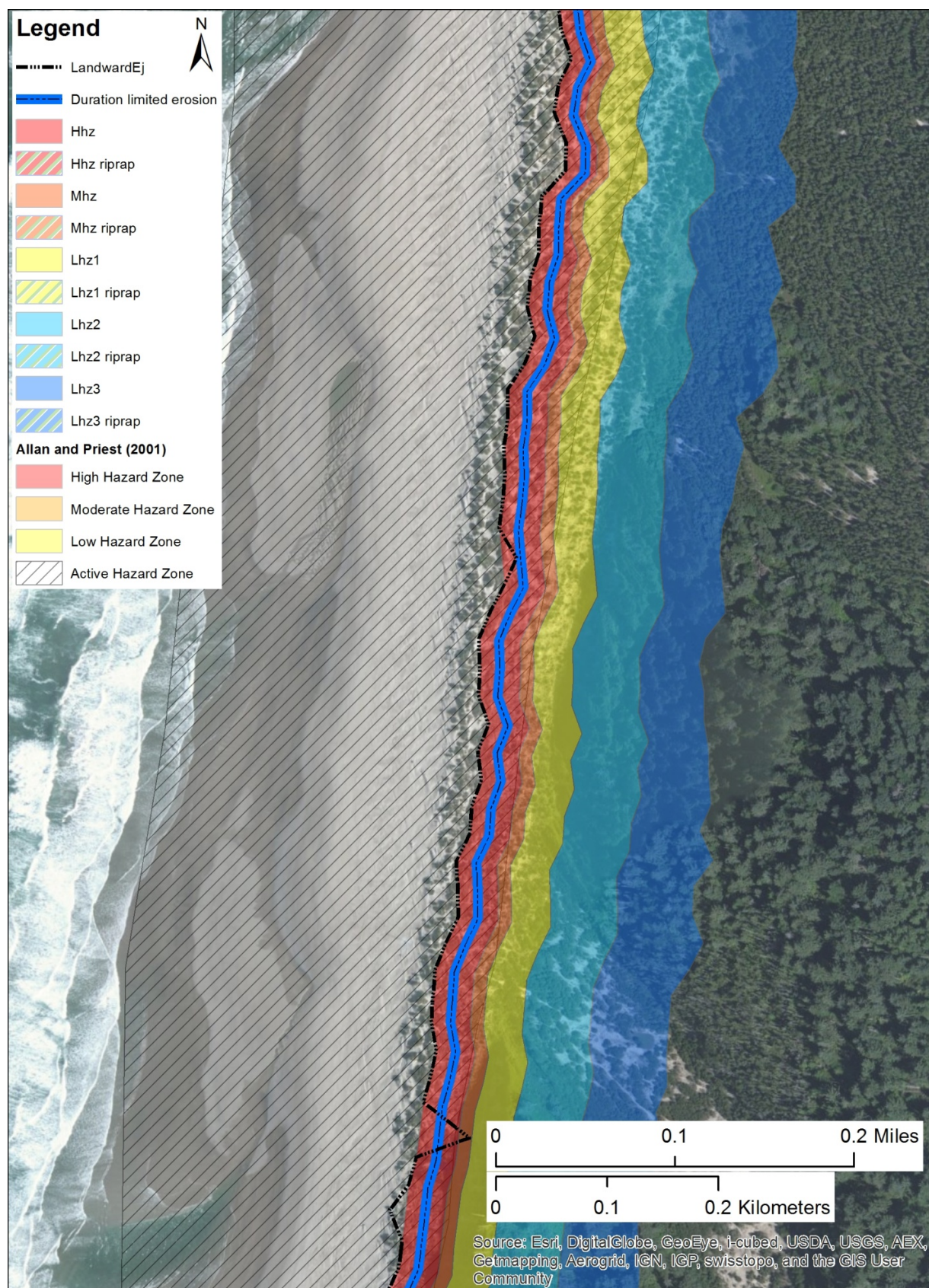




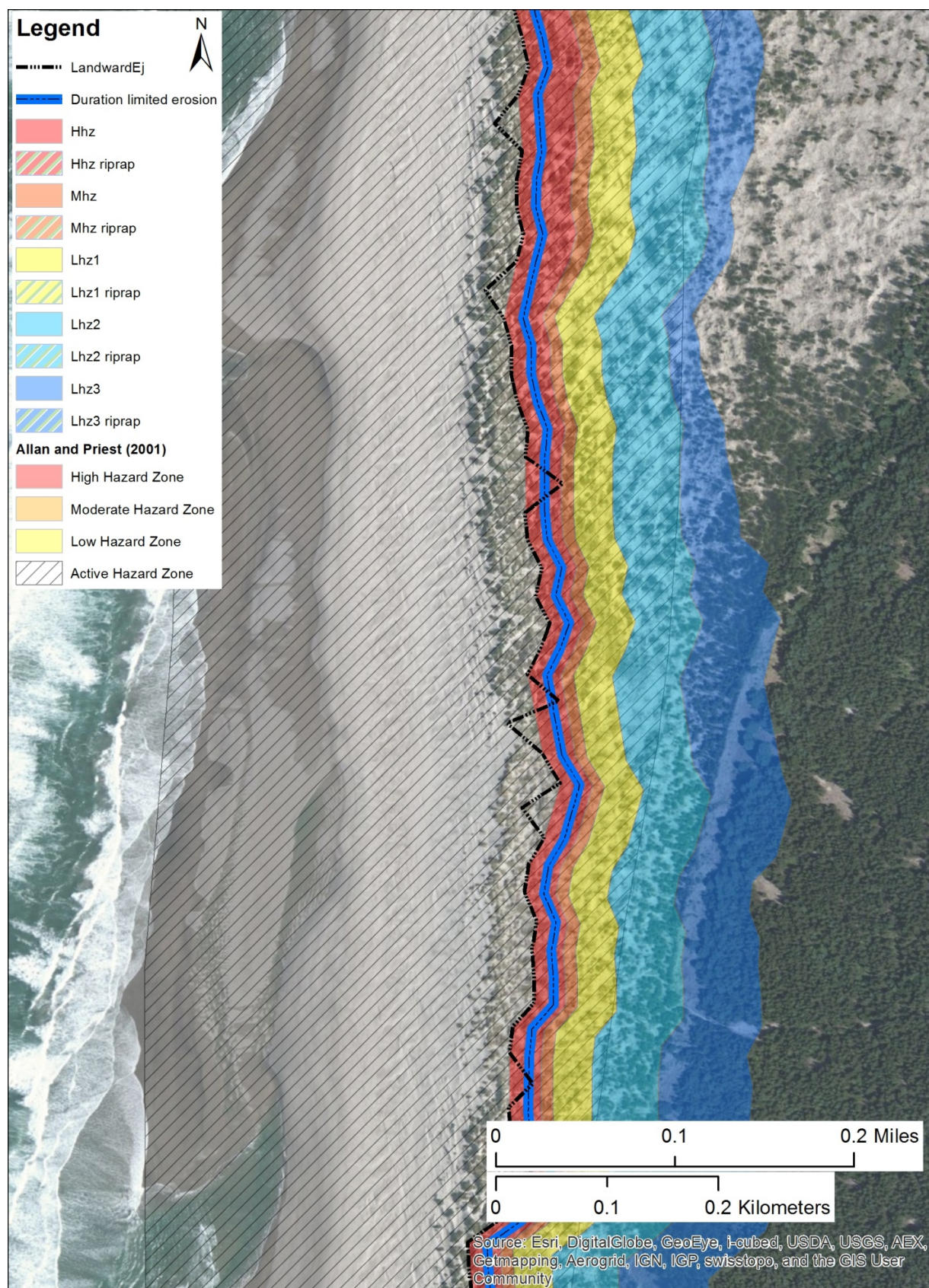




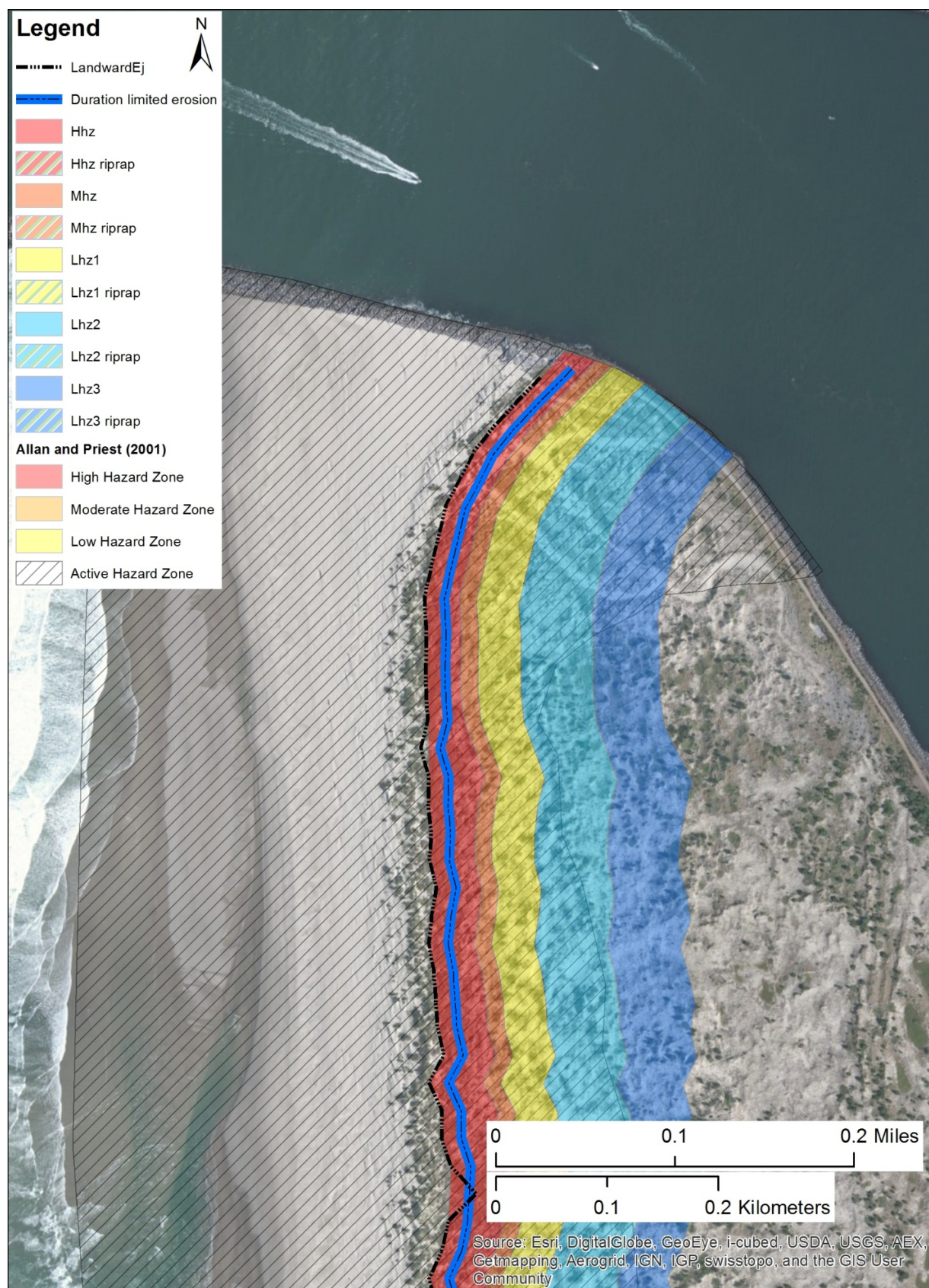






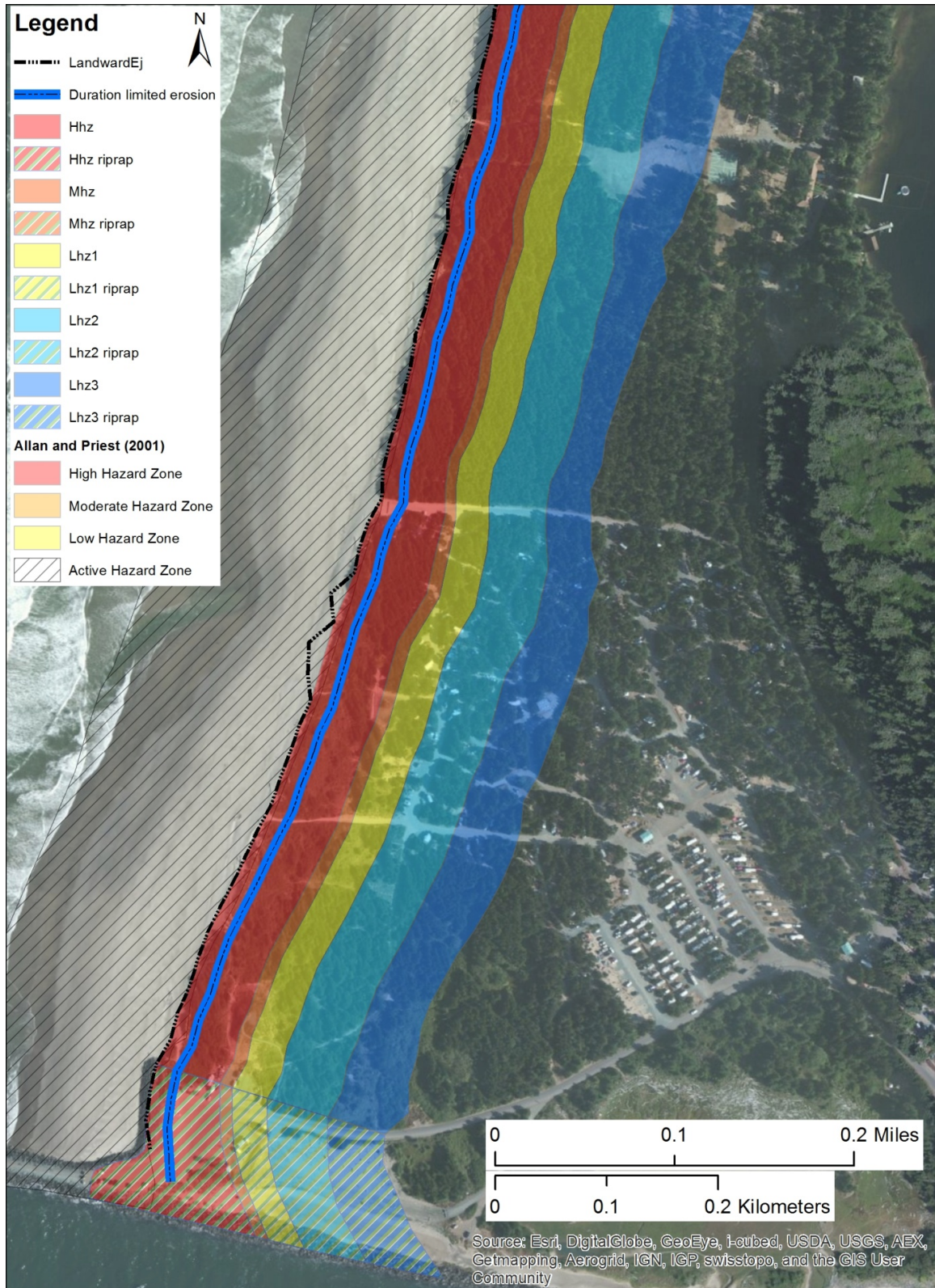




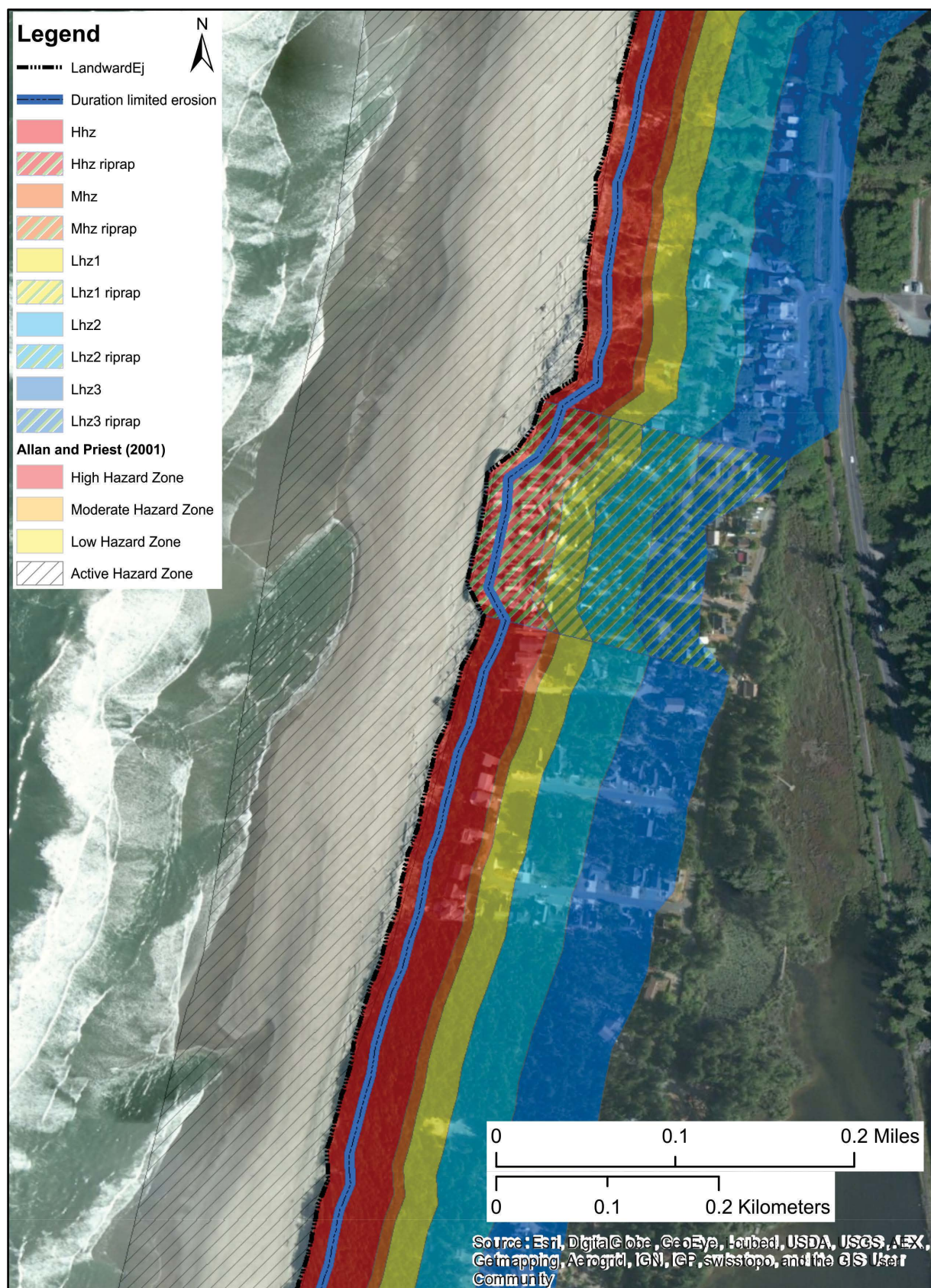




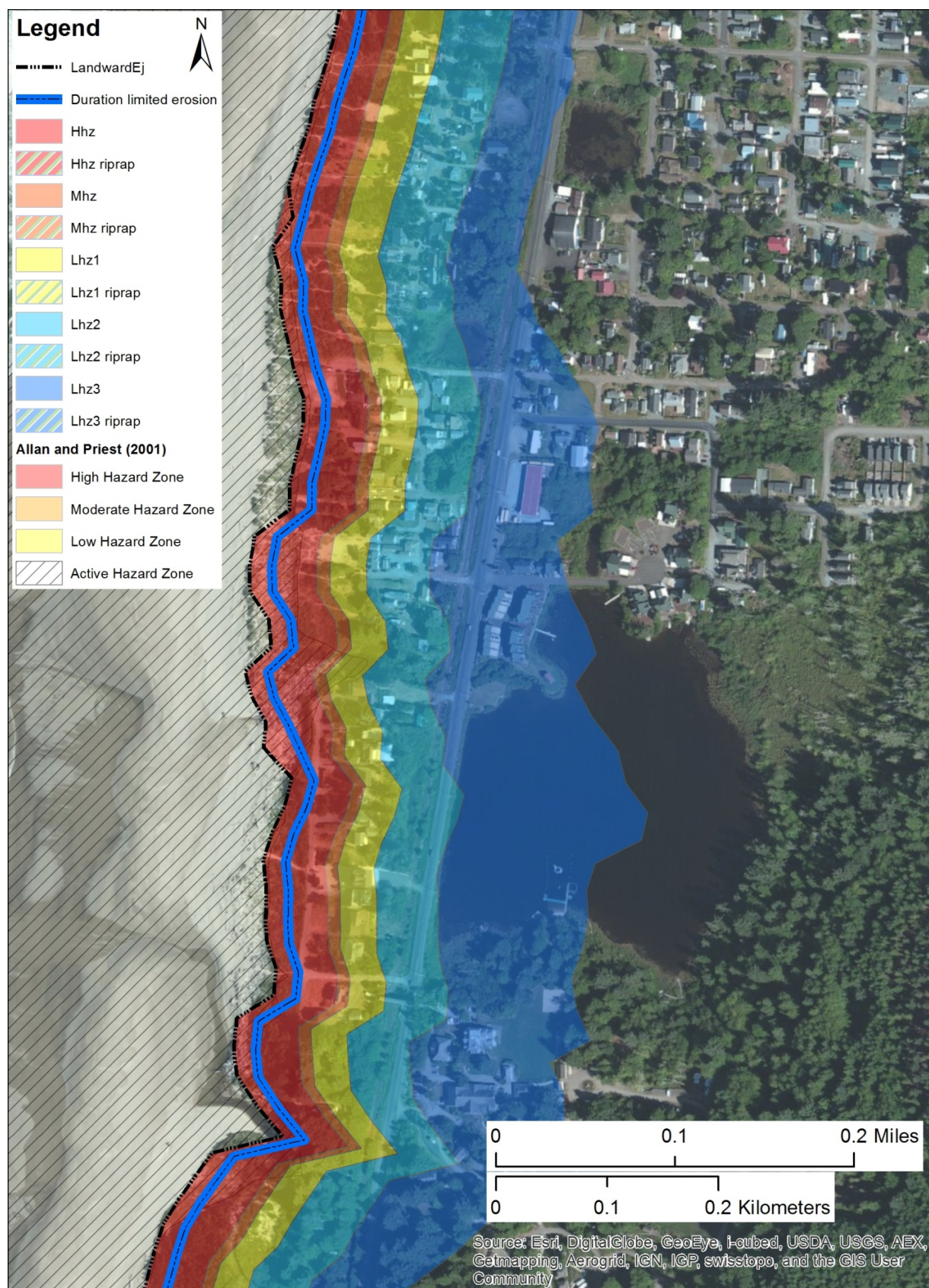
## Rockaway



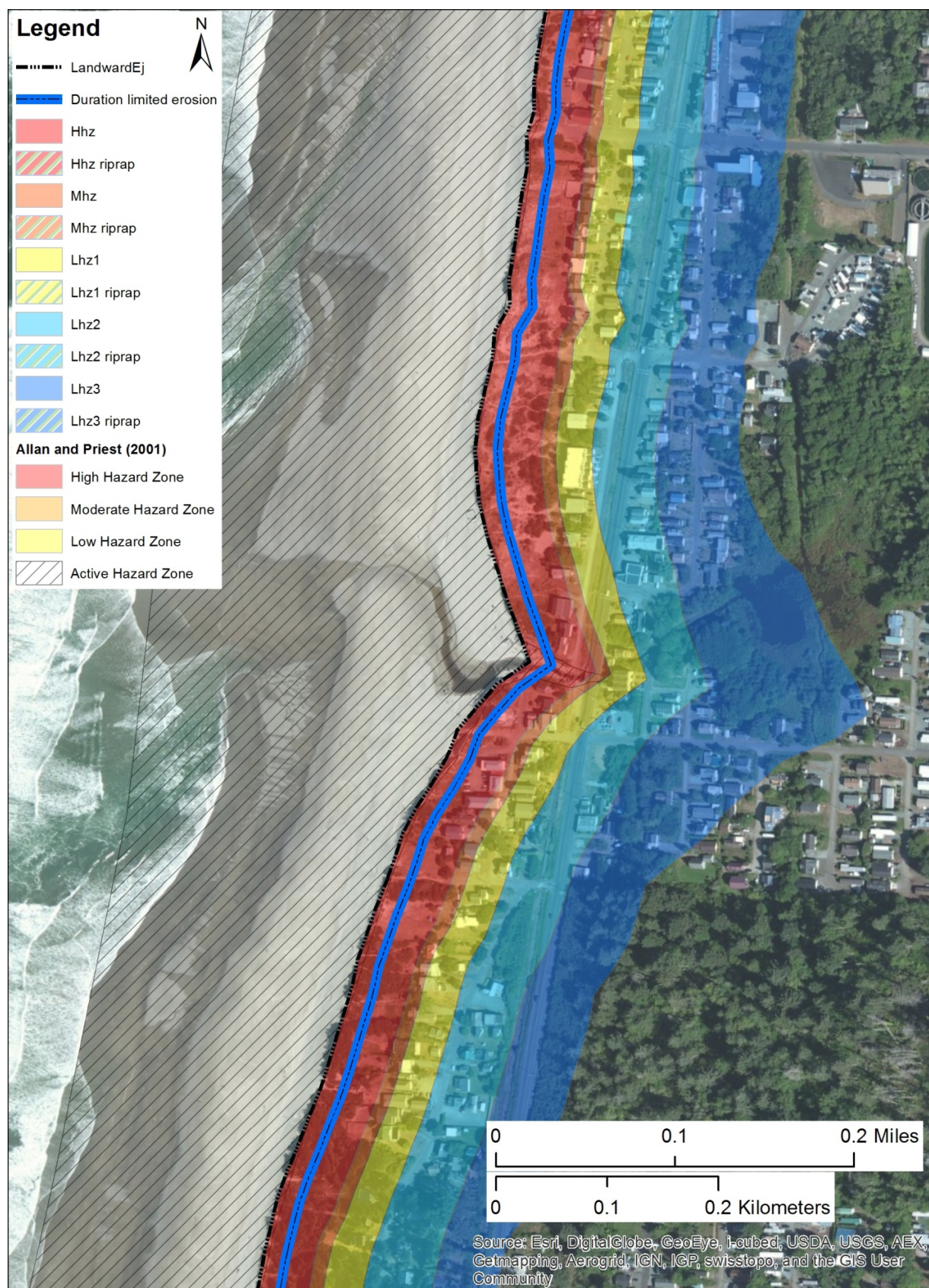




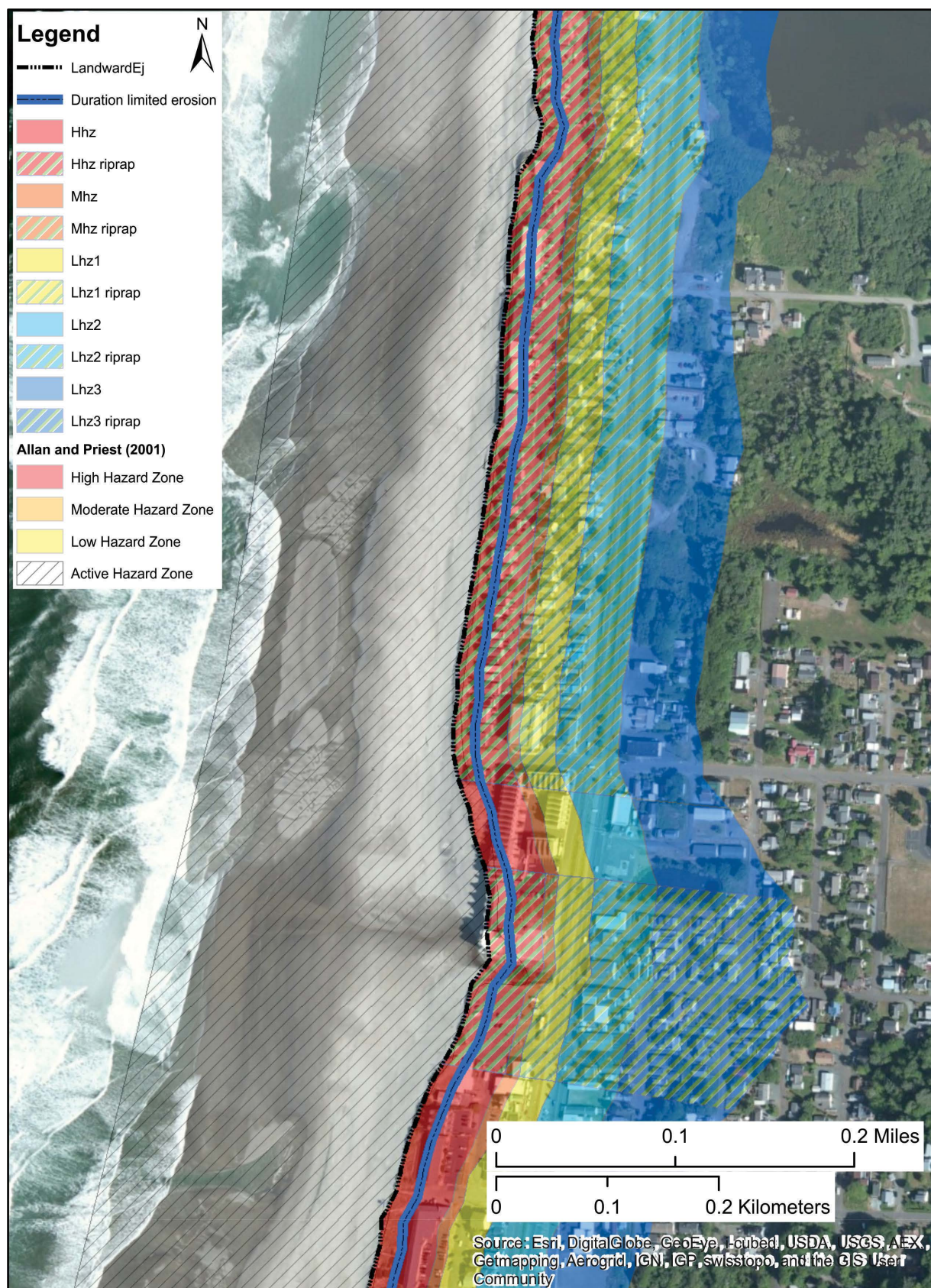




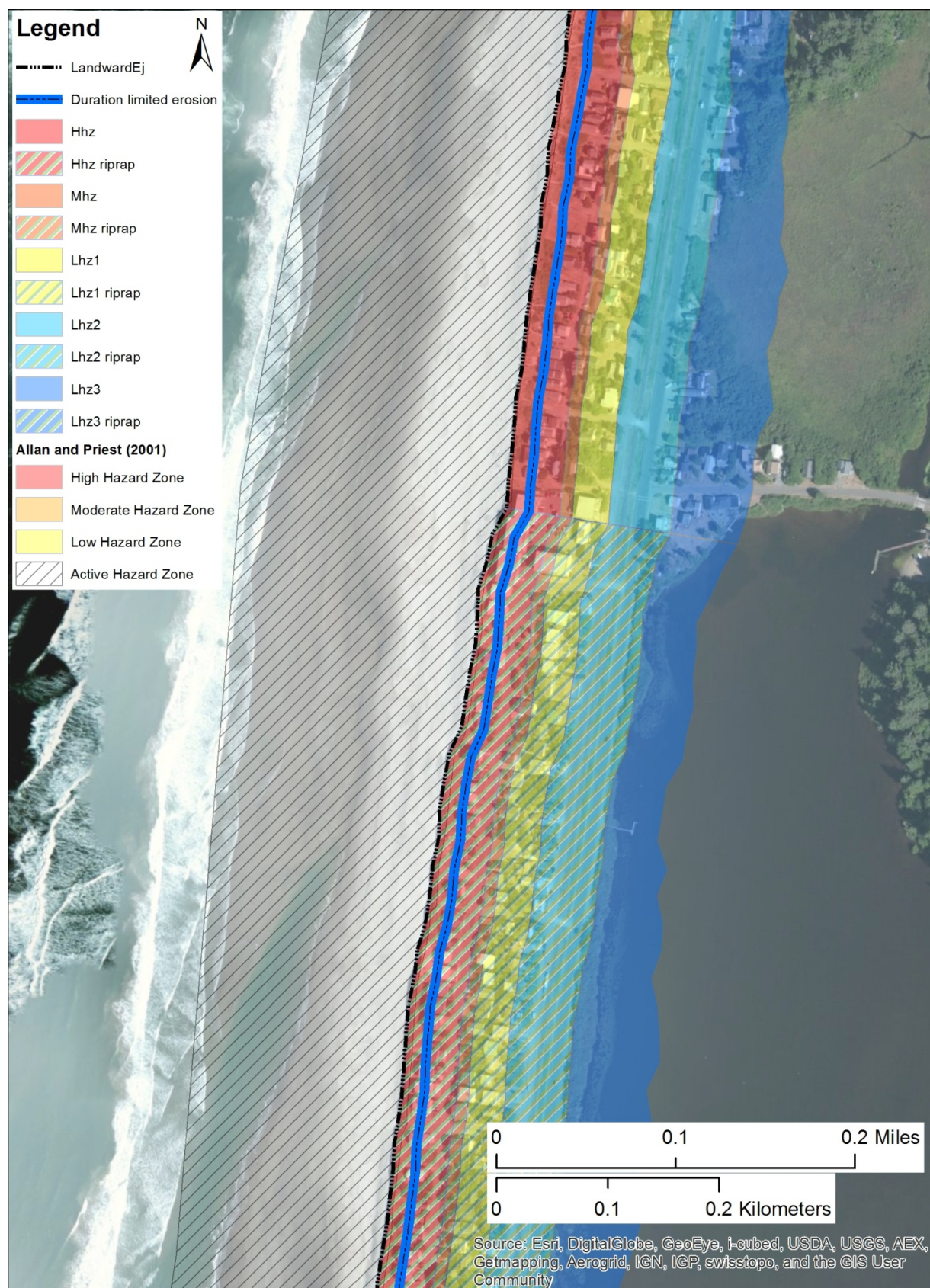




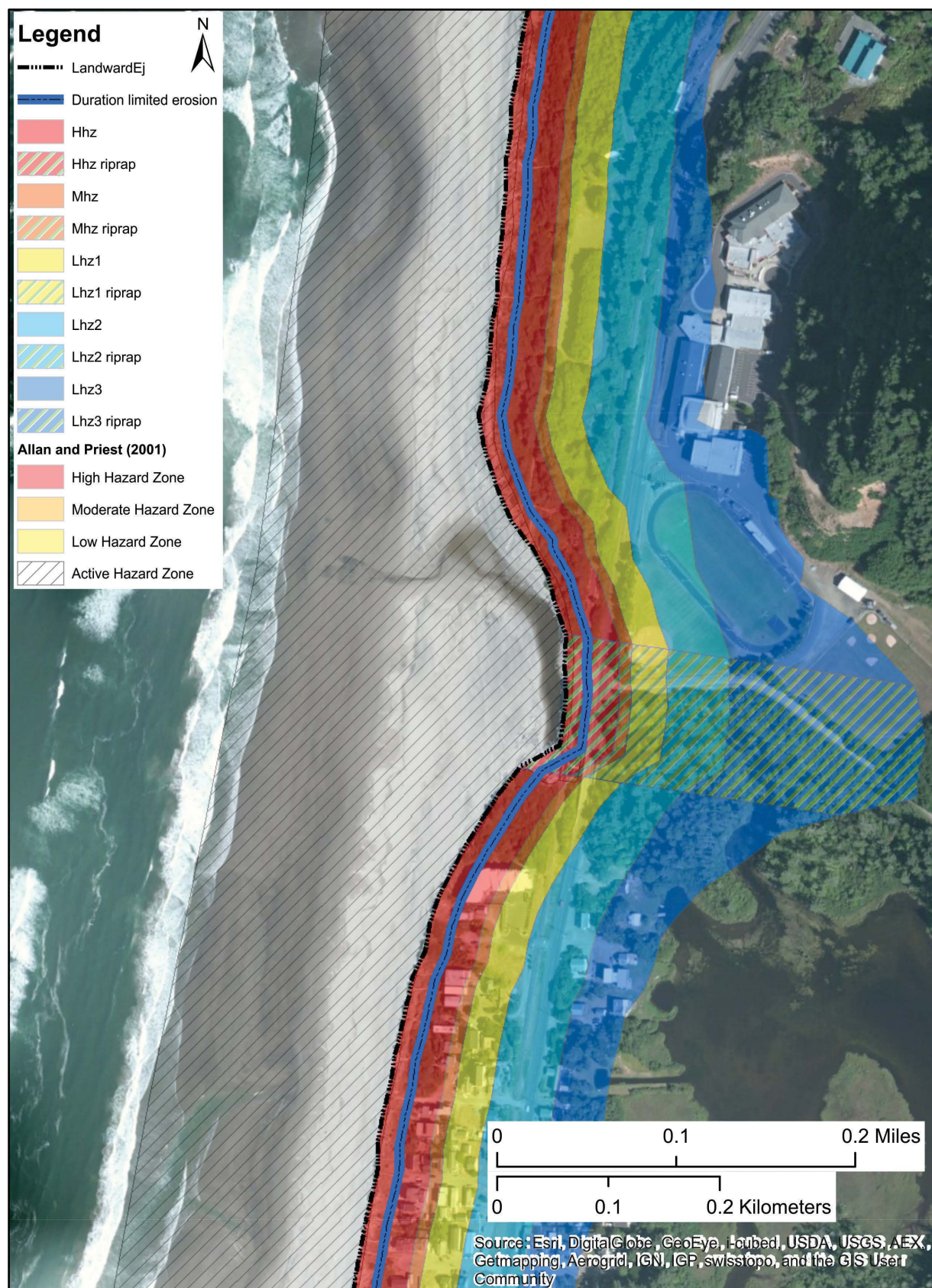








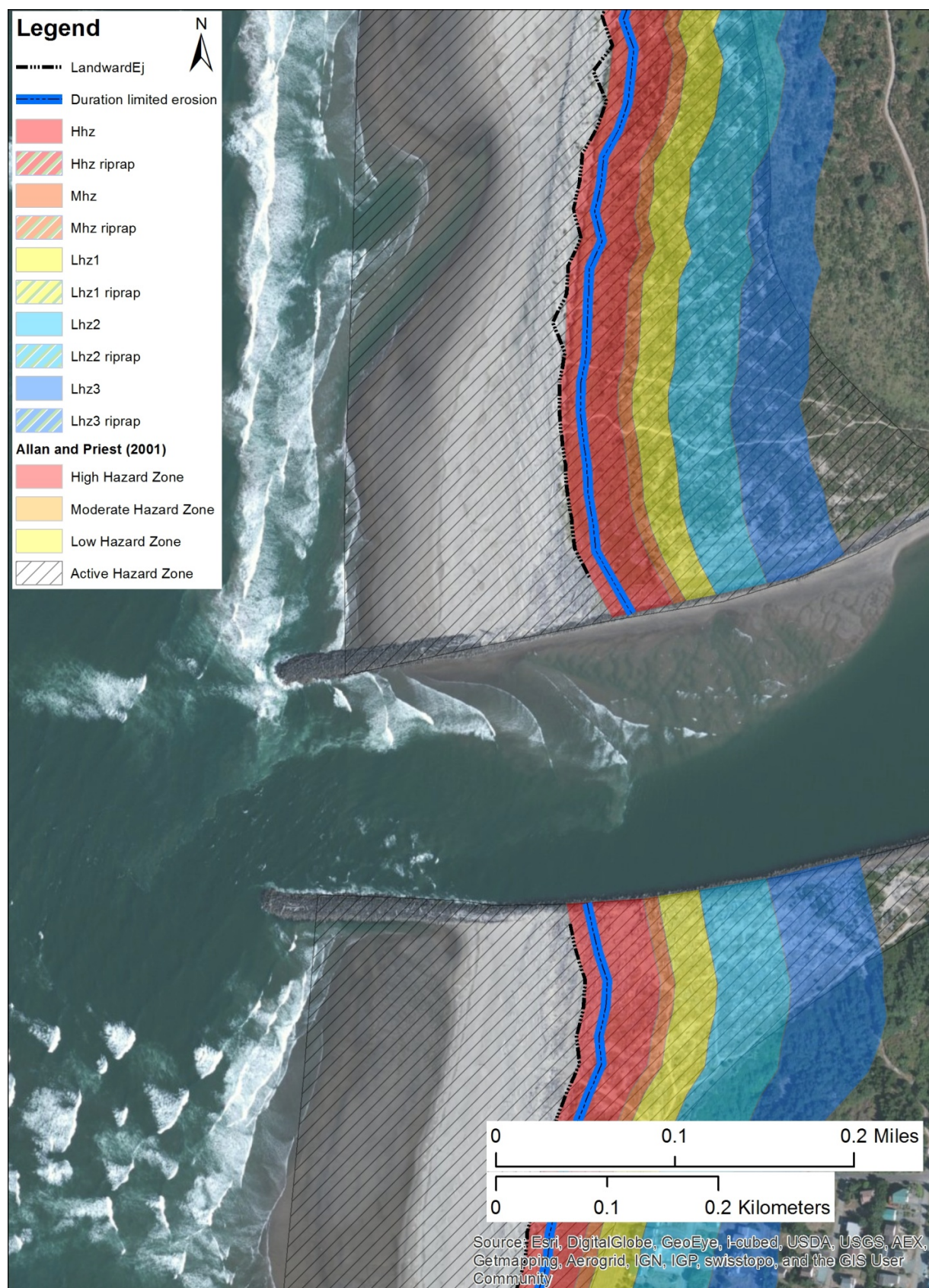






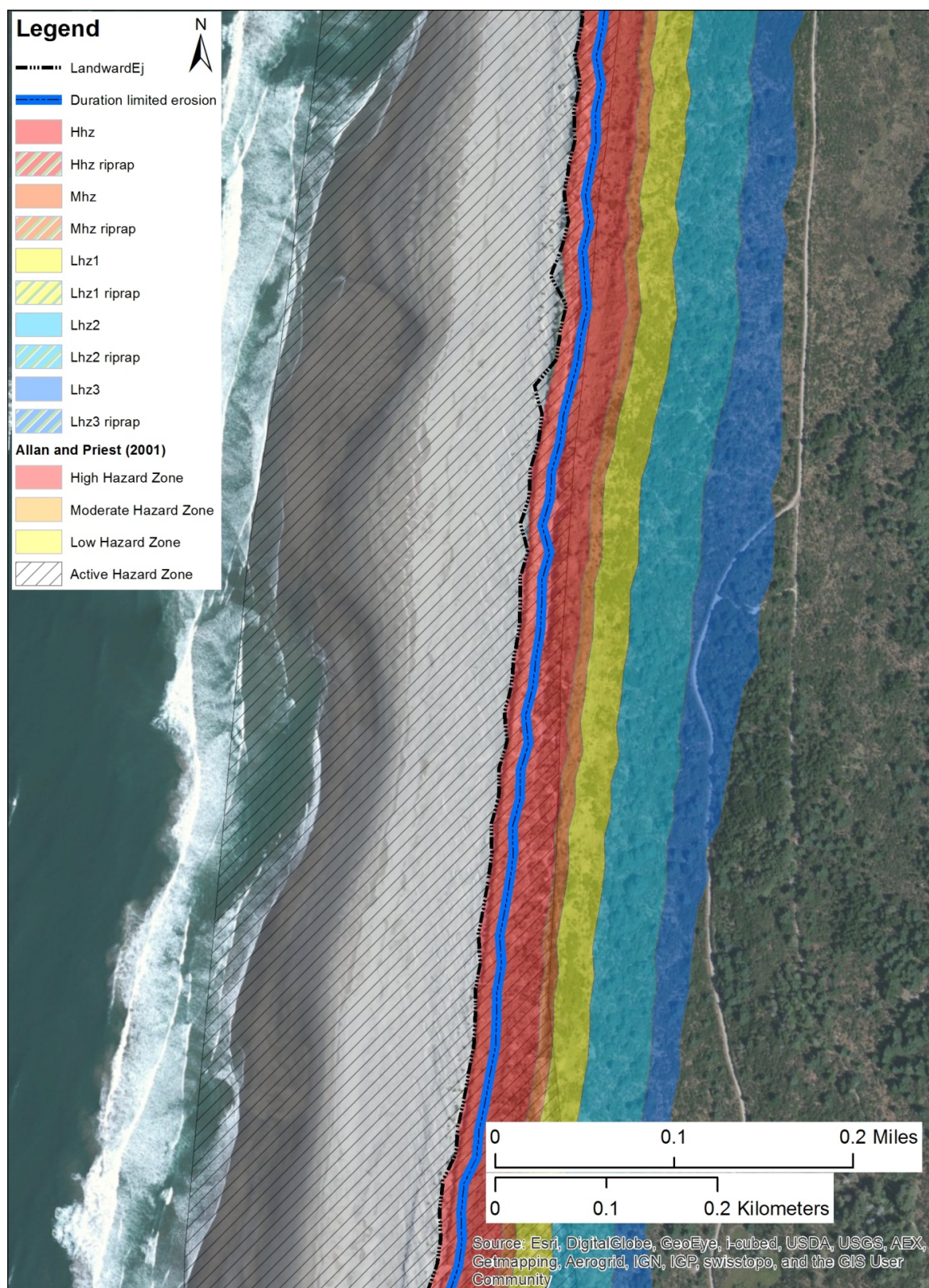




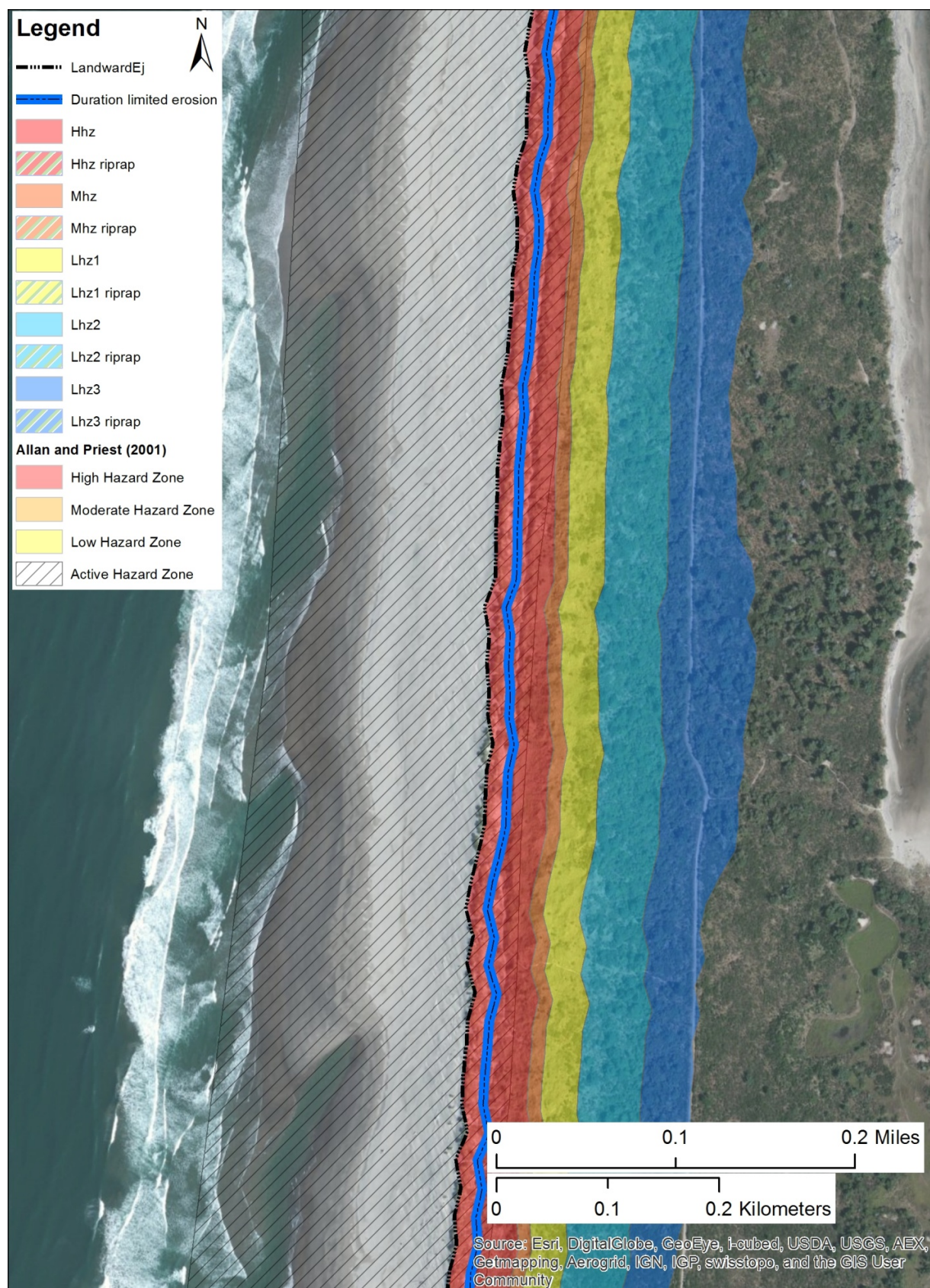




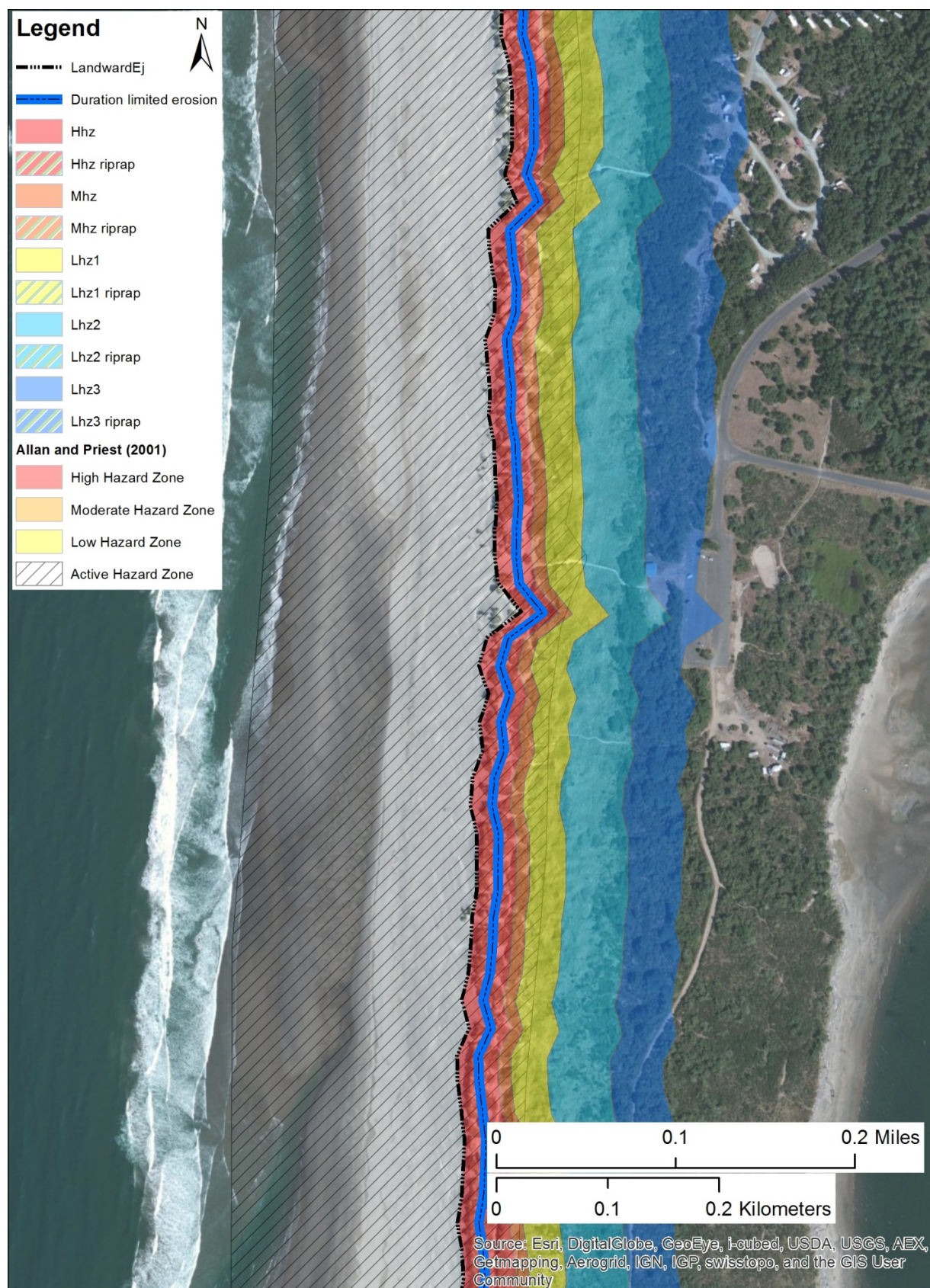
## Nehalem Spit



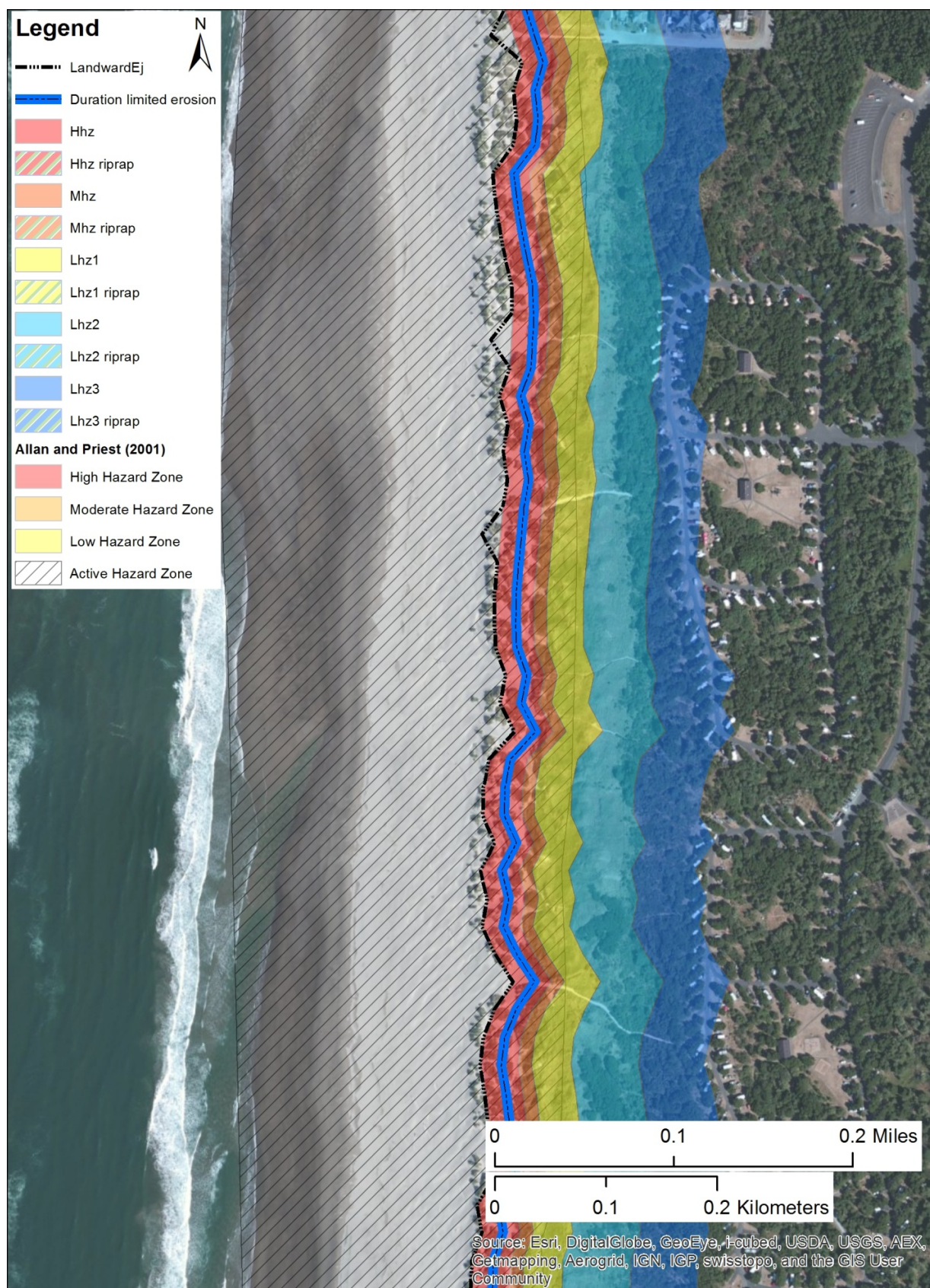














## Manzanita

